MSc Program
Renewable Energy Systems

Large-scale evaluation of rooftop solar potential using raytracing and GIS methods

A Master's Thesis submitted for the degree of
“Master of Science”

supervised by
Univ.Prof. Dipl.-Ing Dr. Reinhard Haas

Joseph Burke. MSc, MBA

11725236

Vienna, 02.04.2021

Affidavit

I, **JOSEPH BURKE. MSC, MBA**, hereby declare

1. that I am the sole author of the present Master's Thesis, "LARGE-SCALE EVALUATION OF ROOFTOP SOLAR POTENTIAL USING RAYTRACING AND GIS METHODS", 91 pages, bound, and that I have not used any source or tool other than those referenced or any other illicit aid or tool, and
2. that I have not prior to this date submitted the topic of this Master's Thesis or parts of it in any form for assessment as an examination paper, either in Austria or abroad.

Vienna, 02.04.2021

_____
Signature

Abstract

The motivation for this thesis is to investigate if synergies between the data, tools and processes already in place for radio network planning can be repurposed effectively towards evaluating solar rooftop potential and at which tiers the effort of that adaptation may be better applied to using purpose made tools and a more detailed study. The objective of this work is to analyse the feasibility of repurposing radio network planning software and cartographic databases in combination with solar irradiation data to calculate region wide rooftop solar potential using GIS & ray tracing techniques. This topic was explored within the framework of the following research questions:

1. Can solar irradiation data be imported into a radio network planning software & filtered to building rooftops?
2. Can cartography data be sourced with fine enough resolution to show roof slope/orientation, and can this data also be incorporated into the rooftop solar irradiation results?
3. Can these results be further refined to include shading effects on building rooftops from the surrounding topography and buildings by simulating the sun as an isotropic radiator and line of sight calculation?

It was found that solar radiation data could be filtered with an accuracy of 0.3m using Open Street Map building outline vectors, however this approach is only suitable at a regional or national level. Applying this process at a macro-level i.e. Western Europe, led to instabilities in the software which made the solution impractical. Furthermore, it was determined that, although cartographic data sets can be sourced with a resolution fine enough to determine roof slope & orientation, this data is discarded during the pre-processing necessary to import the data to a radio network planning software. Finally, it was found that an isotropic radiator simulated as a radio transmitter with a 'Line of Sight' model can accurately simulate the shadowing caused by the sun in specific positions e.g. summer and winter equinoxes, however the parallax effect causes the method to lose accuracy within a 300m radius of the target coordinates, making the solution unsuitable for a regionwide assessment.

The author concludes that if value can be found from a method which employs off-the-shelf radio network planning cartography, to assess regional rooftop solar potential, it would be to generate inputs from the pre-categorised clutter data (building classifications) to improve the results of existing or modified statistical methods.

Table of Contents

1 Introduction

Utility solar in the US and Europe is projected to grow in the next years in greater proportion than residential and non-residential (commercial, industrial) installations, see Figure 1 and Figure 2. However, resistance to ground mounted solar (Saunders, 2020, p. 29) which makes up the majority of utility solar installations, is growing from environmentalists and residents concerned with land use, ecological and visual impact on the landscape. (Mulvaney, 2017, pp. 495, 499 & 511) (Grodsky & Hernandez, 2020, p. 1042) (Wu et al, 2020, p. 8) (Moore-O'Leary et al, 2019, p. 567)

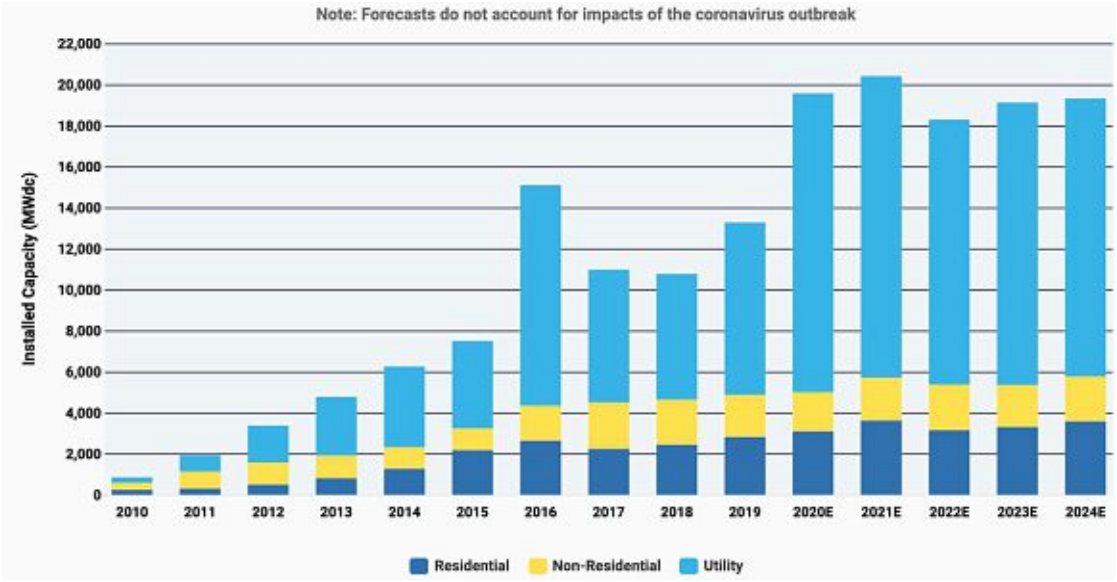

Figure 1: US Solar Deployment Forecast, 2010-2024E
(Solar Energy Industries Association/Wood Mackenzie, 2019, p. 18)

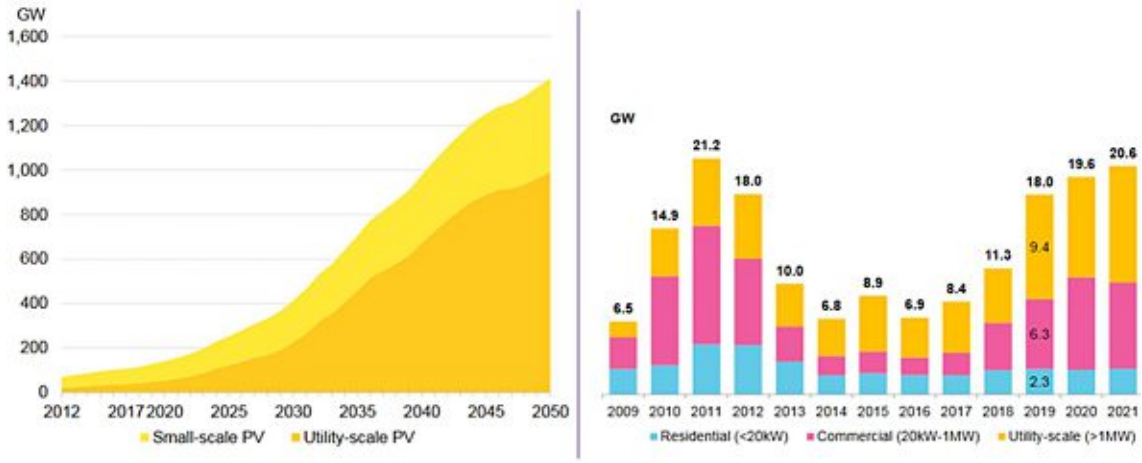

Figure 2: Cumulative PV capacity installed in Europe & PV Capacity additions in Europe by segment
Adapted from (BloombergNEF/Solar Power Summit, 2019, p. 8 & 9)

Land use decisions are often contentious political issues as they involve competing interests (often largely economic), values (conservation, landscapes, development, jobs, clean energy), justice (those negatively impacted sand how benefits are allocated), and rights (liberty, property, expression). Land is perceived to be more available in rural areas and less so in urban communities which leads to regional differences in land use policy and can cause political friction between these communities. Disputes over land use issues with regard to power supply can also be worsened by the fact that urban and rural areas have radically different electricity requirements. (Saunders, 2020, p. 32)

The deployment of rooftop solar in cities, which provide dense markets, could be critical to the de-carbonization of power supply in the future. The sustainability of future building stock can be ensured by proper regulatory support. (OECD/IEA, 2016a, p. 344). Figure 3 shows that approximately nine percent of all urban final electricity demand in 2050 could be met by rooftop photovoltaic (PV) in cities, although this number varies between approximately four to twenty seven percent depending on the region.

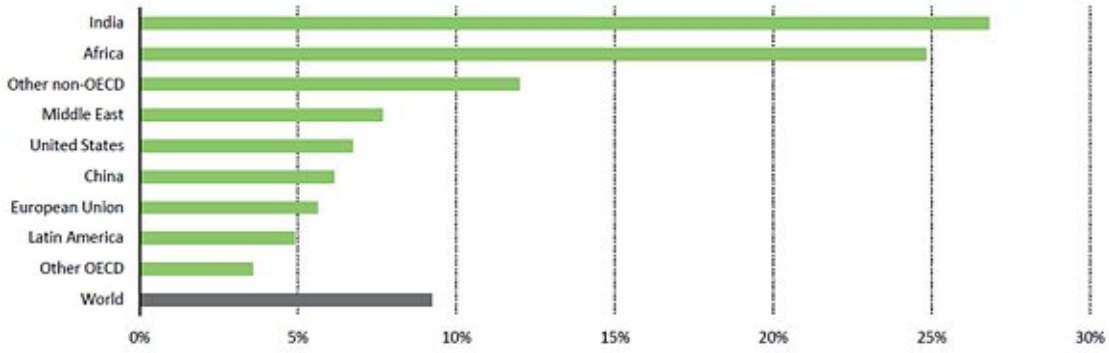

Figure 3: Share of urban final electricity demand met by rooftop PV in cities, 2050 (OECD/IEA, 2016a, p. 285)

Incorporating the findings of a regional solar potential assessment when setting land use policy, building codes and renewables incentive schemes could be used to prioritise large scale solar rooftop implementation. An example of such a policy is the California Solar Mandate, which went into effect on January 1, 2020, and requires newly constructed homes to have a solar photovoltaic system as an electricity source. (State Energy Resources Conservation and Development Commission, 2019, p. 1). However, assessing PV potential, and communicating this data to risk-adverse nontechnical stakeholders is challenging. “Having accurate, accessible, and easily understood tools to assess distributed PV potential estimates

is, therefore, an expected component for appropriate policy development." (Castellanos, Sergio & Sunter, 2017, p. 2)

Currently, when sizing a solar power system (PV or Thermal), solar potential is typically assessed by consulting databases of solar irradiation in this area such as PVGIS (PVGIS, 2019) & Solar GIS (SolarGIS, 2020), see Figure 4. This data can either be combined with statistical methods (OECD/IEA, 2016b, pp. 1-11) on regional population density or used as an input to more complex models which include high resolution cartography and shading models, see Figure 5. (Castellanos, Sergio & Sunter, 2017, p. 5) (Mainzer et al, 2017, p. 562) (Hong et al, 2016, p. 321)

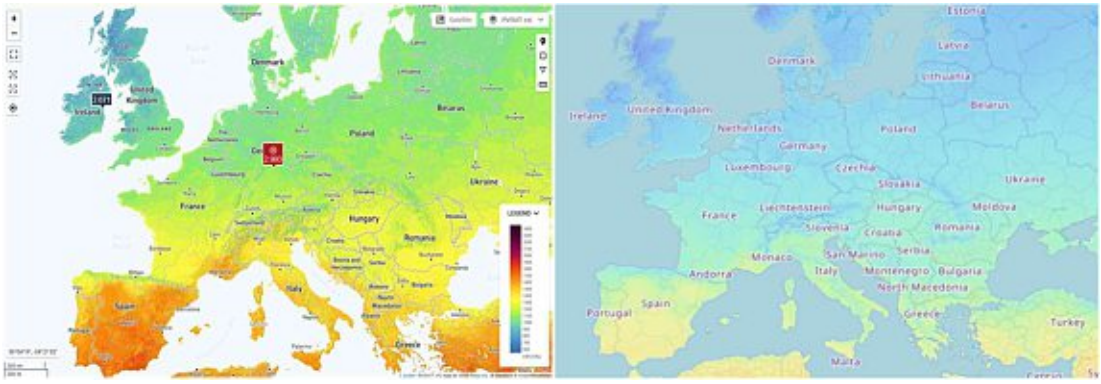

Figure 4: Solar Electricity Potential in Europe (PVGIS, 2019) (SolarGIS, 2020)

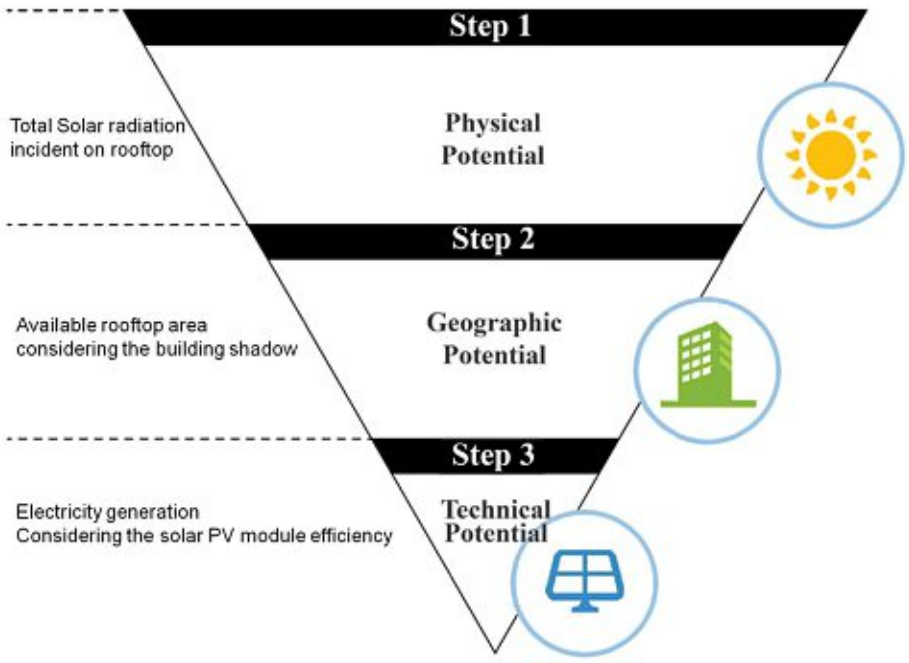

Figure 5: Overview of GIS assessment incorporating shadow modeling
Adapted from (Hong et al, 2016, p. 322)

In a study on the scalability of different evaluation techniques it was noted that policy makers are often faced with the difficult trade-offs between statistical methods based on population density with potentially low accuracy and investing in detailed measurement and modelling campaigns for specific regions. Risk averse decision makers will prefer not to use the less accurate methods but may not have the resources available for those which require expensive data collection, difficult calibration and large computational resources. (Castellanos, Sergio & Sunter, 2017, p. 5)

Radio network planning is the process of optimally locating and configuring telecoms infrastructure to provide the best radio coverage and optimum spectrum usage for the area in question. It is outside the scope of this work to go into all the processes involved in radio network planning, however a brief overview can be seen in Figure 6.

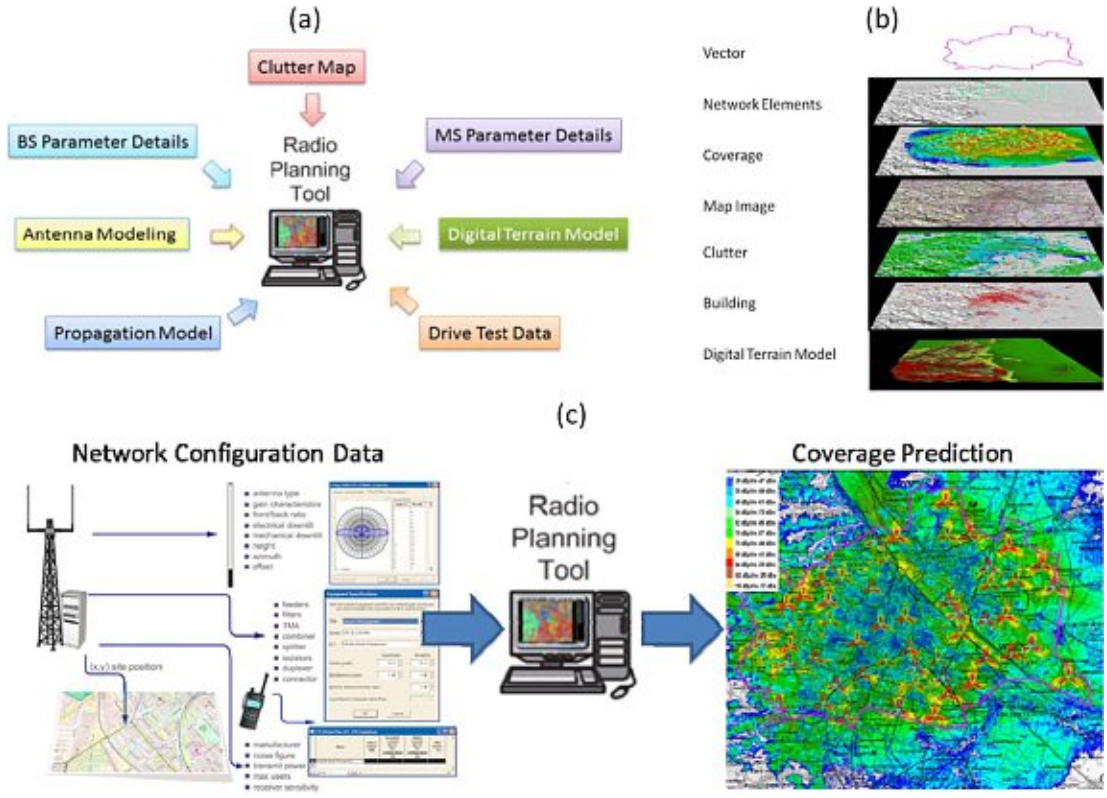

Figure 6: (a) General inputs to a radio planning tool (b) Radio Network Planning Tool Layers for a model of the Vienna area (c) Radio planning tool overview
Adapted from (Burke, 2017, pp. 34, 35 & 37)

Figure 6 (a) shows the general inputs to a radio planning tool. Base Station (BS), Mobile Station (MS) and antennas are modelled on a Digital Terrain Model (DTM) and the radio coverage over this area is calculated using a propagation model which

has been calibrated using drive test data. The simulation is further refined by developing a clutter map which represents different types of ground occupancy e.g., buildings, foliage, water etc., and their respective radio properties at the frequencies available for the network.

Figure 6 (b) shows how this input data is organised in layers within the radio network planning tool. The DTM is the base layer which is a 3D model of the geographic features of the area; the building layer contains height data for the buildings which occupy a particular pixel of the DTM. As already mentioned, the clutter layer defines the properties of the ground occupancy at a particular coordinate on the DTM. The map image layer is a map or aerial photograph of the area under examination, overlaid on the DTM, which gives the user a visual representation of various reference points/landmarks within the area. The network layer represents the characteristics of the infrastructure elements which make up the network. The coverage layer is the coverage which has been calculated by combining the characteristics of all previous layers. Finally, the vector layer, in this case the border of Vienna, is a way to limit the simulation to the required area and also to generate metrics such as percentage or area in km² covered to a specified level.

Figure 6 (c) shows an overview of how the equipment parameters and map data is combined to produce a typical radio coverage prediction.

1.1 Motivation

The motivation for this thesis is to investigate if synergies between the data, tools and processes already in place for radio network planning can be repurposed effectively towards evaluating solar rooftop potential and at which tiers the effort of that adaptation may be better applied to using purpose made tools and a more detailed study.

1.2 Thesis aims and definition of the research problem

The objective of this work is to analyse the feasibility of repurposing radio network planning software and cartographic databases in combination with solar irradiation data in order to calculate region wide rooftop solar potential using GIS & ray tracing techniques. The authors hypothesis is that, based on resources available for the region in question, the methods applied should provide, at minimum, a reliable upper limit for the irradiation of all rooftops within the area which is more reliable than the statistical methods proposed by the IEA. The results of these methods may approach those given by a custom study using specialised tools, depending on the level of processing required, but should be considerably lower effort.

1.3 Research questions

The multiple objectives of the proposed thesis will be addressed by the following research questions:

1. **Can solar irradiation data be imported into a radio network planning software & filtered to building rooftops?**

2. **Can cartography data be sourced with fine enough resolution to show roof slope/orientation, and can this data also be incorporated into the rooftop solar irradiation results?**

3. **Can these results be refined to include shading effects on building rooftops from the surrounding topography and buildings by simulating the sun as an isotropic radiator and line of sight calculation**

1.4 Thesis Structure

An outline of the phases of the constructive research process, thesis research plan and how it fits to the thesis document structure can be seen in Figure 7.

The literature review will commence by studying existing papers available from Google Scholar, the Vienna Technical University Library and other online sources, on the topic of assessing regional rooftop insolation. Key papers will be identified, and the methods used categorised. Companies specialising in the production of regional rooftop insolation studies will be approached with regards to their methodology, tools and typical time frames involved. The results of this research will be presented and summarised in Section 2 of this document: Literature Review.

Sufficient competence will be gained in leading GIS software's (ArcGis, Global Mapper and QGIS) and applied to the problem of assessing regional rooftop insolation. Available cartography data will be selected in order to repeat examples from the papers studied using the tools assessed previously. Studies, examples, or software tutorials from GIS software's will be repeated using both commercial proprietary tools and open-source software in order to gain familiarity with the necessary processes. Once familiarity with the methods has been achieved the exercise will be repeated as closely as possible using radio network planning software. The results of this research will be presented and summarised in Section 3 of this document: Description of methodical approach.

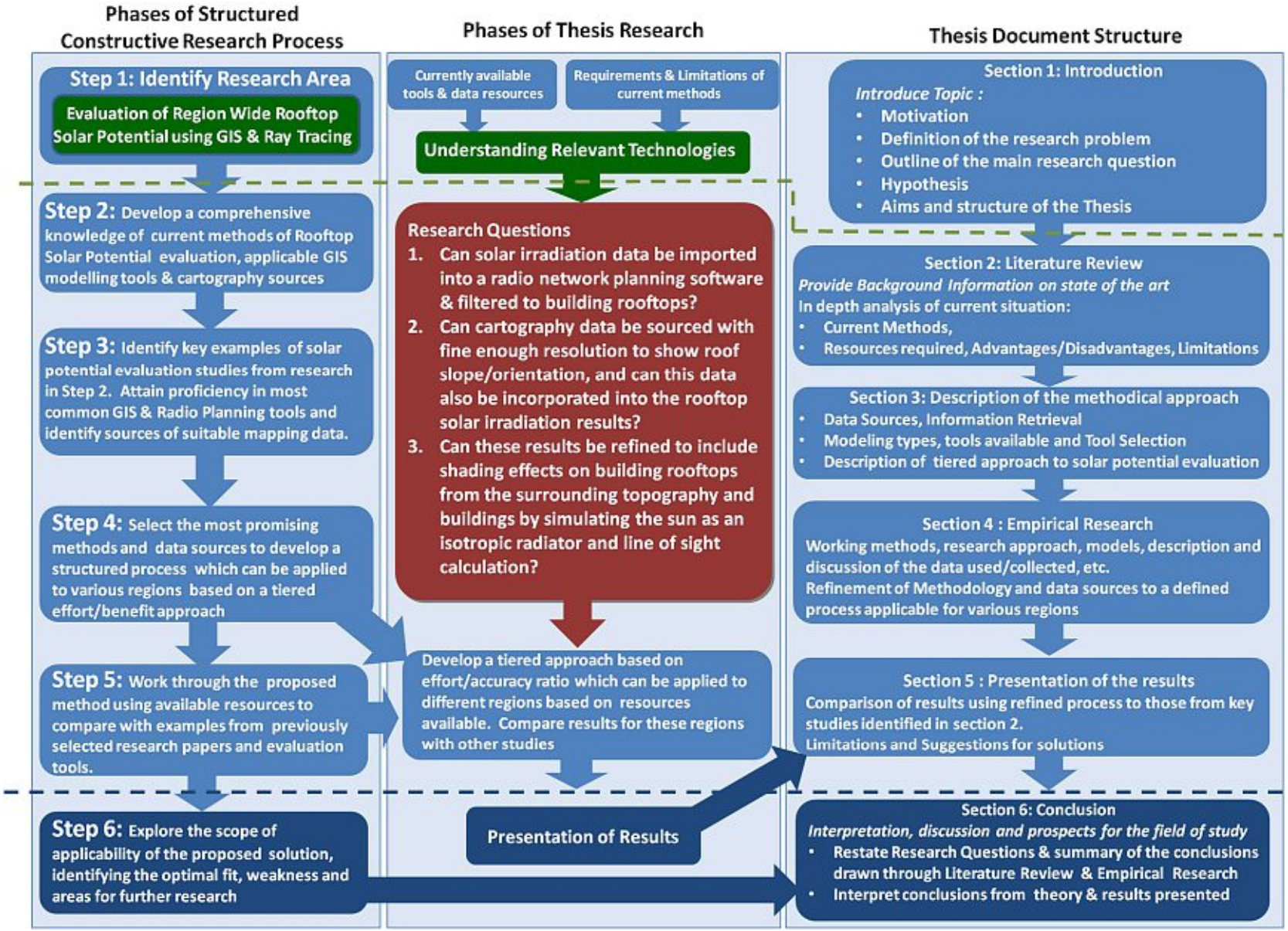

Figure 7: Phases of the thesis research process
(Authors Illustration)

In Section Four: Empirical Research, the process developed will be evaluated, streamlined and the steps necessary to refine the results to levels similar to those approaching the studied papers and examples will be categorised into tiers based on resources necessary (data, resolution, tooling, processing). Granularity and scaling issues will be examined so that the minimum level of resolution for mapping to provide comparative results will be found. This is important as high-resolution data is rare, expensive, difficult to acquire and difficult to process.

In Section Five, results be presented and compared to those achieved using commercial proprietary tools and open-source software, where appropriate. Limitations of the methods employed will be identified and recommendations made on how these limitations could be overcome or how the processes employed may be improved.

Finally, in Section Six: Conclusion, the research questions will be restated and a summary of the conclusions for each will be drawn point by point based on the work in previous sections. The scope of applicability for the proposed methodology will be described including optimal fit, weaknesses and areas for further research based on the theory and results presented.

2 Background information

The International Energy Agency (IEA) has established a methodology for evaluating solar potential of Rooftop Solar Photovoltaics (RTSPV) based on solar insolation and population density. To apply the IEAs' method, first the urban roof area per capita suitable for solar PV is estimated, cities are differentiated by population size, and then the urban roof area is calculated, resulting in the urban potential for RTSPV. (OECD/IEA, 2016b, p. 1)

Figure 8 illustrates the empirical relationship derived by the IEA, based on data from approximately 1600 cities, which links the population density of cities and the roof area per capita available for PV or solar thermal. This relationship ranges from "100 m2/capita in less populated urban areas to 1 m^2/capita in high-density cities". (OECD/IEA, 2016b, p. 2) Logically it follows that larger cities typically have taller buildings/smaller rooms per capita than those in rural areas and therefore less rooftop area per inhabitant. Population densities estimates for cities/city categories worldwide were then combined with the empirical relationship between population density and rooftop area per capita, to produce an estimation of the total roof potential for the cities/city categories. The IEA expects that these estimates are conservative as populations densities tend to decline and that façade installations are not considered. (OECD/IEA, 2016b, p. 4)

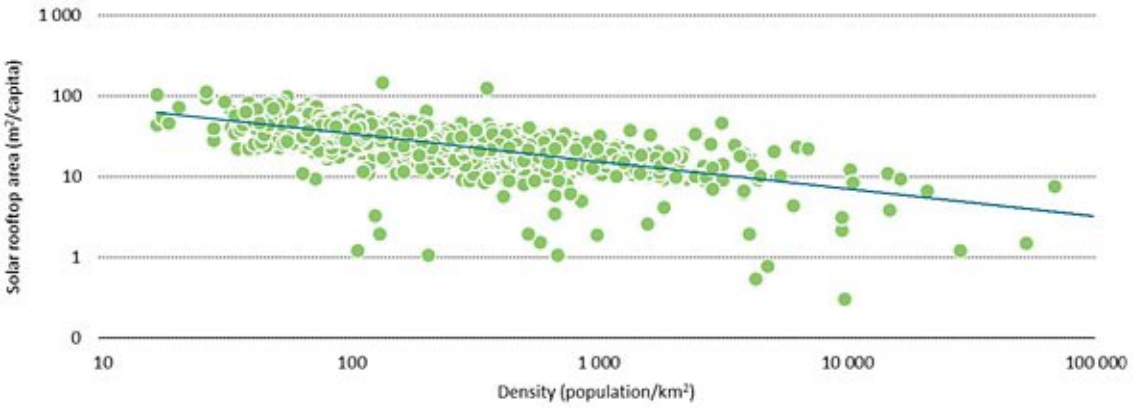

Note: m^2/cap. = square meters per capita; cap. /km^2 = people per square kilometer.

Figure 8: Available solar rooftop area per capita in cities as a function of population density,
Adapted from (OECD/IEA, 2016b, p. 2)

In order to estimate the PVrooftop potential per city according to the OECD/IEA medthod, (OECD/IEA, 2016b, p. 2), the first step is to find the suitable rooftop area per capita, A_{capita}, using equation [1] :

$$A_{capita} = \alpha \cdot \rho^{-\beta} \quad [1]$$

Adapted from (OECD/IEA, 2016b, p. 2)

Where

A_{capita} is the suitable rooftop area per capita, in m^2 per inhabitant

ρ is the population density, to be taken from Table 1, cap/km^2

α is the constant, 172.3, and

β is the constant, 0.352.

As mentioned previously, these constants were found by the IEA after performing a linear regression on 1600 cities, resulting in a correlation coefficient of 44%.

Table 1: Characteristics for large cities (OECD/IEA, 2016b, p. 2)

Population category	Number of cities	Total population (million)	Average population	Total urban area (km^2)	Average city area (km^2)	Average population density (cap./km^2)
100 000 – 200 000	1 694	233	137 792	51 611	30	4 523
200 000 – 400 000	1 009	281	278 198	51 880	51	5 411
400 000 – 800 000	505	280	554 781	47 748	95	5 868
800 000 – 1 600 000	249	282	1 134 387	48 498	195	5 824
1 600 000 – 3 200 000	106	240	2 266 991	38 651	365	6 217
3 200 000 – 6 400 000	47	203	4 321 048	39 077	831	5 197
6 400 000 – 12 800 000	26	226	8 673 664	29 201	1 123	7 723
Greater than 12 800 000	10	179	17 913 610	20 427	2 043	8 770

The next step is to find the the total suitable roof area per city, A_{city} , using equation [2] :

$$A_{city} = A_{capita} \cdot P \quad [2]$$

Adapted from (Castellanos, Sergio & Sunter, 2017, p. 2)

Where

A_{capita} is the suitable rooftop area per capita, found using equation [1],

P, the total population of the city under consideration, and

A_{city} is the total suitable roof area per city, in km^2

The total electricity generation potential, $E_{PV,pot}$, is then calculated, as shown in equation [3],

$$E_{PV,pot} = A_{city} \cdot H_{solar,city} \cdot \eta \cdot PR \cdot f_{orientation} \quad [3]$$

Adapted from (OECD/IEA, 2016b, p. 6) (Castellanos, Sergio & Sunter, 2017, p. 2)

where:

$E_{PV,pot\ is}$ is the total rooftop PV electricity generation potential of the city under consideration, in kWh /yr

$H_{solar,city}$ is the solar insolation (kWh/m^2 /yr), for the area, found from Figure 9,

η is the rooftop PV system efficiency, assumed to be 14% in the IEA study,

PR is the system performance ratio, assumed to be 75% in the IEA study,

$f_{\ orientation}$ is the orientation factor. “In this aggregated approach, no specific information on the gains or losses through tilt or orientation of roof areas is available. The corresponding factor $f_{\ orientation}$ therefore has to be assumed to be 1.” (OECD/IEA, 2016b, p. 6)

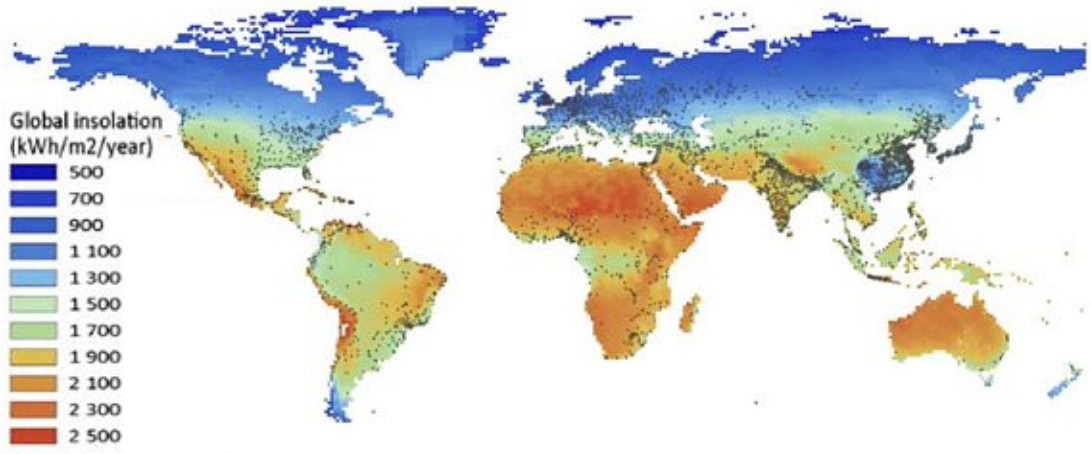

Figure 9: Global average annual solar insolation and location of large cities
Adapted from (OECD/IEA, 2016b, p. 6)

It is intended that these equations, specifically may be used later in this work to validate the methodologies explored at different stages of implementation. From Figure 10 it can be seen that nearly 75% of the technical potential for urban solar rooftop lies in cities outside the OECD while smaller cities with less than 100,000 inhabitants make up almost 40% of this potential. The IEA report further projects that the technical potential of solar rooftop PV in cities is 9100 TWh, and approximately 3650 TWh for buildings in rural areas in 2050. (OECD/IEA, 2016a, p. 268)

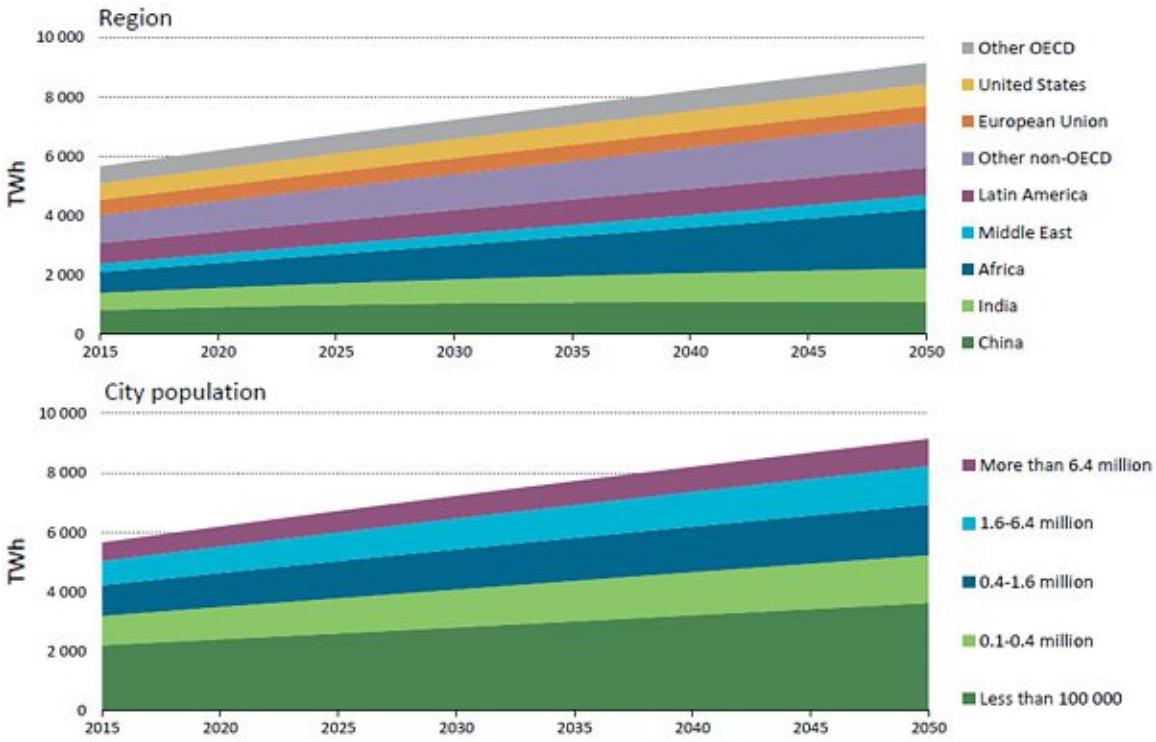

Figure 10: Technical potential for rooftop PV generation by region and city population
Adapted from (OECD/IEA, 2016b, p. 7)

The IEA report concludes that worldwide, cities with a population of ≥1.6 million account for only 25% of the potential rooftop solar PV generation in 2050 and that policies for realizing RTSPV potential need to focus on small cities. The IEA also report also notes that exactly these cities are often, "least prepared for implementing RTSPV, due to lack of data, limited resources, expertise, and constrained governance capacities. Regional or national governments can play a critical role in closing these gaps." (OECD/IEA, 2016b, p. 7)

More detailed and localised academic studies have further refined solar potential evaluation by combining geospatial/statistical data to create a raster of the technical solar potential of rooftops while also taking shading effects into consideration. As part of the literature review process, some key studies were identified and the resolution of the mapping data and methods used were diagrammed and tabulated in Figure 11 and Table 2 respectively, using a study on this topic as a base. (Castellanos, Sergio & Sunter, 2017, p. 4)

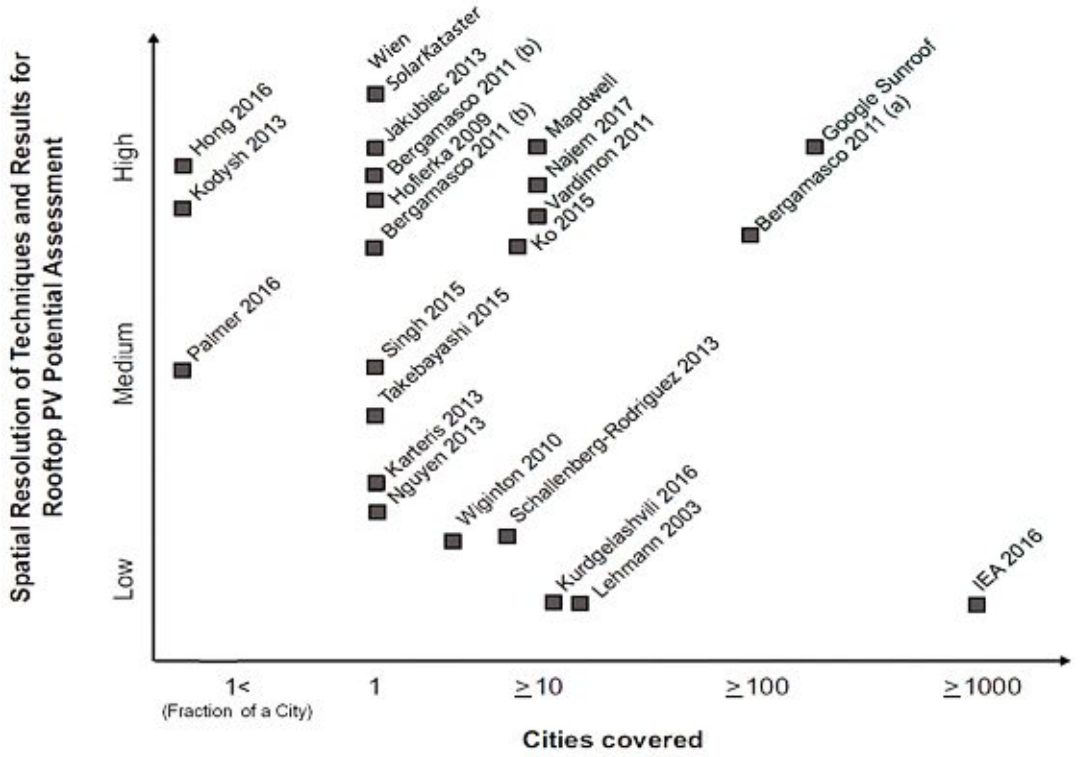

Figure 11: Spatial resolution of studies on rooftop PV potential across different cities, identified from key studies between 2003 and 2016
Adapted from (Castellanos, Sergio & Sunter, 2017, p. 4) (ViennaGis, 2020) (OECD/IEA, 2016b) (Asinari & Bergamasco, 2011) (Asinari & Bergamasco, 2011) (Hofierka & Kaňuk, 2009) (Google LLC, 2017) (Jakubiec & Reinhart, 2013) (Karteris et al, 2013) (Kurdgelashvili et al, 2016) (Lehmann & Peter, 2003) (Nguyen & Pearce, 2013) (Palmer et al, 2016) (Schallenberg-Rodríguez, 2013) (Singh & Banerjee, 2015) (Takebayashi et al, 2015) (Wiginton et al, 2010) (Ko et al, 2015)

From Table 2 it can be seen that the most commonly used softwares for this application are ArcView, ArcGis and ArcMap, part of the ArcGis software suite, created by the Environmental Systems Research Institute (ESRI), as well as Quantum Gis (QGIS) and GRASS Gis, which are open source. QGIS and GRASS GIS are complementary software packages with interconnectivity to execute GRASS processing commands from QGIS menus. QGIS is designed for cartography and map making, while GRASS GIS is used more for data processing and analysis. (QGIS - GRASS-Wiki, 2016)

Table 2: Spatial resolution and techniques for evaluating total rooftop PV potential across different cities, identified from key studies between 2004 and 2016.
Adapted from (Castellanos, Sergio & Sunter, 2017, p. 4) (ViennaGis, 2020) (OECD/IEA, 2016b) (Asinari & Bergamasco, 2011) (Asinari & Bergamasco, 2011) (Hofierka & Kaňuk, 2009) (Google LLC, 2017) (Jakubiec & Reinhart, 2013) (Karteris et al, 2013) (Kurdgelashvili et al, 2016) (Lehmann & Peter, 2003) (Nguyen & Pearce, 2013) (Palmer et al, 2016) (Schallenberg-Rodríguez, 2013) (Singh & Banerjee, 2015) (Takebayashi et al, 2015) (Wiginton et al, 2010) (Ko et al, 2015)

Area	Country	Area (km^2)	Modelling	Spatial Resolution	Authors	Year
Northrhine-Westfalia	Germany	34098	Statistical/Population density	NA	Lehmann	2003
Bardejov	Slovakia	3737	ArcView GIS & GRASS GIS Software	1m	Hofierka	2009
"Renewable Energy Region" of south eastern Ontario	Canada	48000	ArcGis GIS Software with Feature Analyst (FA)	20 cm ortho-photos	Wiginton	2010
Turin	Italy	130.2		mixed	Bergmasaco	2011
Piedmont Region	Italy	25387		mixed	Bergmasaco	2011
Cambridge, Massachusetts	USA	18.5	ArcGis & GRASS GIS Software	1.5 m	Jakubiec	2013
Thessaloniki	Greece	19.31	Statistical/Building Type database	CORINE Land Cover (CLC)	Karteris	2013
Knox County, Tennessee	USA	1362	ArcGIS, Software	1 m horizontal, 0.3 m vertical	Kodysh	2013
Kingston, Ontario	Canada	450.4	ArcGis GIS Software	5 cm	Nguyen	2013
Canary Islands	Spain	7493	Statistical / Spanish Land Registry databse	NA	Schallenberg-Rodriguez	2013
Vienna	Austria	414.6	VERTISOL Software	0.5 m	Wien Solarkataster	2013
Mumbai	India	458.27	Quantum GIS (QGIS) Software	0.5 m	Singh	2015
Osaka	Japan	221.3	ArcGis GIS Software	1 m horizontal, 3.5 m vertical	Takebayashi	2015
Gangnam district, Seoul	South Korea	39.5	ArcMap Software	33 m	Hong	2016
California,Arizona & New Jersey	USA	3 States	Statistical / floor space databse	NA	Kurdgelashvili	2016
England and Wales	UK	130395 & 20735	Strous Sun geometry algorithm	2 & 1 m	Palmer	2016
Worldwide	Worldwide	Worldwide	Statistical/Population density	3 arc seconds/90 m, Shuttle Radar Topography mission (SRTM) 1999	IEA	2016
Portions of 50 states & Washington DC	USA		Shadowing from obstacles 100 to 150m away from each building	15 cm sourced from orthorectified aerial photos	Google Sunroof	Refreshed annually

During the literature review, particular attention was paid to the different methods of assessing usable rooftop area. Examining the methods based on statistics, from Table 2, the study carried out for Northrhine-Westfalia (Lehmann & Peter, 2003) used a statistical method similar to that later used by thee IEA (OECD/IEA, 2016) as already described. Figure 12 (a) and (b) shows the relationship found in this study between roof area on non-residential buildings and residential buildings against population density, respectively. The data on classification of buildings into residential and non-residential categories was taken from a previous study (Unger and Mohr, 1992) which analyzed building structures, site densities and statistical

data, which was in turn was derived from building authorities and land registers to produce an overview of the Northrhine-Westfalia area.

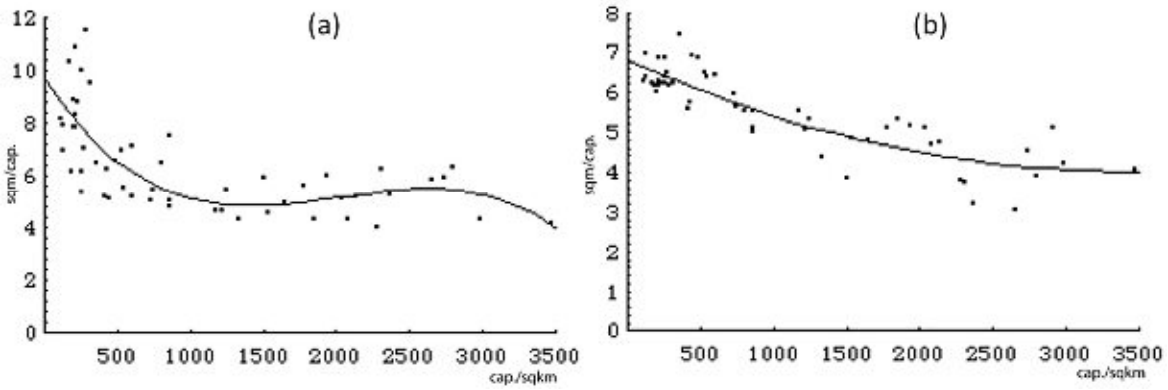

Figure 12(a): Roof area on non-residential buildings and (b) residential buildings against density of population.
Adapted from (Lehmann & Peter, 2003, p. 1 & 2)

The realtionshsip of suitable roof area on non-residential buildings to population density is described by Equation [4]:

$$A\_NR_{city} = 9.625 - 0.008186871\ \rho + 4.42832 \cdot 10^{-6}\ \rho^2 - 7.29043 \cdot 10^{-10}\ \rho^3 \qquad [4]$$

Adapted from (Lehmann & Peter, 2003, p. 1)
where
A_NR_{city} is the total suitable roof area per city on non-residential buildings, expressed in km^2, and
ρ is the population density, expressed as cap/km^2
Similarly, the realtionshsip of suitable roof area on residential buildings to population density is described by Equation [5]:

$$A\_R_{city} = 6.81584 - 0.0016288\ \rho + 2.36943 \cdot 10^{-7}\ \rho^2 \qquad [5]$$

Adapted from (Lehmann & Peter, 2003, p. 2)
where
A_R_{city} is the total suitable roof area per city on non-residential buildings, expressed in km^2, and
ρ is the population density, expressed as cap/km^2

Applying these equations to the EU15 countries, which at the time still included the UK, resulted in approx. 4600 km^2 of rooftops suitable for solar installations. Roof

areas were multiplied by a factor of 0.9 to allow for losses due to non-usable fractions of rooftop areas and shadowing, see Table 3.

Table 3: Roof area and area per inhabitant for all types of buildings in the EU 15. Adapted from (Lehmann & Peter, 2003, p. 3)

Country	Roof Top Area (km^2)	m^2/capita
Austria	103	12.9
Belgium	118	11.8
Germany	985	15.7
Denmark	65	12.7
Spain	528	13.5
France	750	13.2
Finland	72	14.4
Greece	130	12.8
Italy	739	13
Ireland	49	14
Luxembourg	5	12.6
Netherlands	175	11.6
Portugal	137	13.9
Sweden	21	14.7
United Kingdom	692	12
EU15	**4571**	**13.4**

The next study based on a statistical model shown in Figure 11 and Table 2 was carried out for the Canary Islands. (Schallenberg-Rodríguez, 2013) In this study the available roof area for PV purposes was determined per municipality and then within each island/region. Roof surface data was processed from the Spanish Land Registry database (Spanish Land Registry, 2013) by extrapolating from information on number of floors per building and property floor space area. The areas within each municipality were then classified as:

- Industrial buildings
- Services buildings (e.g., Schools, hospital, commercial areas, etc.)
- High-rise apartment buildings
- Semi-detached and terraced houses
- Detached houses

Buildings were then further subdivided by building types according to the regional architectural style and characterization of their roofs.

Figure 13 shows, in overview, the method for computing available roof area which has been derived from a previous study (Izquierdo et al, 2008) on the Spanish mainland with adaptation to local conditions.

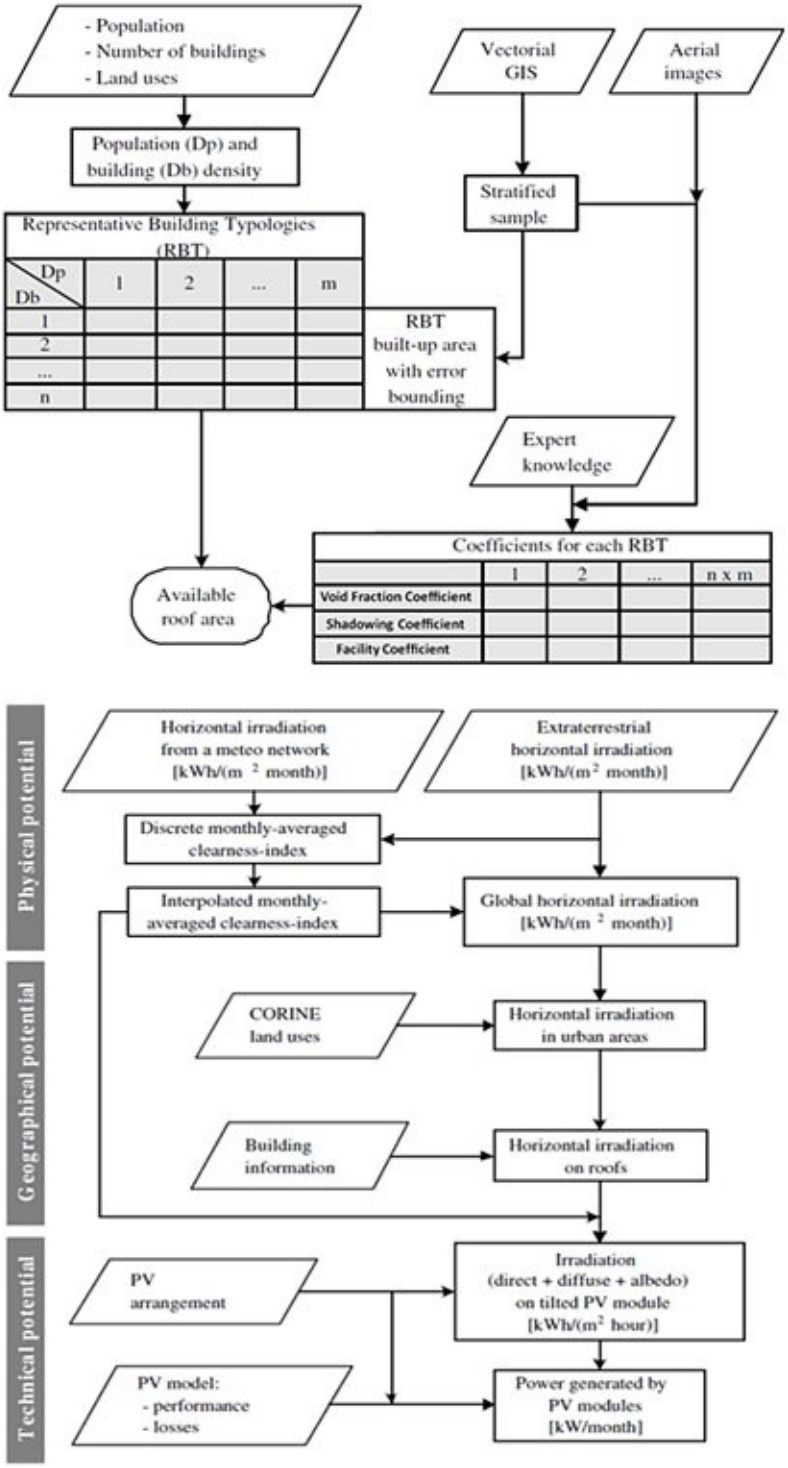

Figure 13: Methodology to compute the available roof area and methodology to compute photovoltaic potential.
Adapted from (Izquierdo et al, 2008, p. 931 & 932)

The available roof area is computed from the total roof area by "progressively applying restrictions defined by the following coefficients (in this order):

(i) the void fraction coefficient C_v to consider voids and recesses in buildings.

(ii) the shadowing coefficient C_s to factor in the effect of shadows generated by other buildings, objects, or by the roof configuration itself; and

(iii) the facility coefficient C_f to exclude surfaces which have other specific applications (e.g., aerials, stacks or Heating, ventilation, and air conditioning equipment)." (Izquierdo et al, 2008).

Instead of using a vector database as in Figure 13, the Canary Islands study used visual inspection of Google Earth and Google Map images for representative areas from each municipality to classify them.

In the Canary Islands study, the total derived rooftop area was reduced by a, ''reduction coefficient'' or "utilization factor" to allow for "shading from other roof parts or from neighbouring buildings and trees; use of roof space for other applications, such as ventilation, heating/air conditioning, stair-wells or chimneys; and installation and tracking of PV panels themselves" (Schallenberg-Rodríguez, 2013, p. 221) in order to find the total available roof area.

As data on roofing types was not available from the Spanish Land Registry database, assumptions on representative roofing types and their characteristics were made based on visual inspection of Google Earth, Google Map images and local knowledge of the region.

Architectural suitability factor, A_{SF}, see Equation [6], is a factor which accounts for the total suitable roof surface area reductions due to construction restrictions, protected building status and shadowing.

$$A_{SF} = CR_C \times S_C \times PB_C \qquad [6]$$

Where

A_{SF} is the Architectural Suitability Factor,

CR_C is the Construction Restriction Coefficient,

S_C is the Shading Coefficient, and

PB_C Protected Building Coefficient,

Note: Using this method, all coefficients were expressed as a percentage of one.

Solar suitability factor is based on orientation and slope of the roof, see Equation [7]

$$R_{SS} = R_{OC} \times R_{SC} \qquad [7]$$

Where

R_{SS} is Rooftop Solar Suitability Factor,

R_{OC} is the Roof Orientation Coefficient, and

R_{SC} is the Roof Slope Coefficient

Note: Using this method, all coefficients were expressed as a percentage of one.

The reduction coefficient or utilization factor, *UF*, see Table 4 and Equation [8] is itself a product of the A_{SF}, Architectural Suitability Factor and $R_{SS,}$ Rooftop Solar Suitability Factor

$$UF = A_{SF} \times R_{SS} \quad [8]$$

Where

UF is Utilization Factor,

A_{SF} is the Architectural Suitability Factor, and

R_{SS} is the Rooftop Solar Suitability Factor

Note: Using this method, all coefficients were expressed as a percentage of one.

The coefficients for Construction, Shading, Protected Building Status, Orientation and Slope were derived from a previous study (Izquierdo et al, 2008) and result in the Utilization Factors for each of the categorised building types as shown in Table 4 by applying Equations [6] [7] and [8]. The resulting available roof surface per island and surface type is given in Table 5.

Table 4: Utilization factors per building type
Adapted from (Schallenberg-Rodríguez, 2013, pp. 225 - 227)

Building Type	Construction Coefficients	Shading Coefficient	Protected Building	Architectural Suitability	Orientation	Slope	Solar suitability	Utilization factor
Industrial	0.95	0.95	1	0.90	1	1	1	0.9
Services	0.85	0.7	1	0.6	1	1	1	0.6
Apartment Building								
Flat roof	0.7	0.64	0.95	0.43	1	1	1	0.43
Mansard roof	0.7	0.64	0.95	0.43	0.50	0.50	0.25	0.11
Semidetached / Terraced House								
Flat roof	0.8	0.48	0.9	0.35	1	1	1	0.35
Pitched roof	0.9	0.48	0.9	0.39	0.50	0	0	0
Detached House								
Flat roof	0.8	0.66	0.9	0.48	1	1	1	0.48
Pitched roof	0.9	0.66	0.9	0.53	0.50	0	0	0

Table 5: Available roof surface per island and surface type.
Adapted from (Schallenberg-Rodríguez, 2013, p. 228)

Available roof surface (1000 m^2)								
Surface type	Gran Canaria	Lanzarote	Fuerte-ventura	Tenerife	La Palma	La Gomera	El Hierro	Total
Industrial	5706	1153	1000	8088	615	154	68	16,784
Services	2913	790	598	4434	206	74	45	9062
Tourist	707	313	318	464	30	18	0.9	1851
Residential	5426	1690	1243	6279	689	186	144	15,656
Total	**14,753**	**3946**	**3160**	**19,265**	**1540**	**453**	**258**	**43,374**

The three use case scenarios and available rooftop surface, shown in Table 6, describe different mixes of rooftop use:

- Scenario 1: Total available roof area dedicated to PV energy production.
- Scenario 2. Total available roof area dedicated to a mix of Solar Thermal and PV energy production.
- Scenario 3: available roof area shares its surface between energy uses (both solar thermal and PV as in scenario 2) and other purposes e.g., drying clothes or recreational space not related to energy production. 1m^2 per capita was allocated for non-energy production purposes.

Table 6: Available roof surface per scenario.
Adapted from (Schallenberg-Rodríguez, 2013, p. 228)

	Available roof surface (km2)							
Scenario	Gran Canaria	Lanzarote	Fuerte-ventura	Tenerife	La Palma	La Gomera	El Hierro	Total
Scenario 1	14.8	3.9	3.2	19.3	1.5	0.45	0.26	43.4
Scenario 2	13.9	3.8	3.1	18.4	1.5	0.43	0.25	41.3
Scenario 3	13.1	3.7	3.0	17.5	1.4	0.41	0.24	39.1

Similarly to other studies mentioned already, the yearly PV production per municipality was found from the available rooftop area, annual mean global solar irradiation on optimally tilted plane, per municipality and PV system efficiency (Module Efficiency * Performance Ratio). For each municipality, data on the annual mean global solar irradiation, was taken from a radiation map of the Canary Islands developed by the Instituto Tecnologico de Canarias (Instituto Tecnologico de Canarias, 2020).

Table 7: Annual PV production in a sample of municipalities
Adapted from (Schallenberg-Rodríguez, 2013, p. 235)

Municipality	Usable roof msurface (1000 m2)	Global Irradiation 23° tilted plane	Yearly PV production (GWh/a)
Las Palmas de Gran Canaria	4938	5057	1023
S/C de La Laguna	2958	5424	657
S/C de Tenerife	2787	5317	607
Telde	2304	5371	483
Arona	1936	5482	469
S. B. de Tirajana	1652	5534	374
Betancuria	25	5864	6
Puntagorda	26	5438	6
Artenara	25	5376	5.6
Garafia	27	5204	5.7
Tejeda	20	5234	4
Agulo	17	4821	3.4

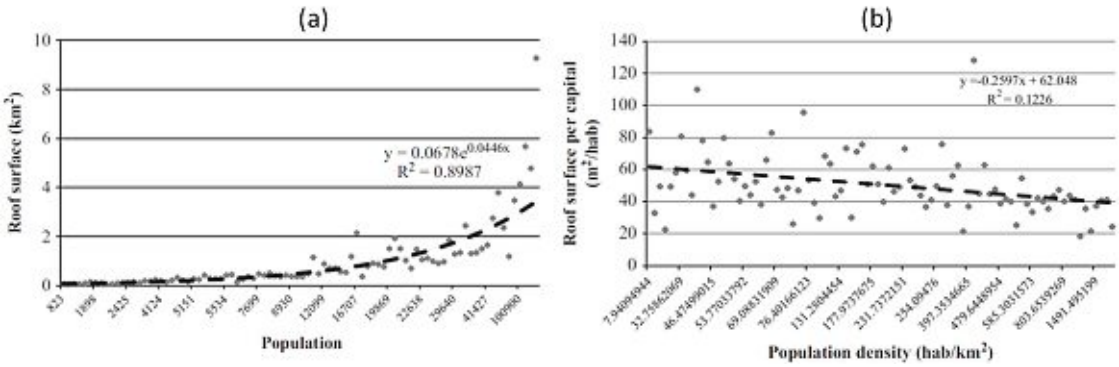

Figure 14: (a) Roof surface vs. population (b) Roof surface per capita vs. population density.
Adapted from (Schallenberg-Rodríguez, 2013, p. 290)

Figure 14 (a) shows that there is a exponential relationship between roof surface area and population and (b) shows that roof surface per capita decreases when the population density increases. This is in line with the relationship between these parameters found in the IEA study, see Figure 8 and for Northrhine-Westfalia, see Figure 12.

In 2016, a study (Kurdgelashvili et al, 2016) was carried out on the potential for rooftop photovoltaics in California, Arizona and New Jersey which also used statistical methods, see Figure 15, based on public databases maintained by the Energy Information Administration's (EIA) Commercial Buildings Energy Consumption Survey (CBECS).

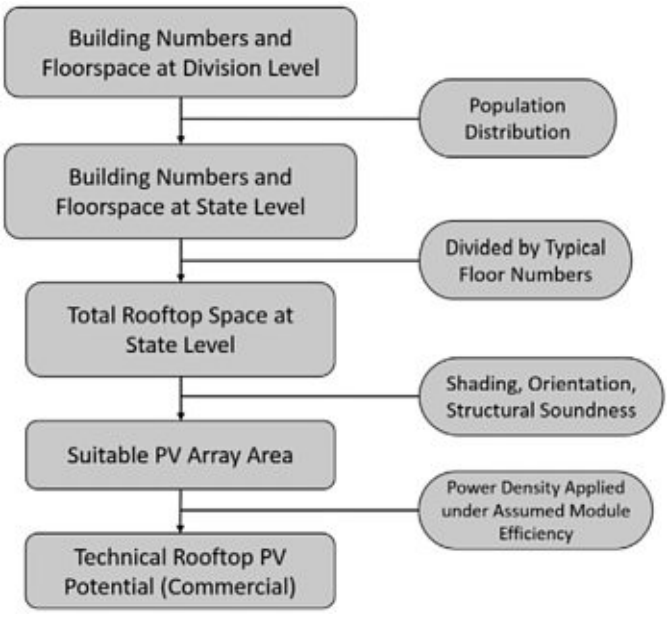

Figure 15: Methodology for the estimation of technical rooftop PV potential in commercial sector.
(Kurdgelashvili et al, 2016, p. 288)

Similarly to the Canary Islands study where buildings were categorised by municipality and Island, buildings from these databases were categorised by division and state level. In the first step, division level, buildings are divided into categories by building utilization and size. In the next step, state level, commercial building floorspace and subsequently, rooftop area, was estimated based on correlation with the population density for each region.

Again, as with previous studies, it was found that census divisions with larger population tend to have more floorspace. Wherever necessary, missing data was extrapolated from reference values developed by U.S. Department of Energy (USDOE), the National Renewable Energy Laboratory, Pacific Northwest National Laboratory and Lawrence Berkeley National Laboratory, see Table 8.

Table 8: USDOE-CBECS Category matching table and number of commercial building with aggregated floorspace in three states
Adapted from (Kurdgelashvili et al, 2016, pp. 289-291)

Matched building type Categories			
EIA Category system	USDOE Category system	Floor area (ft^2)	No. of floors
Education	Primary School	73,960	1
	Secondary School	210,887	2
Food Sales	Supermarket	45,000	1
Food Service	Quick Service Restaurant	2500	1
	Full Service Restaurant	5500	1
Health Care-Inpatient	Hospital	241,351	5
Health Care-Outpatient	Outpatient Health Care	40,946	3
Lodging	Small Hotel	43,200	4
	Large Hotel	122,120	6
Mercantile Retail (other than malls)	Stand-alone Retail	24,962	1
Mercantile Enclosed & Strip Malls	Strip Mall	22,500	1
Office	Large Office	498,588	12
	Medium Office	53,628	3
	Small Office	5500	1
Warehouse & Storage	Warehouse	52,045	1

States	Estimated number of commercial buildings	Estimated floorspace of commercial buildings (million ft2)
California	693,473	9987
Arizona	97,931	1443
New Jersey	108,445	2416

After the total floor spaces for each type of building in California, Arizona and New Jersey was estimated, calculations were performed, see equations [9], and [10], to give an estimate of total rooftop space is needed to calculate technical rooftop solar potential.

On flat roofs where solar panels are installed in rows, panel-to-panel shading must be considered. A setback ratio (SBR) or the ratio of gap between rows to vertical distance between the highest edge of the panel and the ground must also be considered. An SBR of 3:1 was taken for all locations in the Arizona, California and New Jersey studies. The influence on available PV array area from panel-to-panel shading can be estimated using the Ground Cover Ratio (GCR), defined as the array area divided by the ground area. Equation [9] gives the relationship between tilt angle $\measuredangle$, SBR and GCR for multi-row systems.

$$GCR = (\cos(\measuredangle) + SBR * \sin(\measuredangle))^{-1} \quad [9]$$

Where

GCR is the Ground Cover Ratio, expressed as a percentage

SBR is the Setback Ratio, expressed as a percentage and

$\measuredangle$ is the Tilt Angle, in degrees

For the US 3-state study, the tilt angle was assumed to be 10 degrees for all locations with flat roofs, which gives a GCR of 66.4%. Therefore for flat roofs, equation [10] can be applied:

$$Af_{pv} = H_{GRS} \times AF \times GCR \quad [10]$$

where

Af_{pv} is the Total PV Array Area for flat roofs in square feet,

H_{GRS} is the Estimated Gross Horizontal Roof Space in square feet,

AF is the Access Factor, based on roof pitch, and

GCR is the Ground Cover Ratio

As noted in the previous studies, the total area available for PV array installation is affected by various factors: roof pitch, orientation, structural soundness, building obstruction and shading etc. From the CBECS database, the rooftops of commercial buildings were categorised as: flat, shallow pitch and steeper pitch. Access Factor coefficients were developed from reference values available in literature on rooftop PV market penetration (Paidipati et al, 2008). In California, Arizona and New Jersey, over 50% of commercial buildings have flat roofs. In warm states e.g. California and Arizona, flat roofs have an Access Factor of 60% and pitched roofs have an Access Factor of 24.3%. In cooler climates such as New Jersey, the Access Factor of flat roofs is 65% and that of pitched roofs is 17.55%.

For commercial buildings with pitched roofs, no GCR coefficient is necessary as panels are assumed to be installed directly on the along the roof surface. Instead a Geometric Factor, *GF*, must be applied, see equation [11]. Shallow pitched roofs were are assumed to have a tilt of 10° while steeper ones were assumed to have a tilt of 30°.

$$GF = 1/\cos(\measuredangle) \quad [11]$$

where

GF is the Geometric Factor, expressed as a percentage and

$\measuredangle$ is the Tilt Angle, in degrees

The Geometric Factor, *GF*, is then used in combination with the Estimated Gross Horizontal Roof Space, H_{GRS}, to find the Total Estimated Pitched Roof Space, P_{RS}, as shown in equation [12].

$$P_{RS} = \sum_i^2 H_{GRS_i} \times GF_i^7 \quad [12]$$

where

P_{RS} is the Total Estimated Pitched Roof Space, in square feet,

H_{GRS} is the Estimated Gross Horizontal Roof Space, in square feet, and

GF is the Geometric Factor, expressed as a percentage.

Therefore, in order to find the Total PV Array Area for pitched roofs, $AP_{pv,}$ equation [13] is applied:

$$AP_{pv} = P_{RS} \times AF \quad [13]$$

where

AP_{pv} is the Total PV Array Area for pitched roofs in square feet,

P_{RS} is the Total Estimated Pitched Roof Space in square feet,

AF is the Access Factor, expressed as a percentage, and

The resulting Feasible PV array area for commercial buildings in Arizona, California and New Jersey can be seen in Table 9

Table 9: Feasible PV array area for commercial buildings in Arizona, California and New Jersey
Adapted from (Kurdgelashvili et al, 2016, p. 294)

State	Roof type	Rooftop space (million ft2)	Access factor (%)	GCR (%)	Feasible PV array area (million ft2)	Total PV array area (million ft2)
Arizona	Flat	445.84	60.0%	66.4%	177.66	**361.90**
	Shallow Pitch (10°)	259.98	60.0%	N.A.	155.99	
	Steeper Pitch (30°)	116.28	24.3%	N.A.	28.26	
California	Flat	3592.91	60.0%	66.4%	1431.67	**2629.82**
	Shallow Pitch (10°)	1670.79	60.0%	N.A.	1002.47	
	Steeper Pitch (30°)	805.26	24.3%	N.A.	195.68	
New Jersey	Flat	869.32	65.0%	66.4%	375.26	**526.48**
	Shallow Pitch (10°)	170.96	65.0%	N.A.	111.12	
	Steeper Pitch (30°)	228.46	17.55%	N.A.	40.09	

For residential buildings, buildings were categorised as shown in Table 10 based on information from the US Energy Information Administration's Residential Energy Consumption Survey (RECS).

Table 10: Characteristics of residential buildings in three states.
Adapted from (Kurdgelashvili et al, 2016, p. 295)

Characteristics	California	Arizona	New Jersey
With Attic			
Yes	17.98%	18.75%	53.85%
No	82.02%	81.25%	46.15%
With Basement			
Yes	6.74%	6.25%	57.69%
No	93.26%	93.75%	46.31%
Housing Type			
Detached	78.89%	93.75%	77.78%
Attached	10.00%	6.25%	7.41%
Appt. 2-4 units	11.11%	0.00%	14.81%
Number of			
1	78.51%	86.96%	53.33%
2	19.83%	13.04%	43.33%
3	1.65%	0.00%	3.33%

Similarly to the method for commercial rooftops potential, Access Factors of 24.3% (for Arizona and California) and 17.55% (for New Jersey) were used for single-family detached, single-family attached, and apartments with 2-4 units (Paidipati et al, 2008). The total horizontal rooftop spaces for these categories were estimated using equation [13] above. Large apartments which have similar characteristics as flat roofed commercial buildings were calculated using equation [10] above. The calculated results for residential technical PV potential can be seen in Table 11.

Table 11: Residential technical PV potential in three states.
Adapted from (Kurdgelashvili et al, 2016, p. 297)

State	Residential Category	Horizontal rooftop space (million ft^2)	PV array area (million ft^2)	PV array area (million m^2)	Technical PV potential (GW)
California	Single-Family Detached, Attached & 2-4 Unit Apts.	13,105.45	3677.29	341.63	54.66
	Large Apartments	1179.30	467.00	43.39	6.94
	Total	**14,284.75**	**4144.29**	**385.02**	**61.6**
Arizona	Single-Family Detached, Attached & 2-4 Unit Apts.	3031.96	850.74	79.04	12.65
	Large Apartments	201.17	79.66	7.40	1.18
	Total	**3233.13**	**930.41**	**86.44**	**13.83**
New Jersey	Single-Family Detached, Attached & 2-4 Unit Apts.	3590.9	727.7	67.61	10.82
	Large Apartments	245.81	105.45	9.8	1.57
	Total	**3836.71**	**833.15**	**77.40**	**12.38**

PV generation potential is different in each state due to solar resources (higher in Arizona and California) building characteristics and distribution, e.g., in California and Arizona most houses are one-floor, single-family detached units without attic and basement. New Jersey has a smaller solar resource base, but also more housing units tend to be multi-occupant and multi-storey, leading to comparatively lower solar potential, see Table 12.

Table 12: Result table for PV potential and ratio to total annual electricity consumption in three states
Adapted from (Kurdgelashvili et al, 2016, p. 298)

State	PV capacity (GW)			Potential PV generation (GWh)	Total state electricity consumption (GWh)	Ratio of PV generation to total electricity consumption
	Comm.	Res.	Total			
California	39.10	61.6	100.7	159,046.70	261,524.91	60.82%
Arizona	5.38	13.83	19.21	32,301.01	75,668.22	42.69%
New Jersey	7.83	12.38	20.21	26,363.76	74,642.40	35.32%

The next study reviewed was for the Piedmont Region, North-Western Italy, (Asinari & Bergamasco, 2011) which also assessed the available roof area usable for PV per municipality. This study used a hierarchical method, see Figure 16, by estimating the physical, geographical and technical potential of the region. The theoretical PV potential is eventually achieved by aggregating the results of the calculations carried out in the various levels. In this case the roof surface computation was based on a cartographic database of the complete region combined with coefficients to find the usable area instead of representative samples as in the previous studies.

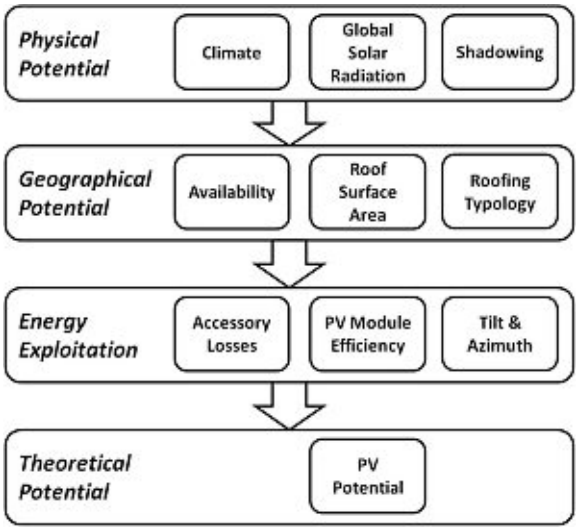

Figure 16: Hierarchical method of assessing PV potential.
Adapted from (Asinari & Bergamasco, 2011, p. 1043)

In the first step, roof areas within the region, defined by vectorised polygons in the GIS tool were filtered to ascertain the number of residential and industrial buildings per municipality and their total available roof area. These rooftop polygons are 2 dimensional outlines of the building area and contain no data on the slope of the roof pitch. For the Piedmont region, representative slopes for the pitches of residential and industrial buildings were taken as 20° and 30° respectively.

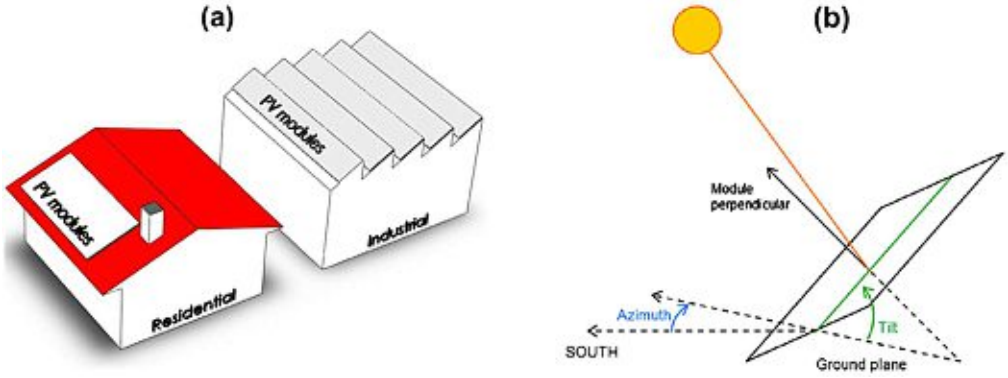

Figure 17(a): representative roof types for residential and industrial buildings in Piedmont with roof-top integrated PV installations (b) Definition of tilt and azimuth angles for PV applications
Adapted from (Asinari & Bergamasco, 2011, p. 1046)

The available roof surface is calculated using equation [14]

$$S_{roof}^{avail} = C_{RT} \cdot C_F \cdot C_{ST} \cdot C_{COV} \cdot C_{SH} \cdot \frac{S_{roof}}{\cos(\theta_{res})} \qquad [14]$$

Where:

C_{RT} is the roof-type coefficient, considered to be 0.5 as only 50% of the roof is typically exposed to the sun for residential buildings and 75% for industrial buildings as a greater percentage of industrial buildings in the area have flat roofs or.

C_F is the feature coefficient, considered to be 0.7 as only 70% of the roof on residential buildings is typically available for PV installation as the remaining space is occupied by windows, chimneys and antennas. 0.9% is taken for industrial buildings as these roofs tend to be larger and have less proportional space occupied by obstructions such as HVAC installations and chimneys.

C_{ST} is the solar thermal coefficient, considered to be 0.9 as 10% of the roof of residential houses may not be available for PV installation due to pre-existing solar-thermal installations. No allowance for existing solar-thermal installations was for industrial buildings.

C_{COV} is the covering index coefficient, considered to be 0.45 which represents the spacing necessary between modules to prevent inter-row shadowing. (Lorenzon, 1994) The same spacing is necessary for both residential and industrial buildings.

C_{SH} is the shadowing coefficient, representing the shadowing from other buildings, in residential areas considered to be 0.46 (Izquierdo et al, 2008) No shadowing is considered for industrial buildings as they tend to be located in less built-up areas.

S_{roof} is the roof surface area.

θ_{res} is the roof pitch, taken as 20° for residential and 30° industrial buildings.

A summary of the coefficients and cumulative total of all coefficients, C_{tot} can be seen in Table 13.

Table 13: Result table for PV potential and ratio to total annual electricity consumption in three states
(Asinari & Bergamasco, 2011, p. 1046)

Coefficient	Residential	Industrial
C_{RT}	0.500	0.750
C_F	0.700	0.900
C_{ST}	0.900	1.000
C_{COV}	0.450	0.450
C_{SH}	0.460	1.000
C_{tot}	0.065	0.304

In the study, the authors presented the results as a series of histograms with number of buildings and their corresponding roof surfaces, an example shown in Figure 18, are the results for the municipality of Turin, which was carried out by the authors in a second paper using the same principles in the same year. (Asinari & Bergamasco, 2011) The calculation of solar insolation values and energy output of the modelled PV systems will not be dealt with in more detail here as it follows the methods described previously for other papers.

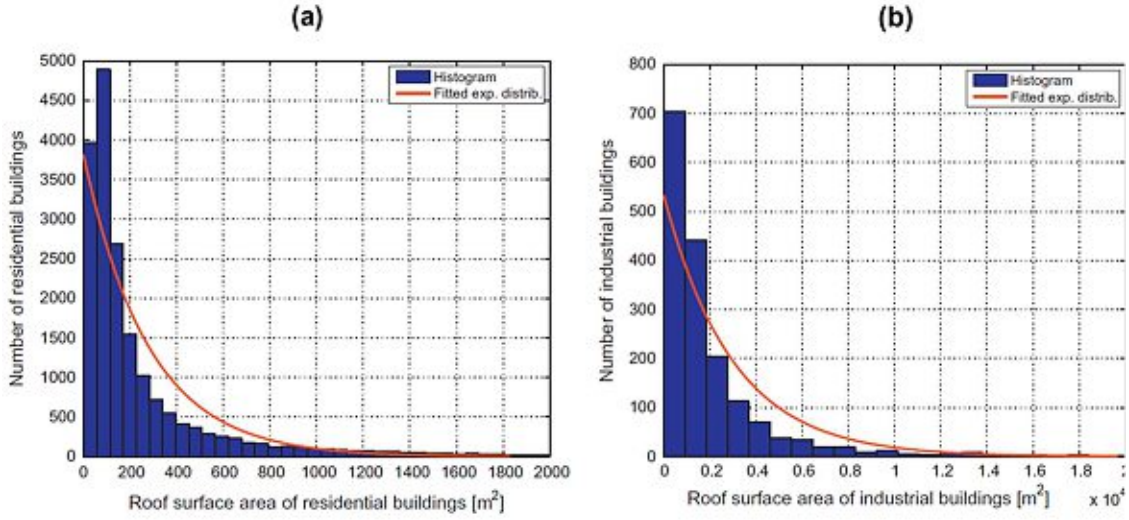

Figure 18: Histogram and fitted exponential distribution roof surface area in the municipality of Turin (a) residential buildings and (b) industrial buildings.
Adapted from (Asinari & Bergamasco, 2011, p. 1053)

The next study analyzed as part of the literature review is the first one mentioned so far which relies on GIS modeling without using statistical methods and focused on Bardejov, a small city in eastern Slovakia. (Hofierka & Kaňuk, 2009) The method used for the Bardejov study consists of three steps:

1. Creation of a 3-D city model implemented in a GIS database including creation of a digital elevation model and building models which include all properties that may affect the utilization of solar energy.
2. Modeling of solar radiation on the 3-D city model including variation in solar irradiance over a complete year using the r.sun solar radiation model. (Hofierka et al, 2007)
3. Calculation of potential electricity production using PVGIS for the area from parameters derived from the 3-D city model in the GIS database.

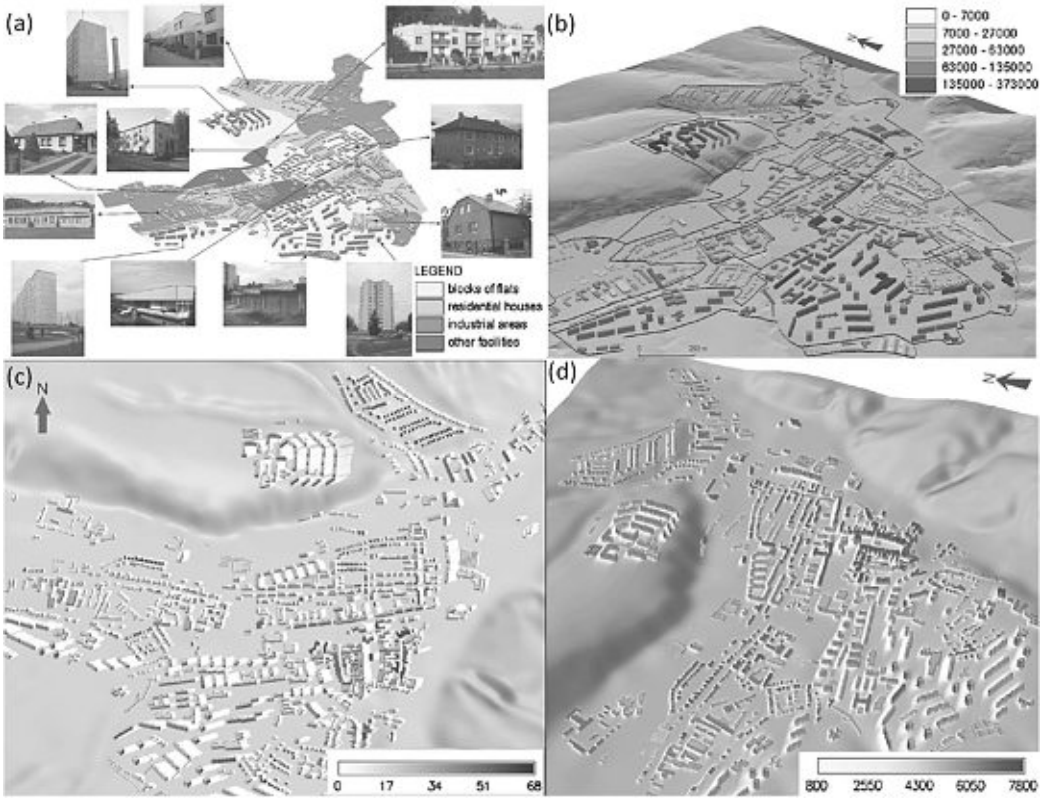

Figure 19(a): Subdivision of urban zones in Bardejov, (b) Estimated annual PV electricity production in kWh per building, (c) r.sun model for March 21, 4 PM local time incident on the 3-D city model. (d). Clear-sky irradiation [Wh/m2] simulated by r.sun for March 21.
Adapted from (Hofierka & Kaňuk, 2009, pp. 2210-2213)

In this study, the authors built a 3-D model of the complete area in question using the following steps:

- Collection of hardcopy and digital topographic, orthophoto-maps and city maps.
- Digitization of individual building footprints from available maps using GIS tools.
- Survey to ascertain each buildings construction type, height and solar-related roof attributes.
- Creation of a digital surface model (DSM) of the area including digital elevation model (DEM) and building surfaces.
- Classification of urban zones according to building construction type and utilization. see Figure 19 (a) and Table 14.

The underlying model was created with a resolution of 1m and the building outlines were digitised from the data sources mentioned using ArcView GIS. Attributes such as building height, roof type, inclination and available roof area were developed from a measurement surveying campaign using a laser distance measuring device, see Figure 19 (a), Table 14 and Table 15.

Table 14: Building attributes stored in the GIS database
(Hofierka & Kaňuk, 2009, p. 2209)

Attribute	Description
Roof type	Flat, sloped (for example, gable, shed, etc.)
Roof inclination	9 Categories with 10-degree steps
Roof orientation	8 Categories with 45-degree steps
Building height	Measured in [m] from the baseline to the building's top
Building footprint area	Measured in [m^2]
Total roof area	Measured in [m^2]
Roof area for PV	Free roof area available for installation of a PV system in [m^2]
Building functionality	Residential houses, garages, schools, multi-function buildings, etc.

Table 15: Statistical characteristics of categorised urban zones
(Hofierka & Kaňuk, 2009, p. 2210)

Urban zone	Total area [ha]	Number of buildings	Buildings footprint area [ha]
Residential houses	104.5	802	14.9
Blocks of flats	142.9	329	19.6
Industrial areas	98	253	14.1
Other facilities	28.3	60	2.7
Total	**373.7**	**1444**	**51.3**

Data from PVGIS (PVGIS, 2019) was draped over the 3-D model and the resulting PV potential estimation was draped over the surface of the buildings is shown in Figure 19(b). The r.sun module of GrassGis, mode 1, is used to develop the shadows cast by buildings and other objects for a specific time, see Figure 19(c). Using mode 2 of the r.sun module, a solar irradiation map was calculated for an entire day, March 21, with snapshots made in 15-minute intervals. The resulting shadows cast over the complete day cause lower irradiation values around the buildings, see Figure 19(d). The PV potential previously estimated from Figure 19(b) was masked using a shading model using the methods as shown in Figure 19(c) and (d) and the results presented for each urban zone in Table 16. The authors concluded that a more detailed 3-D city model should be developed which also includes the effects of foliage and that future versions of the r.sun module should include the ability to account for facade surfaces.

Table 16: Estimated PV electricity production per urban zone
(Hofierka & Kaňuk, 2009, p. 2210)

Urban zone	Total area [ha]	Buildings footprint area [ha]	Roof area for PV systems [ha]	Estimated PV electricity production [MWh/year]	Annual PV electricity production per footprint area [kWh/m²]
Residential houses	104.5	14.9	5.2	4425.216	29.7
Blocks of flats	142.9	19.6	14.7	12037.794	61.4
Industrial areas	98	14.1	8.6	7222.258	51.2
Other facilities	28.3	2.7	1.8	1462.226	54.2
Total	**373.7**	**51.3**	**30.3**	**25147.494**	**49**

The next study to be reviewed was an analysis of the solar potential of Cambridge, Massachusetts, (Jakubiec & Reinhart, 2013), where the city model was developed from a Light Detection And Ranging (LiDAR) survey of the city made in 2010. The original LiDAR data was simplified and de-speckled to remove noise (e.g. adjacent pixels with neighbouring pixels that have more than 0.3m vertical variance were removed) and the resolution down sampled to 1.25m taking the mean of overlapping data points. The data from the resulting LiDAR cloud was then categorised from lower resolution existing GIS data sets to differentiate between the buildings and local topography. An example of the processing carried out on the LiDAR and GIS data is shown in Figure 20.

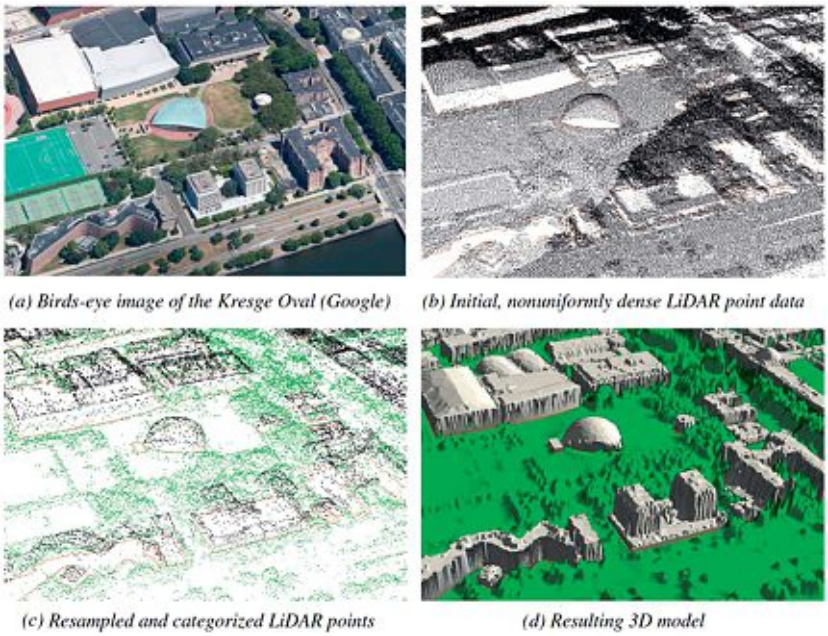

Figure 20: Process images of 3D model generation from LiDAR and GIS data.
(Jakubiec & Reinhart, 2013, p. 130)

As part of developing a new method for shade modelling the authors compared the results of their algorithm with measurements made on 2 buildings, the MIT Student Centre and a private residence. The detailed building models created using the LiDAR processing previously described can be seen in Figure 21(a) and (b).

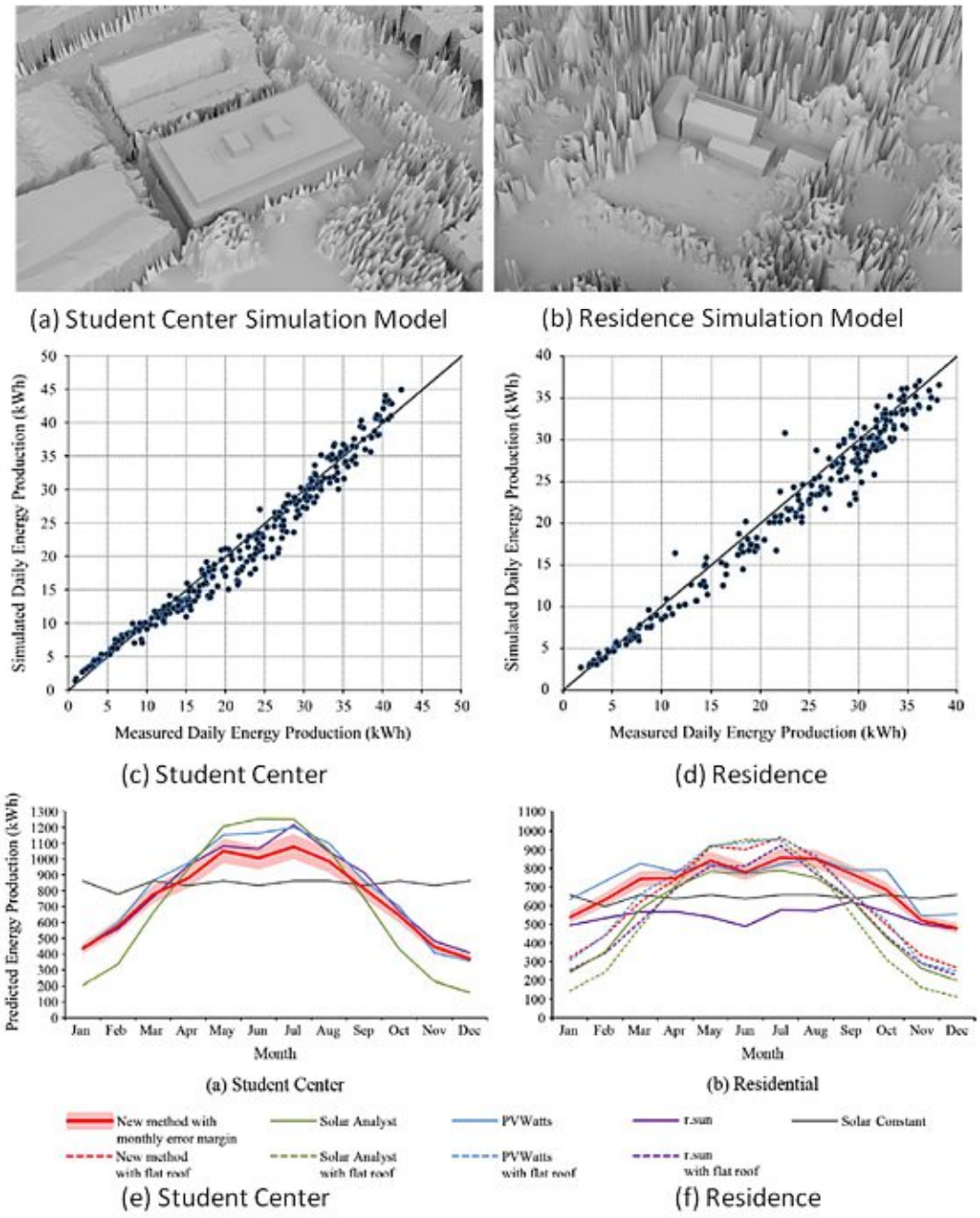

Figure 21: Detailed building simulation models in urban context of (a) Student Center and (b) Residence, Measured vs. simulated daily PV energy production of (c) Student Center (d) and Residence, Monthly comparison of typical energy prediction methods for (e) Student Center (f) and Residence.
(Jakubiec & Reinhart, 2013, pp. 134-137)

The measured daily PV energy production output of PV systems located on both of these buildings was used to validate the authors' new method of generating a shading model, see Figure 21(c) and (d). Figure 21(e) and (f) shows monthly comparisons of the predicted PV system output using the different calculation methods for both the student centre and residential PV systems respectively. The red line shows the results of the new model with the pink outline indicating the Root Mean Square Error when compared to the measured results shown in Figure 21(c) and (d). The blue line is the output of the simulated results using the PVWatts model. (National Renewable Energy Laboratory, 2020) A notable difference between the red line and the blue during summer months indicates that the PVWatts model does not account for heating of PV systems on dark rooftops. r.sun (purple line) follows the predictions of the new model for flat roofs well but also does not consider the effects of inefficiencies cause by solar panel heating in the summer months. r.sun (purple line) also under-predicted the PV systems summer output on pitched roofs. (Hofierka et al, 2007) The Solar Analyst algorithm (green line) predicts less PV output than other models during the winter. (ESRI, 2021) The examined models when applied to flat roof scenarios (dashed lines) with the exception of Solar Analyst which again underperforms, have similar monthly energy yields. From both graphs, it can also be seen that the solar constant (grey line) method, based on statistical modelling, does not track seasonal changes well.

The useful roof area and PV production from the new shading model based on LiDAR data for the whole city of Cambridge, Massachusetts is shown in Table 17.

Table 17: Useful roof area and annual PV production
(Jakubiec & Reinhart, 2013, p. 139)

Method	Useful roof area (m^2)	PV production (MW h/yr)
New method	10,949	2539
Solar Analyst	11,041	2301
R.sun	11,967	2183
Flat roof	13,279	3323
Constant value	13,336	3439

The method developed in this paper, using finer resolution LiDAR data, was used to develop the results for the Mappedwell online platform which at the time of writing, in January 2021, is available for eight US cities and three cities in Chile. (Jakubiec & Reinhart, 2013) (Mapdwell Inc, 2014) The assumptions made for the calculation of PV output based on the modelling method previously described are presented in Table 18 and a sample screenshot from the tool is shown in Figure 22.

Table 18: Mappedwell Solar System Assumed Values
(Mapdwell Inc, 2014)

Description	Value
Installed System Cost Curve	5kW, 3.71 $/watt
	30kW, 2.84 $/watt
	350kW, 2.24 $/watt
Panel Efficiency	18%, configurable
System Age	Photovoltaic degradation rate of 0.5% per year
Inverter Efficiency	Assumption is 96%, constant
Other Losses	5%, configurable
Solar Panel Size	39" x 65"
Optimum Angle (for tilted panels on flat areas)	35.0°
Panel Spacing (at optimum angle on flat areas)	77"

Figure 22: Example screenshot from Mappedwell rooftop photovoltaic potential map in Cambridge, MA
(Mapdwell Inc, 2014)

A study of the PV potential carried out for the Gangham district of South Korea (Hong et al, 2016) was of particular interest to the author due to the type of 3-D city model used. In this study, 27,774 building outline polygons were overlaid on a Digital Elevation Map (DEM) of the region and then each polygon was allocated an additive height to produce flat roofed models each building in the region shown as the blue areas of Figure 23(a). These building heights were supplied from local sources (Spatial Information Industry Promotion Institute, 2014), but did not include any surface detail beyond the averaged height of each building or building section.

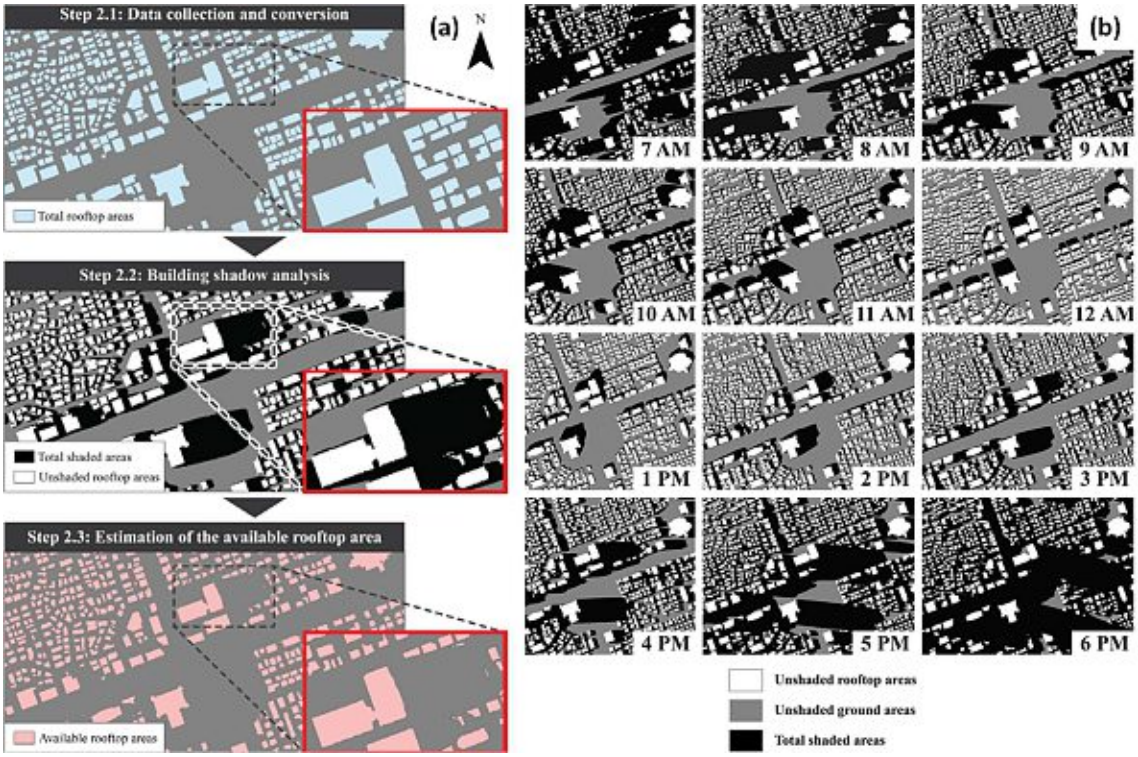

Figure 23(a) Framework for estimating the geographic potential (b) Hillshade shade analysis results by hour.
Adapted from (Hong et al, 2016, p. 3)

This method is of particular interest for this thesis as the building models used in radio network planning software are developed using the same process and are available off the shelf for many regions of the world at resolutions varying from 30m to 1m. (Advanced Topographic Development and Images, 2021) Figure 23(b) shows how the ArcGis Shading model, as previously mentioned in the summaries of several other studies, was applied to the city model at hourly intervals throughout the day. White areas indicated unshaded areas, Black indicated shadowed areas and grey areas are located outside the building outlines and are therefore not of interest. The results of these calculations were summed as shown in the second tile of Figure 23(a). These areas which remained unshaded for the entire day were categorised as available rooftop area, indicated in pink in the bottom tile of Figure 23(a). A 33 m^2 installation area was defined as the minimum for future PV installations based on local guidelines (Hong et al, 2016, p. 4) and therefore areas smaller than this were also removed from the GIS layer of available rooftop area. A further assumption of this study is that the solar PV panels are installed horizontally with no tilt on the entire rooftops.

Upon cursory inspection of the area in GoogleEarth from the author of this thesis, it was found that nearly all roofs in this area are flat and that the Hong et al analysis

method may fit well. However, it must also be noted that no margin was left for already occupied area of the rooftop (e.g. HVAC installations and Lift machinery housings), so a derating factor for this purpose as used in the Turin study (Asinari & Bergamasco, 2011) should be applied in many cases.

The authors of the Gangham study concluded that the utilised method is superior to constant value/statistical methods, several of which are previously described in this literature review (Izquierdo et al, 2008) (OECD/IEA, 2016) in terms of accuracy and reliability in that it

> "(i) considers the actual buildings' elevation in a macro scale.
>
> (ii) considers the location of the sun, which changes throughout the year, for calculating the shaded rooftop area; and
>
> (iii) considers the hourly solar radiation and hourly rooftop conditions."
>
> (Hong et al, 2016, p. 12)

A further study which was reviewed for this thesis was an evaluation of the potential rooftop solar PV in Taiwan. (Ko et al, 2015) The flow chart for the process of calculating the shading in Taiwan can be seen in Figure 24.

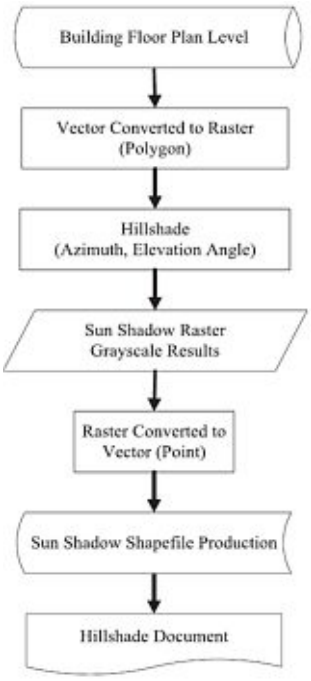

Figure 24: Shading calculation process carried out in Taiwan
(Ko et al, 2015, p. 585)

As previously described, from other studies, 1 m^2 GIS data for the region had the ArcGis Solar Analyst algorithm applied to produce shade values from the sun's hourly position during the spring equinox, summer solstice, autumn equinox, and

winter solstice of 2011. The novelty of this study was that the shading results were supplemented using binarization image theory to implement pattern recognition. Hillshade values from the ArcGis shading analysis were defined as a target object, and the resulting grayscale values under different sunlight conditions were defined to calculate the area of shadows and subsequently the area usable rooftop area. This geo-referenced data was used as a mask to remove values on a separate layer which consisted of the average annual solar radiation. This process was carried out for several representative counties in Taiwan and then the results were then applied across the complete island based on statistical methods for areas of similar ground occupancy.

Another tool for estimating solar potential, this time for the US, is Google Project Sunroof, (Google LLC, 2021) a service similar to the previously mentioned Mappedwell, which was launched in 2014. The process used by Project Sunroof is not as transparent as those published in academic papers, however the author has endeavoured to piece it together based on information disclosed on the Project web page (Google LLC, 2021) and various press releases (Google LLC, 2017) (McClendon, 2012). Project Sunroof covers portions of 50 states and Washington DC, including more than 60 million buildings. The 3D buildings models are derived from orthorectified aerial imagery with a resolution of 15cm which is refreshed annually. These aerial photos are made through a process called Photogrammetry which involves photographs of the same area being made from 2 or more angles at the same time and then the heights of each pixel are extrapolated using the differences between the perspectives of the different images, see Figure 25.

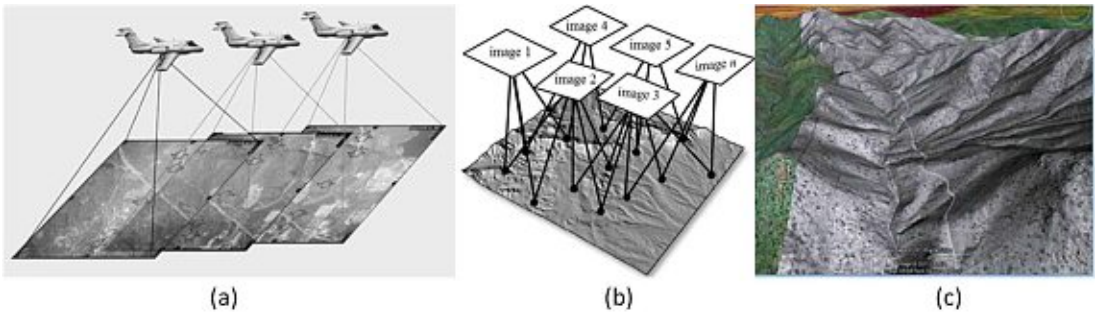

Figure 25: Aerial Photogrammetry process: (a) Aircraft takes multiple photographs simultaneously from different angles, (b) resulting images to be tiled together in an overlapping mosaic and (c) an orthorectified mosaic geometrically corrected so that it aligns with geospatial data in software such as Google Earth
Adapted from (Pan Tech World, 2016) and (Pritt, 2014)

The resulting 3-D model allows estimation of all positions of the suns path and the shading for every pixel of the roofs model. The shading model used in Project Sunroof takes all obstacles into account, including foliage, from between 100 to 150m away from each building. The 3-D models also enable the estimation of the amount of available space for solar panels, including the pitch and azimuth of each roof plane. Solar irradiance data includes “Direct Normal Irradiance (DNI- energy received directly from the sun), and Diffuse Horizontal Irradiance (DHI- received from other parts of the sky.) Shadowed regions receive no DNI.” (Google LLC, 2017) Typically, historical weather data of 10km resolution is sourced from commercial databases or NRELs’ closest weather station when that is not available. The sky is divided into a grid with a separation of 7.2° and the suns path is then modelled from 200 distinct grid points along azimuth and zenith lines to represent the suns path and the shadows it casts over one year. Available roof space is identified using machine learning and the Random Sample Consensus (RANSAC) algorithm.

Only areas which can host an array of four contiguous solar panels with a sum of at minimum 2KW are considered viable. A summary of the key assumptions and criteria of Google Project sunroof can be seen in Table 19.

Table 19: Google Project Sunroof Summary of Key Assumptions and Criteria (Google LLC, 2017)

Variable	Assumed value
Module efficiency	15.30%
Module dimensions	1.650m x 0.992m
Module power rating	250w
Panel mounting tilt	In the plane of the roof
Maximum installable pitch	60 degrees
Temperature coefficient	-0.50%
Annual power degradation	0.50%
Number of sun positions per year	~50, depending on latitude
DC to AC derate factor	0.85
Minimum subarray size	4 panels
Minimum rooftop capacity for inclusion in technical potential	2kW
Minimum sun threshold	75% of optimum in the county or city
Packing Density	1.0

In 2017 Google Project Sunroof was rolled out in Germany in partnership with E.ON. and Tetraeder, a German software development company.

(Conkling, 2017) (Google LLC, 2021)

A study on the scalability and resolution of assessment approaches for rooftop solar potential which compares the IEA methodology with more complex techniques combining varying resolutions of map data and shading models concluded that the generic IEA method varied significantly with an average absolute percent difference of 110%. (Castellanos, Sergio & Sunter, 2017, pp. 4,5) As shown in Figure 26(a) the delta between the output power using the IEA method and the previously summarised as part of this literature review, studies made in Gangham, South Korea and Bardejov, Slovakia was 115.7% and 15.2% respectively. (Hofierka & Kaňuk, 2009) (Hong et al, 2016) Note there is a misprint in the graph of Figure 26(a) and the study referenced for Bardejov, Slovakia was carried out in 2009 and not 2016 as shown in the diagram. Also, in Figure 26(a), comparing the IEA method to the Mappedwell methods applied to the cities for San Francisco and Boston resulted in a delta of 207.1% and 84.2% respectively. (Mapdwell Inc, 2014) (Jakubiec & Reinhart, 2013)

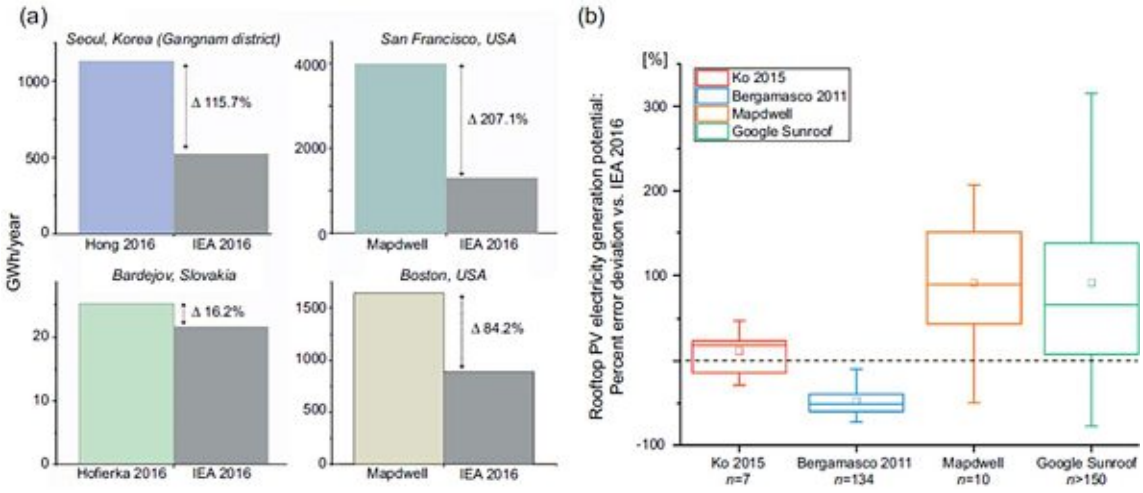

Figure 26(a): Rooftop PV electricity generation potential (GWh yr−1) comparison between selected high spatial resolution methodologies that focus on individual cities (Hong et al, 2016), (Hofierka & Kaňuk, 2009), and Mappedwell (2017): San Francisco, USA and Boston, USA) and the low spatial resolution methodology from (OECD/IEA, 2016a) (Castellanos, Sergio & Sunter, 2017)
(b) Percent error deviation between four different high resolution and low resolution methodologies involving multiple reported cities: (Ko et al, 2015), (Asinari & Bergamasco, 2011), Mappedwell (2017), and Google Project Sunroof vs. (OECD/IEA, 2016a) (Castellanos, Sergio & Sunter, 2017)

The box plots of Figure 26(b) show the 25th, 50th, and 75th percentiles of the data, with cap ends showing the 5th and 95th percentiles to exclude outliers. The square signifies the mean values while the dashed line indicates 0% error deviation against

the IEA 2016 method. The units of the plotted values are percent, with a range of -78% to 315%. (Castellanos, Sergio & Sunter, 2017)

The city of Vienna has a map of rooftop and facade solar potential available at: https://www.wien.gv.at/umweltgut/public/grafik.aspx?ThemePage=9
(ViennaGis, 2020).
The 3-D city model was made in 2013, using Airborne Laser Scanning (ALS), see Figure 27, and has a resolution of 50 cm. (Stadt Wien-Stadtvermessung, 2020) The resulting Digital Surface Model (DSM) includes the areas topography including vegetation and buildings. The solar potential analysis is based on global insolation data averaged over 18 years. (ViennaGis, 2020) The 3-D Solarpotental tool which shows the solar potential of Viennese building facades was made available in November 2016 and has been updated in March 2017 (MA 41 - Stadtvermessung, 2020), see Figure 28. The software tool used to develop both the 2-D and 3-D versions was VERTISOL. (Petrini-Monteferri et al, 2014)

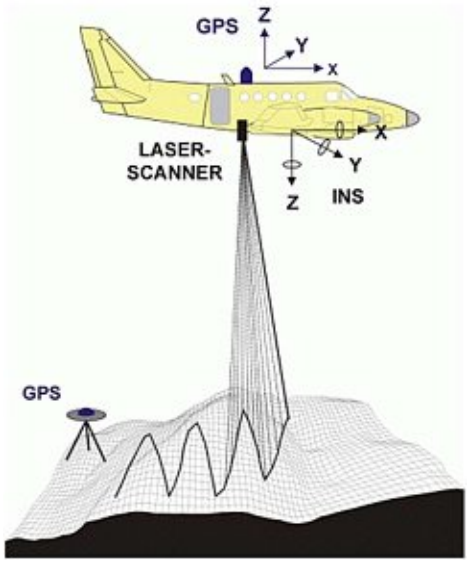

Figure 27: Airborne Laserscanning (ALS)
(Stadt Wien-Stadtvermessung, 2020)

The two colours used in the solar potential models, see Figure 28, indicate the suitability of roof/facade areas where:

Orange = very good, solar energy potential in excess of 1200 KWh/m^2 per year

Yellow = good, solar energy potential in the range of 900 to 1200 KWh/m^2 per year

Areas with a solar energy potential of less than 900 KWh/m^2 per year or less than 5 m^2 of contiguous area are not considered viable.

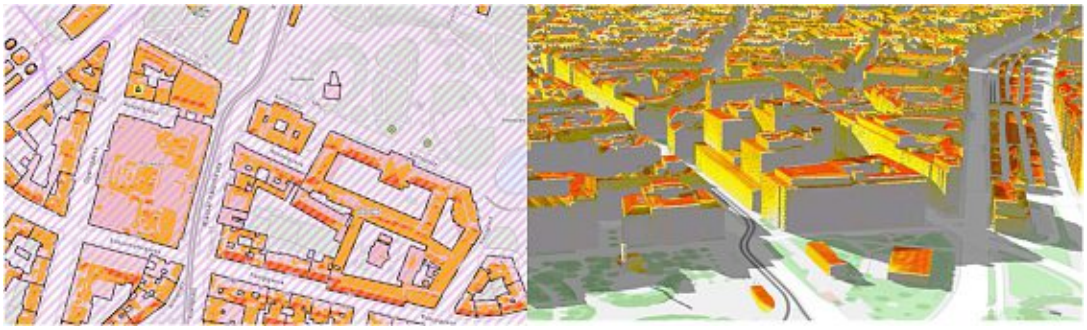

Figure 28: Extract from Wien Solarpotenzialkatastar and Solarpotenzial3D websites (ViennaGis, 2020) (MA 41 - Stadtvermessung, 2020)

A study on assessing rooftop solar potential using publicly available geodata used machine learning to develop a 3-D city model from open street map data. (Mainzer et al, 2017) (OSM Buildings, 2020) The method described utilised advanced image recognition algorithms and machine learning – methods too complex to be reproduced within a radio planning tool; however the work carried out was validated against a 3-D city model of Freiburg. (Stadt Freiburg i. Br. - Vermessungsamt, 2018) This data may be used to validate the processes and results of the methods developed after conversion to a suitable format, an extract from the 3-D city model can be seen in Figure 29.

Figure 29: Extract from Freiburg 3-D city model
(Stadt Freiburg i. Br. - Geodatenmanagement, 2018)

From the literature review, six different methods for evaluation of solar potential were identified. The first category is statistical or constant value methods where statistical methods are combined with applicable coefficients or constants. These methods are based on one or more of the following:

1. Finding the ratio of available roof surface per inhabitant within the area.

2. Determining the correlation between available roof area and population density

3. Determining available roof space derived from floor plans/building area divided by number of floors using information from land registry database or similar. This gives roof surface data (not geo-referenced) and can be combined with solar radiation values for the area.

4. Method based on a variation of the previous methods, carried out for representative subset/s of the complete area (district or municipality) and then applied to the complete target region by matching similar areas or making assumptions relative to the initial subset/s.

GIS methods may involve some of the previously mentioned steps based on data availability, however they tend to fall into the following two categories:

1. Pure GIS method: Geo-referenced surface data and geo-referenced solar radiation map are cross referenced to allow the PV production to be calculated.

2. GIS method combined with machine learning – machine learning used to either automatically find the roof surfaces for orthorectified aerial photographs or to find suitable areas within the roof surfaces for PV system installation using exact PV array dimensions.

The most popular software utilised in evaluating PV potential from the studies reviewed was ArcGis from ESRI and the opensource tools QGis and GrassGis, see Table 2.

The methods for calculating insolation factor varied only in the source of the insolation data, using either international online databases or data from more local sources. Calculation of PV system performance was very similar in all studies reviewed, with only slight variation in parameters.

Finally, it can be noted that up until approximately 2013, most of the studies reviewed utilised statistical methods with, at most, GIS tools used for pre-processing of the cartographic data to supply various inputs. Since 2017, the majority of papers reviewed have been utilising purely GIS methods with a growing trend of machine learning utilization to automatically generate roof surfaces from ortho-rectified aerial photographs, categorise roof slopes or to find spaces based on pre-defined solar array dimensions within the available roof space.

3 Description of the methodical approach

A listing of major data sources for Digital Elevation Model (DEM), LiDAR data which can be used to generate Digital Surface Models (DSM) and vector polygons or raster data which can be used to classify different geographical features has been compiled by the author in Appendix A1 (International) and A2 (National).

The data available from these different sources may need to be reprojected, scaled/resampled, interpolated and saved to specific file formats before it can be combined to carry out a solar potential assessment. Unless stated otherwise, the author has used Global Mapper v21 to perform this data conversion, as it supports over 300 proprietary and opensource data formats. (Blue Marble Geographics, 2021)

From the literature review, it was be concluded that the main GIS tools currently used for solar potential evaluation are ArcGis and QGis with GrassGis plugin, see Table 2. In order to better understand and evaluate the processes using both these tools, a worked example was carried out in both, before applying these methods to attempting to evaluate regional rooftop solar potential using a radio network planning tool. As the operations involved in these processes are CPU intensive, and calculation time will be a criterion for evaluating the ease of use for these processes, all calculations will be carried out on the same PC Hardware, specifications as follows:

Processor: Intel Xeon W-2235, 3.8 GHz, 12 core

RAM: 64 GB

Hard Disk: 2TB SSD

Operating System: Win 10

Graphics: NVIDIA Quadro RTX 4000

3.1 ArcGis

ArcGis Pro 2.7 was installed, including sample mapping for Washington, DC, USA, available from (ESRI, 2020). Using the software, ArcGIS Pro with ArcGIS Spatial Analyst extension, a tutorial from the Learn ArcGis platform was worked through. (Khanna, 2020) An overview of the process used in the tutorial, to perform an evaluation of the solar potential for can be seen in Figure 30.

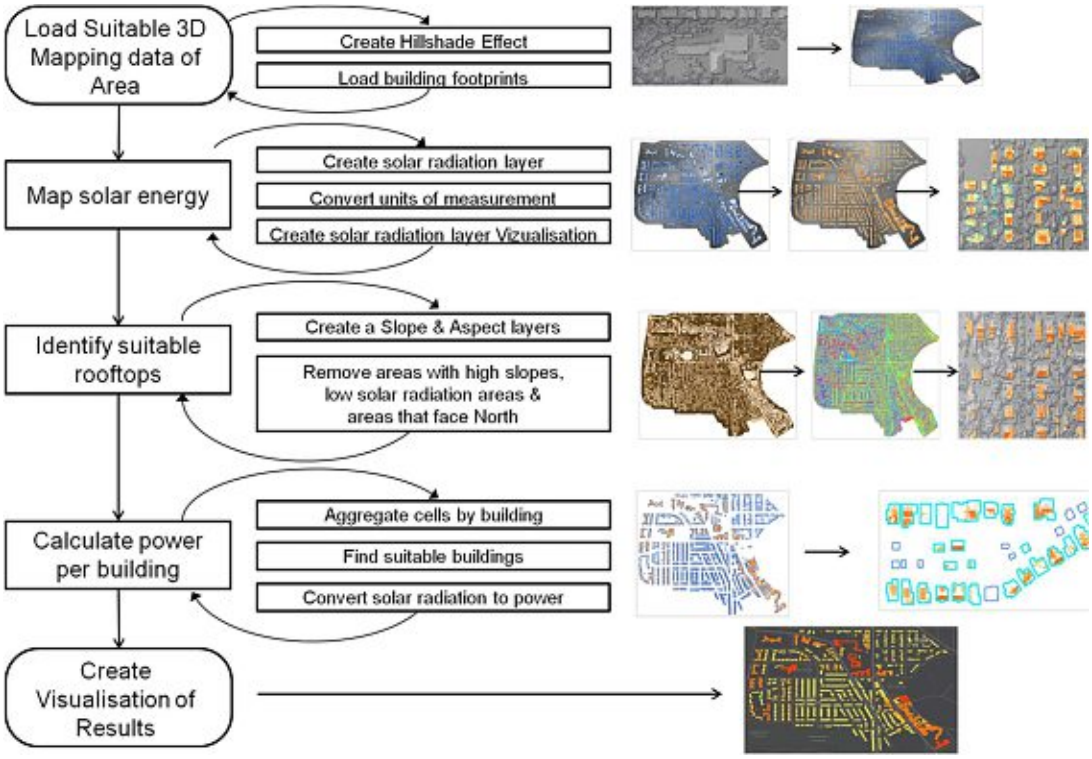

Figure 30: Overview of method to estimate rooftop solar potential using ArcGis (Authors Illustration)

In step 1, the data is loaded and a hillshade effect activated in order to get an impression of the types of buildings and vegetation in the area under analysis. As can be seen in Figure 31, the majority of buildings have flat roofs, buildings have many different orientations, some vegetation is higher than the roofs and some buildings have sloped roofs. In the next step, shown on the right side of Figure 31, building outlines (indicated in blue) were added to the project as an overlay.

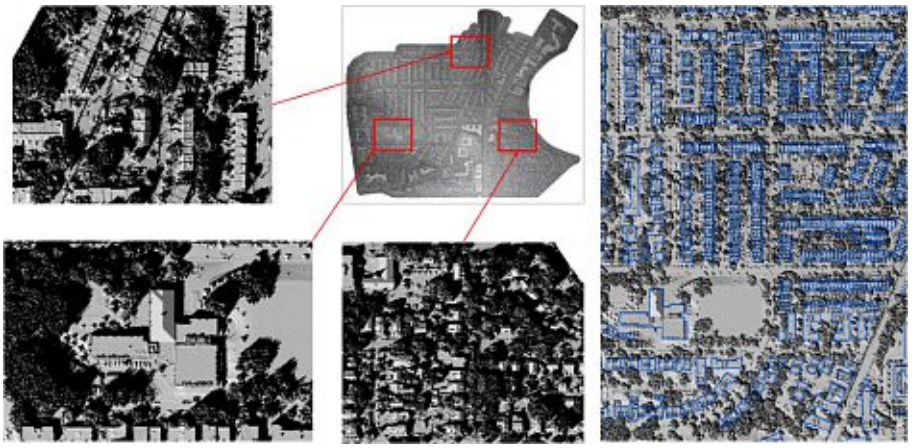

Figure 31: ArcGis Project buildings, vegetation and activated building outline layer (Authors Illustration) Screenshots from ArcGis Pro 2.7, Washington DC area

A solar radiation layer is now calculated and added to the project by calculation using the Area Solar Radiation Tool. This tool automatically calculates the latitude of the sun based on the regions location and allows for options such as specific date and time, daily, weekly, monthly or whole year averages. In this case the average solar radiance, in 16 directions, within each building outline was calculated for 2021 at hourly intervals. The result of this operation can be seen in Figure 31. It is to be noted that the area under examination is approximately 0.9 km^2, contains 1490 buildings and that this calculation took roughly 15 min to perform.

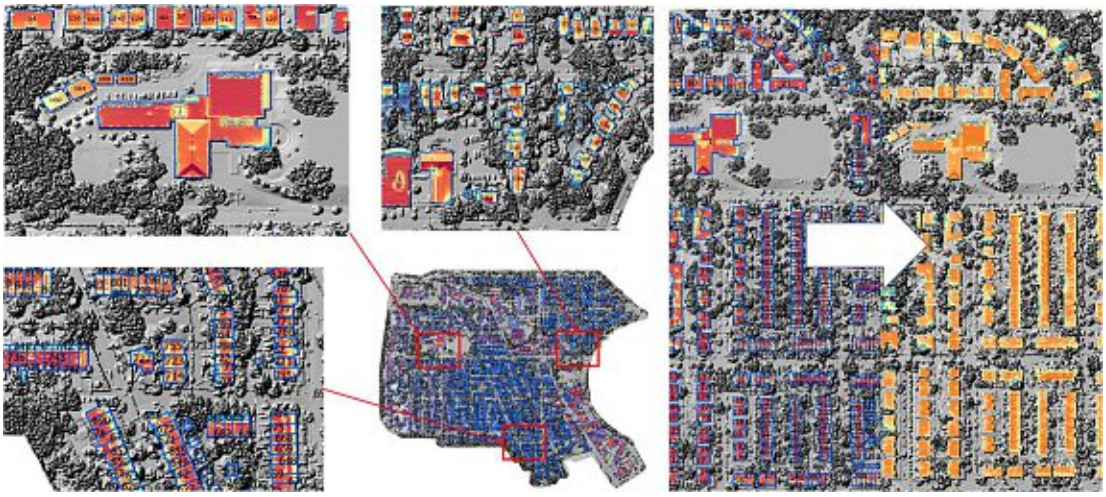

Figure 32: ArcGis Project results of Area Solar Radiation tool with results converted to and displayed in $KWhm^2$
(Authors Illustration) Screenshots from ArcGis Pro 2.7, Washington DC area

This layer displays values in Whm^2 and is converted to $KWhm^2$ by dividing all active layer values by 1000 using the raster calculator function, see left side of Figure 32. Now, having allocated a solar radiation value to each pixel on a rooftop using the building outlines for the entire area, the next step is to identify suitable rooftops for solar array installation. A suitable rooftop, for the purposes of this exercise, is defined as having:

- a slope of 45 degrees or less
- receive at least 800 kWh/m2 of solar radiation
- should not face north; area under analysis is in the northern hemisphere, and north-facing rooftops receive the least sunlight.

Using the Spacial Analysis tool, a slope and Aspect layer is created as per Figure 33, and then used to filter the solar radiation layer to remove areas which face north or have an azimuth of greater than 45°.

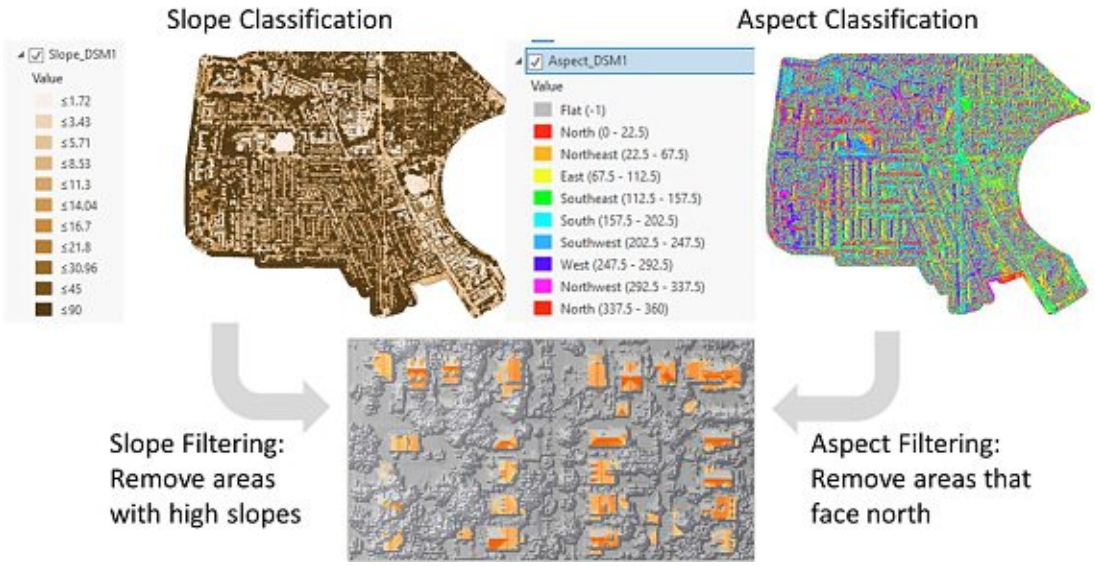

Figure 33: Slope and Aspect Filtering
(Authors Illustration) Screenshots from ArcGis Pro 2.7, Washington DC area

The slope classification layer displays all slope values on the map from 0 to 90 degrees, with darker colors indicating higher slope values. The aspect classification layer allocates colors to surfaces facing different directions in 22.5 degree steps, with grey indicating a flat surface. Both of these layers are combined and used to filter out the solar radiation layer to remove areas facing north or have a slope of less than 45 degrees. Each of these parameters can be changed in the geospatial analyst menu and needs to be setup appropriately by the user. As the last step of identifying suitable rooftops, areas with less than 800 kWh/m2 are removed. This achieved by setting up a conditional filter using the “Input conditional raster” within the Geoprocessing menu.

The next step is to calculate the power per building, given that current map shows how much solar radiation each raster cell (0.5 square meters) receives. The first step to calculate the power per building is to aggregate the raster cells on the solar layer using the Zonal Statistics as Table tool and the Buildings_Footprints layer. This generates a table where the mean value of solar energy per roof is calculated, see Table 20.

Table 20: Extract from ArcGis “Zonal Statistics as Table” results

Rowid	BUILDING_ID	COUNT	AREA	MEAN
1	39380	9276	2319	1178,644096
2	39416	6635	1658,75	1185,2639
3	39461	5686	1421,5	1204,371294
4	39489	5958	1489,5	1141,522492
5	39496	5727	1431,75	1111,957379
6	39524	5172	1293	1172,654719
7	39526	4645	1161,25	1193,94474
8	39548	4800	1200	1170,321213
9	39591	3780	945	1209,790254
10	39597	3879	969,75	1147,604858
11	39603	3466	866,5	1098,339543
12	39731	2627	656,75	1214,043129

This table is then associated with each individual building outline by the Building_ID field, those with an area of less than 30 removed, and outputted to file named Suitable_Buildings which is a new class of building outlines visible on the map, see Figure 34. After this step is completed, an attribute table is generated for the “Usable Buildings” layer each building's usable area is multiplied by its average solar radiation and converted from kilowatt-hours per square meter to megawatt-hours per square meter. This is achieved by a call to Python scripting language and performing the operation: (!solar_rad_table_AREA! * !solar_rad_table_MEAN!) / 1000.

Which results in an estimate of the yearly amount of solar radiation every building receives on areas suitable for solar panel installation.

The conversion from incident solar radiation to power is carried out in similar fashion to methods described previously where the solar panels efficiency and the system performance ratio is applied. In this example 15% efficiency and 86% performance ratio is applied based on United States Environmental Protection Agency (EPA) recommendations. (EPA, 2020)

Figure 34: Suitable buildings for Solar Array installation
(Authors Illustration) Screenshot from ArcGis Pro 2.7, Washington DC area

The final step of the process is to output the results, each building can be given a colour for the complete building footprint based on power output potential, or the usable surfaces can be kept as per previous calculation. The author feels that the usable surface results are more useful as they give an indication for each building where the solar panels should be located. A cumulative sum for the entire community of the area under analysis, in this case 21,135 MWh, is also produced, see Figure 35.

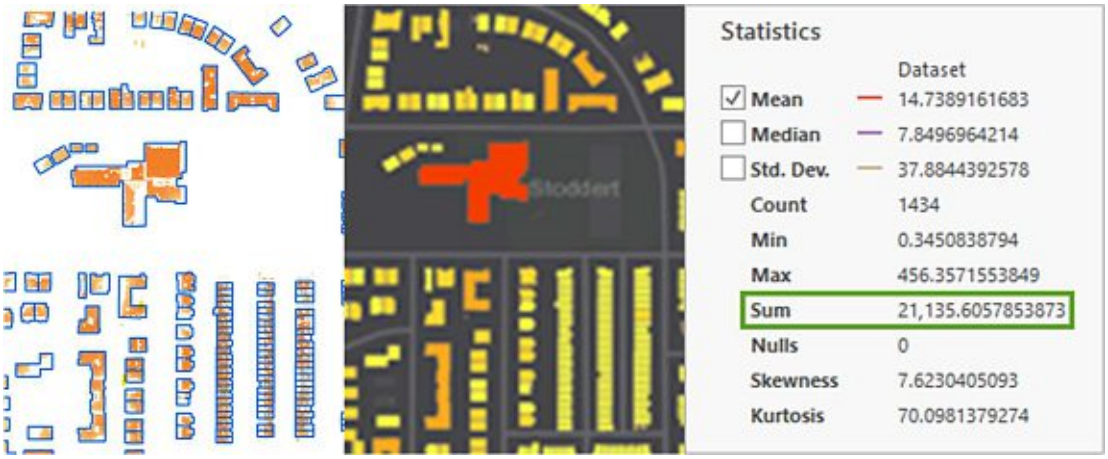

Figure 35: Extract from the final results: usable surface, potential per building, and cumulative results for complete area under analysis
(Authors Illustration) Screenshots from ArcGis Pro 2.7, Washington DC area

3.2 QGis

QGis 3.16 64 bit, latest stable release, with GrassGis 7.8.5 was downloaded and installed, including sample mapping for Gothenburg, Sweden, available from (Lindberg et al, 2018). Using the software, QGIS with Urban Multi-scale Environmental Predictor (UMEP) extension, which needs to be installed separately, a tutorial from the QGis Solar Energy on Building Envelopes (SEBE) was worked through. (Lindberg et al, 2018) The area under analysis covered approx. 0.5km2 and portions of roughly 12 to 18 building/city block outlines. An overview of the method used to estimate rooftop solar potential using QGis is shown in Figure 36.

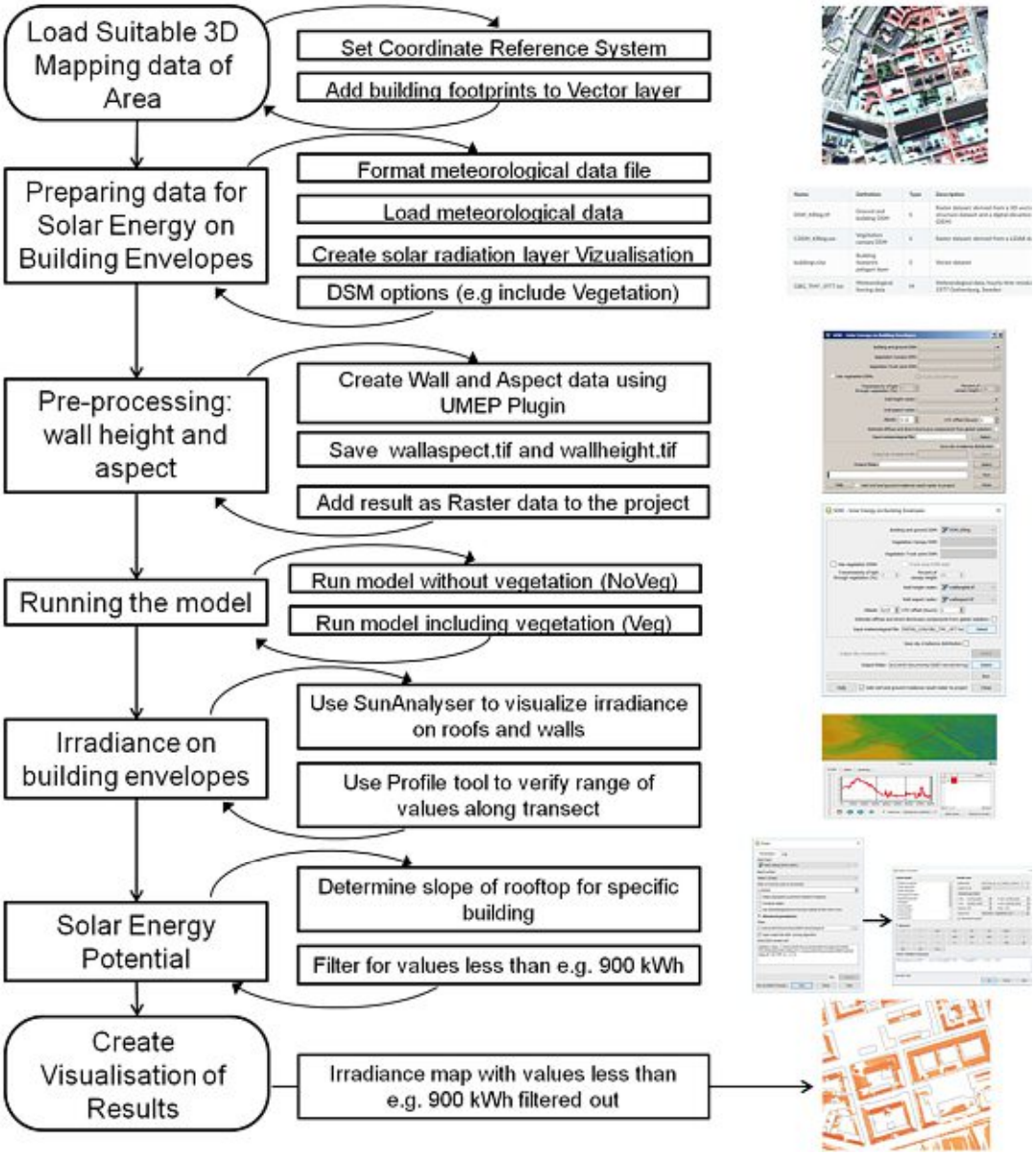

Figure 36: Overview of method to estimate rooftop solar potential using Qgis (Authors Illustration)

A list and description of the data sets required to carry out a solar potential evaluation is shown in Table 21.

Table 21: Input data and parameters required to carry out solar potential evaluation using QGis, in this case from the Gothenburg dataset.
Adapted from (Lindberg et al, 2018)

Name	Definition	Type	Description
DSM_KRbig.tif	Ground and building DSM	Spatial	Raster dataset: derived from a 3D vector roof structure dataset and a digital elevation model (DEM)
CDSM_KRbig.asc	Vegetation canopy DSM	Spatial	Raster dataset: derived from a LiDAR dataset
buildings.shp	Building footprint polygon layer	Spatial	Vector dataset
GBG_TMY_1977.txt	Meteorological forcing data	Meteorological	Meteorological data, hourly time resolution for 1977 Gothenburg, Sweden

The Gothenburg data geodata was added to the project by adding the .tif and .asc raster files to Raster Layers and the building footprint polygons to the vector layer and the appropriate coordinate reference system (CRS), EPSG:3007 for this region, was selected. The meteorological data was then (GBG_TMY_1977.txt) loaded to the SEBE plugin. The required format of the meteorological data can be found in Appendix A3. After this, the Solar Energy on Building Envelopes (SEBE) was setup, see Figure 37. The inputs for the SEBE are the meteorological file, building, ground DSM, and optionally the vegetation (trees and bushes) models. If the vegetation effects of shadowing are to be included in the simulation, two models are required, a Canopy DSM (top of the vegetation) and the Vegetation Trunk Zone (the tree trunks). The vegetation trunk zone file can be generated automatically if a Canopy DSM is present.

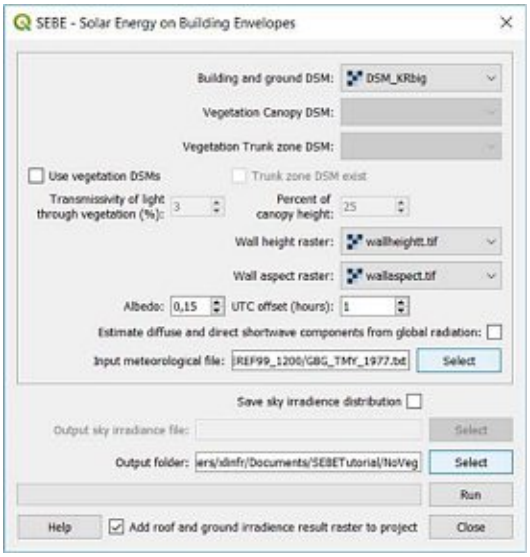

Figure 37: QGis settings for running Solar Energy on Building Envelopes (SEBE) without vegetation in Urban Multi-scale Environmental Predictor (UMEP)
(Lindberg et al, 2018)

The simulations of the model must be run twice, with and without vegetation. and the results are saved to different files which are merged consecutively to the irradiance layer. Irradiance on building walls can also be calculated by including two raster datasets, wall height and wall aspect which need to be setup as part of data pre-processing.

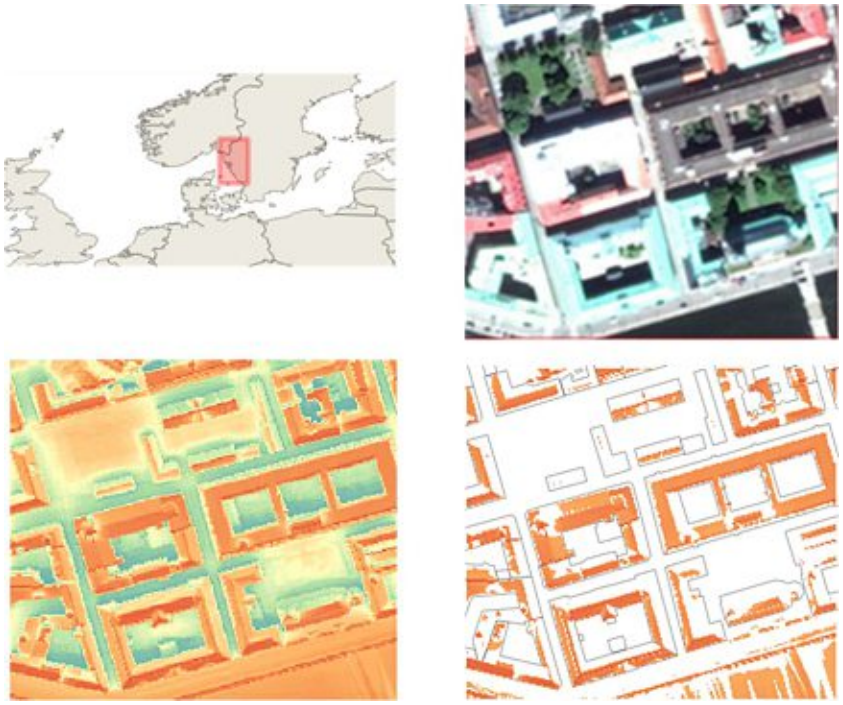

Figure 38: Steps in producing Irradiance map on building roofs in Gothenburg using QGis
(Authors Illustration) Screenshots from QGis 3.16/GrassGis 7.8.5, Gothenburg area

In order to obtain the solar energy for each building (termed Irradiance on building envelopes within the tool). The actual roof area needs to be calculated, including those surfaces which are sloped. The area of sloped roofs can be calculated using equation [15]:

$$A_A = A_P / cos(S_i) \quad [15]$$

where

A_A is the area of the sloped roof, in m^2

S_i is the slope of the raster pixel, in radians (1 degree = pi/180 radians), and

A_P : is the area of each pixel, read from the resolution of the data set in map properties e.g. in this case 1 m^2

To perform this operation on the complete data set, a slope layer is created using the DSM as the elevation layer, using the Raster-Analysis-Slope command and inputting the following formula to the Raster Calculator, Expression Window: “Energyyearroof@1” / cos (((“slope@1”<65) “ “slope@1”) * 3.141 / 180).
Note that in the ArcGis project where slopes greater than 45° where disregarded, here 65° is selected as the cut-off, as Gothenburg has a higher latitude than Washington and optimally tilted solar panels have a tilt of 65°.

In order to visualize where to locate solar arrays optimally, only areas which receive an irradiance above a certain threshold are considered to be cost effective. In this example an irradiance of above 900 kWh is taken to be minimum cut off for effective solar energy production. A custom transparency is added to the Energy/year/roof/layer by setting values between 0 and 900 to 100% transparency. This now generates a layer which is an Irradiance map displaying pixels which are equal to or greater than 900 kWh. Finally, from the Zonal statistics tool menu, the energy per square meter is selected on after calculating on the roof area raster layer (energy_per_m2_slope roof area) created while using building shape file as the polygon layer to filter as the zonal layer. Note that the performance of the solar panels needs to be calculated externally as QGis does not support this functionality.

4 Description of the research problem

Radio network planning software tools are used to calculate and assess radio coverage of telecommunications networks over defined areas, typically entire countries or regions. In this thesis it will be investigated if these tools can be repurposed to assess region-wide solar potential. A block diagram of the proposed process to be used to assess solar potential using a radio network planning software, based on research of the previously described GIS tools methodology can be seen in Figure 39. In summary, apart from creating a virtual workspace and outputting the results, the proposed process involves three main steps:

1. Loading and filtering solar potential map data into the tool and filtering this data against a database of building outlines for the region.
2. Acquiring Digital Surface Model (DSM) data of sufficient granularity to recognise the slope and azimuth of the roofs in this area and eliminate those roof areas with no visibility to the sun from the previous results.

3. Filtering this data for shadowing effects by generating shadows equivalent to the suns path over a complete year using the simulated composite power-sum coverage of several omnidirectional radio transmitters with line of sight (LOS) coverage over the complete area.

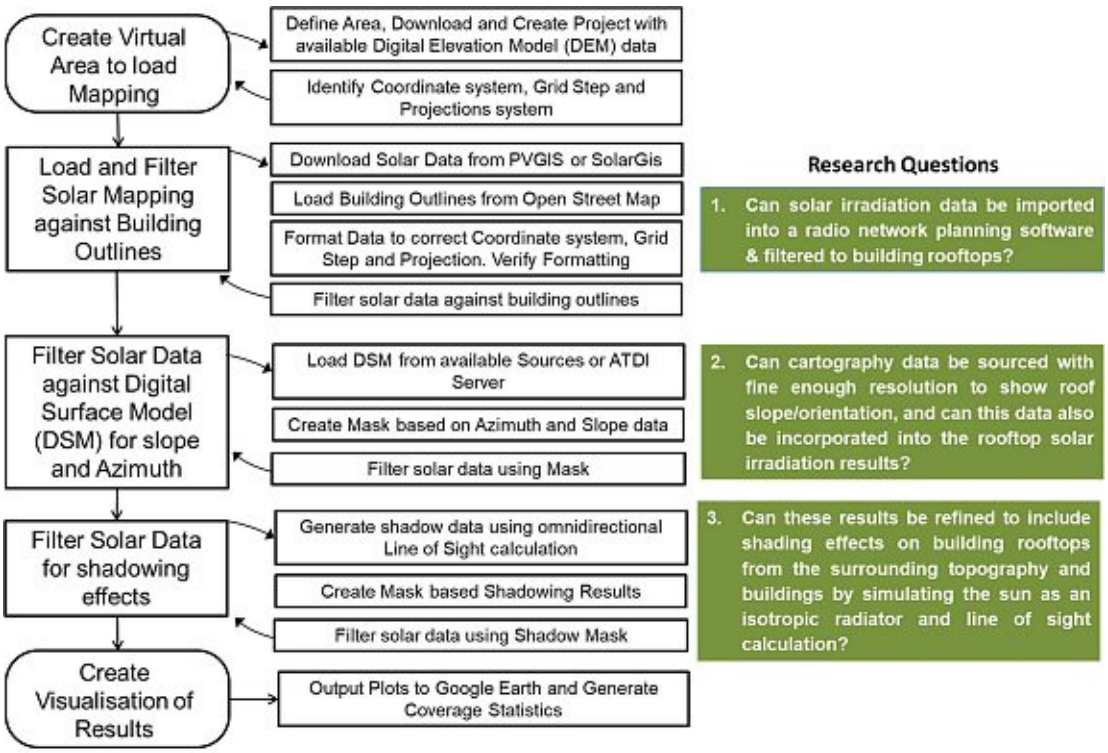

Figure 39: Proposed steps in evaluating rooftop solar potential using a Radio Network Planning tool and formulation of research questions.
(Authors Illustration)

These steps will be investigated within the framework of the following research questions:

1. Can solar irradiation data be imported into a radio network planning software & filtered to building rooftops?
2. Can cartography data be sourced with fine enough resolution to show roof slope/orientation, and can this data also be incorporated into the rooftop solar irradiation results?
3. Can these results be further refined to include shading effects on building rooftops from the surrounding topography and buildings by simulating the sun as an isotropic radiator and line of sight calculation?

As shown in Figure 39, to begin with the analysis, a virtual workspace needs to be created within the radio network planning software. The main bottleneck when evaluating the solar potential for a region using GIS methods is the availability of high-resolution cartographic data and the ability to process large areas of this data. To establish the limits of scalability of the solution under investigation, three virtual workspaces were prepared:

Macro-Level: covering a larger region, in this case a rectangular area of 3000 x 3500 km covering the majority of western Europe, with a resolution of 100m per pixel, Cartographic Projection: European Petroleum Survey Group (EPSG). See Figure 40 (a). Note that although 100m resolution would seem to be too coarse to assess solar potential, the building outline vector layer can be loaded at higher resolutions.

Regional Level: covering an entire country, in this case a rectangular area of 610 x 350 km which encloses the borders of Austria, with a resolution of 20m per pixel, Cartographic Projection: Austrian Gauss Krueger. See Figure 40 (b).

City Level: covering a complete city, in this case a rectangular area of 33.5 x 27.5 km which encloses the entire city limits of Vienna, with a resolution of 1m per pixel, Cartographic Projection: Austrian Gauss Krueger. See Figure 40 (c).

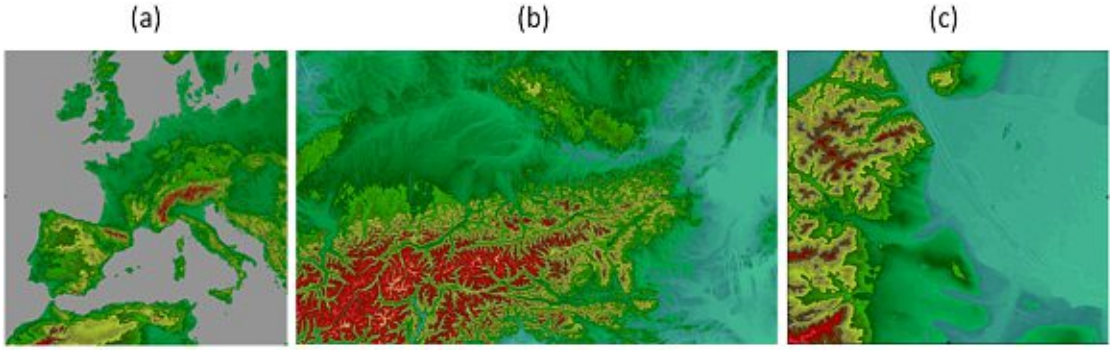

Figure 40: Virtual workspaces created for analyzing (a) Macro-Level (b) Regional Level, and (c) City Level evaluation of solar potential
(Authors Illustration) Screenshots from ATDI HTZ communications v23

1. **Can solar irradiation data be imported into a radio network planning software & filtered to building rooftops?**

Geo-referenced data on solar radiation (kWh/ m2) and the photovoltaic electricity potential (kWh) in a certain area (and for an assigned installed peak power) can be downloaded from both the Photovoltaic Geographical Information System (PVGIS) and SolarGis (SolarGis). Both sources provide daily and monthly mean values, as well as the yearly sum of solar irradiance which can be downloaded for specific regions. Building outlines as geo-referenced vectors are available for download in shape file format from Open Street Map (OSM Buildings, 2020). It is proposed to combine this data to quantify and visualize the solar irradiation of a region by combining this data as show in Figure 41.

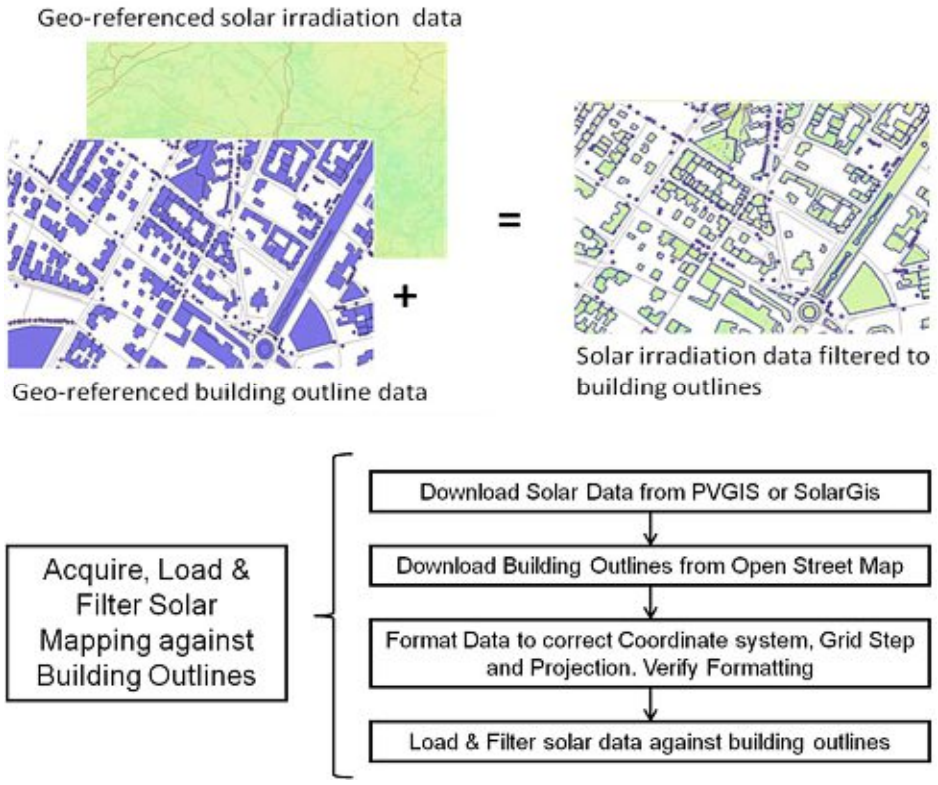

Figure 41: Concept for filtering solar irradiation data of an area using freely available Solar irradiation data and OSM building outlines.
(Authors Illustration)

The solar radiation data set containing the "Yearly average global irradiance on an optimally inclined surface (W/m2)," was downloaded from PVGIS (European Commission's Joint Research Centre, 2020). This data was imported to Global Mapper (Blue Marble Geographics, 2021) and converted to ATDIs' Coverage layer format, *.FLD, using the ATDI Global Mapper Plugin, see Figure 42.

Figure 42: Start-up screens from Global Mapper equipped with the ATDI plugin and ATDI HTZ Communications, Radio Network Planning Software
(Advanced Topographic Development and Images, 2021) (Blue Marble Geographics, 2021)

Using the macro level workspace, shown in Figure 43 (a), the Yearly average global irradiance on an optimally inclined surface (W/m2), was loaded as a coverage file overlaid on this DEM, see Figure 43 (b).

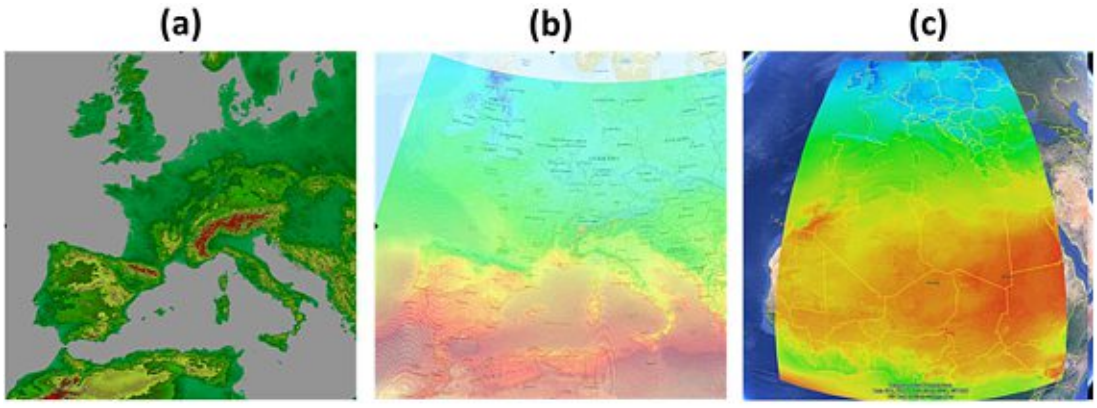

Figure 43: Virtual workspace loaded with (a) DEM of Western Europe, (b) Irradiation data overlaid as coverage layer in the radio planning tool and (c) Irradiation layer exported to Google Earth for verification
(Authors Illustration) Screenshots from ATDI HTZ communications v23 & Google Earth (Advanced Topographic Development and Images, 2021) (Google LLC, 2021)

In order to verify the data import, the data was immediately exported to google earth, see Figure 43 (c) and verified by spot checking the colour codes at various locations against the values on the PVGIS online map database, which shows that the data import to the tool was successful.

It must be noted that during this process, which took approximately six hours to complete, the software was unstable and crashed several times during the verifications process. For practical purposes this means that although the irradiation data for a large part of Western Europe could be successfully converted, imported, and saved, it is not possible to work at this level to carry out a meaningful analysis on such a large area.

At this stage, the irradiation data within the radio planning tool has no meaning, and is only a representative set of colour codes, allocated to each pixel of the map data. By cross-checking against the data on the PVGis website, the colour data was scaled from 256 colours to 12 for usability, and a scale/colour palette representative of kWh/m2 was setup, see Figure 44.

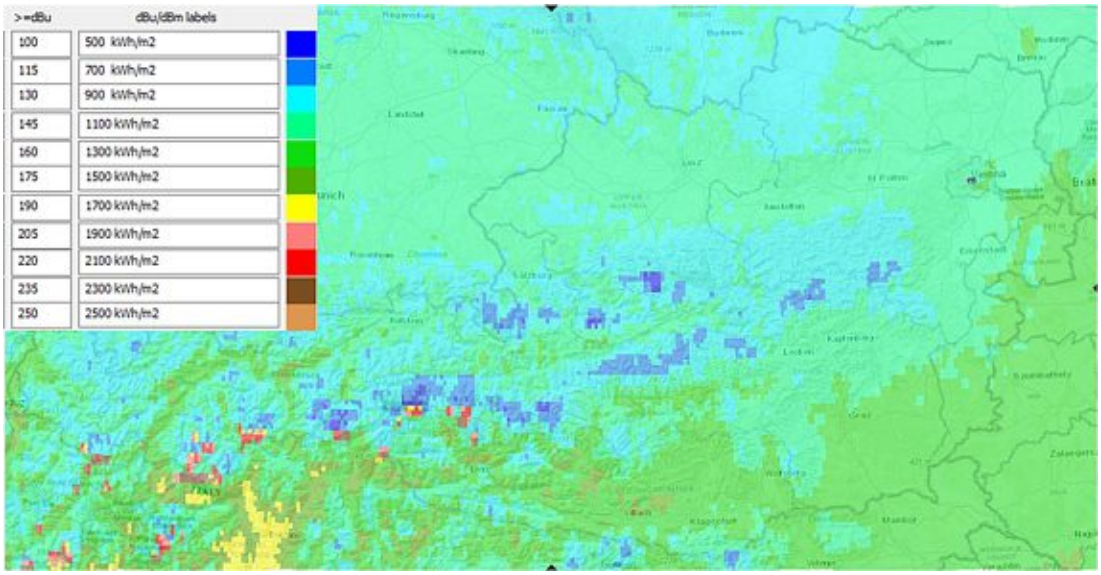

Figure 44: Twelve colour palette representing kWh/m2 set in the radio planning tool (Authors Illustration) Screenshot from ATDI HTZ communications v23

OSM data (OSM Buildings, 2020) for building polygons was now loaded as a vector layer into the radio planning tool, see

Figure 45. Although the statistics office of Austria indicated that there are approx. 2.2 million buildings in Austria as of 2011 (STATISTIK AUSTRIA, 2013), the building outline database contains over 15 million polygons which also include voids within

buildings as well as structures which do not qualify as buildings by the Austrian census offices criteria.

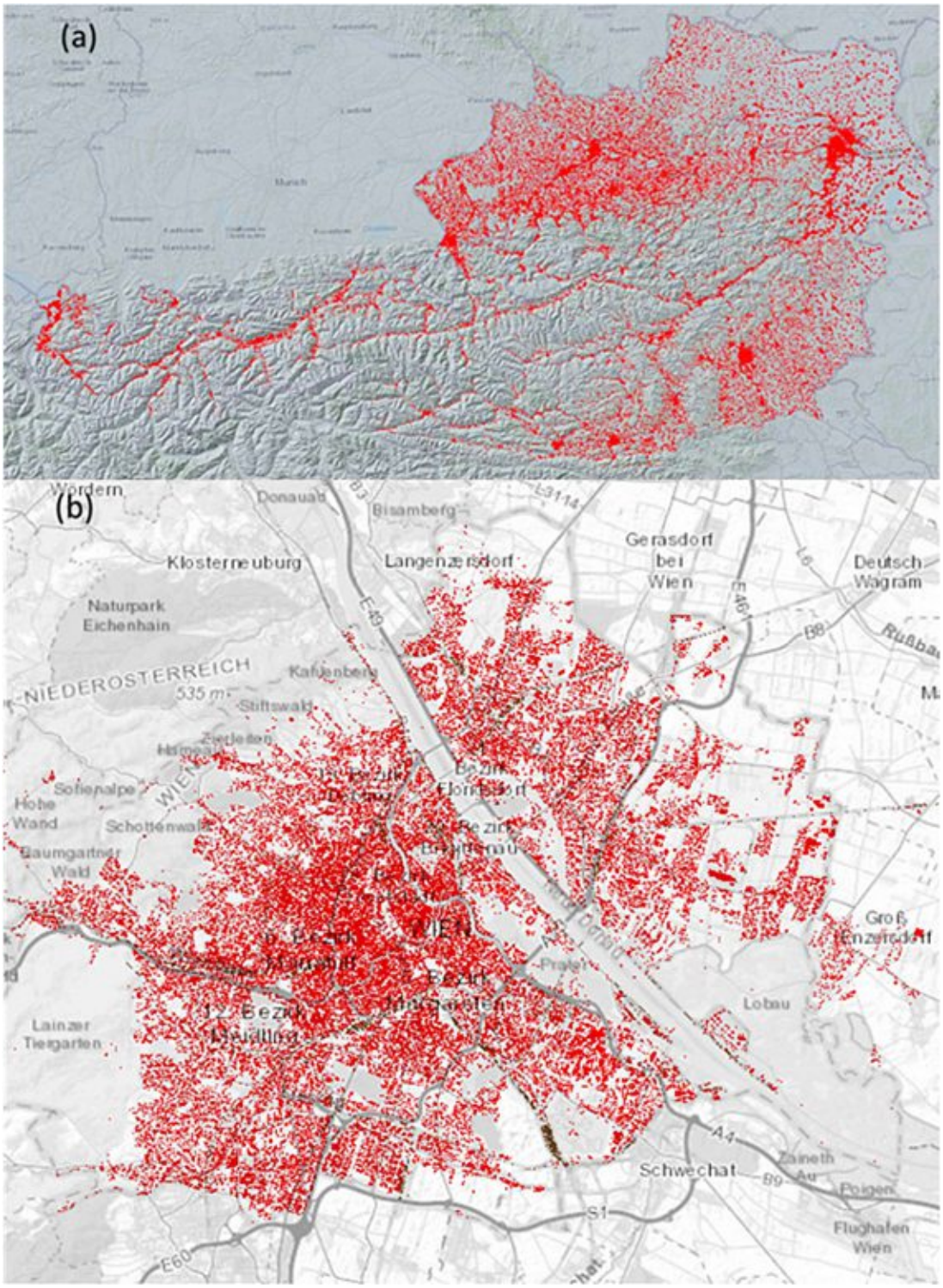

Figure 45: OSM Building outlines for (a) Austria and (b) Vienna loaded into the Regional and City Level virtual workspaces
(Authors Illustration) Screenshots from ATDI HTZ communications v23, (OSM Buildings, 2020)

When importing the vector polygons, a 1:1 ratio, i.e., 20m was initially selected, as this is the resolution of the underlying DEM for the Austrian data set. This led to many sampling errors, see Figure 46, so the import was repeated, iteratively increasing resolution until 0.3m was selected, where sampling errors were observed to be insignificant when compared to aerial photography of the area.

Figure 46: Sampling errors when importing building outline polygons at (a) 20m and (b) 0.3m resolution
(Authors Illustration) Screenshots from ATDI HTZ communications v23, Vienna Area

This vector layer was then converted to a raster layer for both the Austria and Vienna map set and used as a filter to give the percentage of the whole area, and area in km2 of the cumulative area of building outline polygons covered. These results are presented in Table 22 and Table 23, section five of this document.

Note that the output of this process gives total rooftop solar irradiated area and irradiated intensity for the region under examination but can only be used as an upper limit for estimation this potential as it does not account for roof slope and shading from e.g., topography, foliage, and buildings.

2. Can cartography data be sourced with fine enough resolution to show roof slope/orientation, and can this data also be incorporated into the rooftop solar irradiation results?

Data sets with resolution as fine as 1m can be sourced for radio planning which is the same resolution as the ArcGis and QGis examples worked through previously in section 3.1 and 3.2 of this document. This would suggest that this data can be used to evaluate rooftop solar potential. A 2D and 3D screenshot of a 1 m data set for Vienna which has been developed for radio planning can be seen in Figure 47.

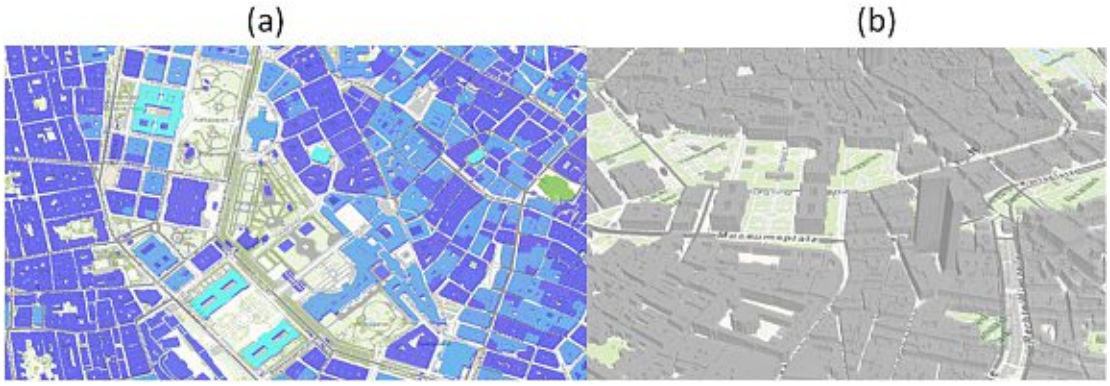

Figure 47: (a) 2D and (b) 3D screenshot of a 1 m data set for Vienna used for radio network planning
(Authors Illustration) Screenshots from ATDI HTZ communications v23, Vienna Area

As radio network planning is primarily concerned with coverage on ground level, roof geometry typically plays only a small role, in simulating radio coverage, see Figure 48. For that reason, roof slope and orientation data, even when available, is discarded when preparing mapping data for radio planning, with buildings being represented as one, or several polygons with a uniform height for the entire polygon. This can be observed in Figure 47 (a) where each buildings height is represented by a single colour, or in Figure 47 (b) where all buildings can be seen to have been modelled with flat roofs.

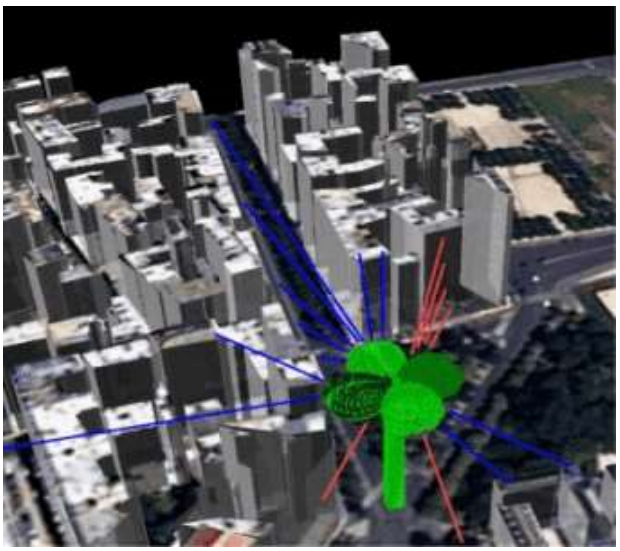

Figure 48: Typically, radio network planning is primarily concerned with coverage on ground level and neglects roof geometry
(Software Informer, 2021)

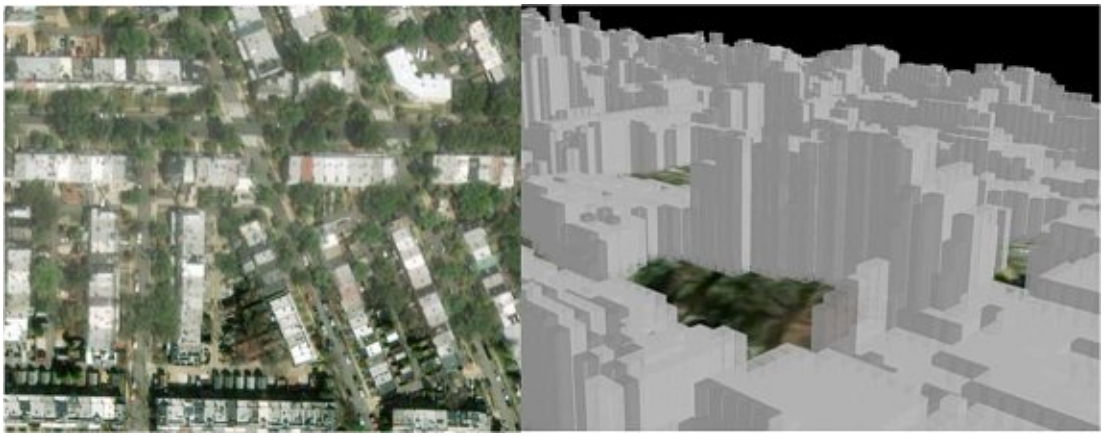

Figure 49: Section of Washington DC mapping imported to radio planning tool (Authors Illustration) Screenshot from ATDI HTZ communications v23, Vienna area

In order to test the possibility of retaining altitude granularity when creating building layer data for import into the radio planning tool, the mapping data previously used in the ArcGis example for assessing solar potential in Glover Park, Washington DC was processed using Global Mapper with the ATDI plugin. As can be seen in Figure 49:

- It is possible to have multiple altitudes within one building polygon.
- Granularity is limited to the pixel resolution of the underlying DEM data (1m in this case)
- Each pixel can only hold the information for one discrete altitude, it is not possible to have a pixel which has a different altitude on one side than another, i.e. containing slope data.

This demonstrates that even when it is possible to source cartography data sets with fine enough resolution to show roof slope/orientation, this data cannot be imported into the radio planning tool without loss of fidelity (all slope data is lost).

3. **Can these results be refined to include shading effects on building rooftops from the surrounding topography and buildings by simulating the sun as an isotropic radiator and line of sight calculation?**

In order to generate a shadow model, as a proof of concept, two radio transmitters with omnidirectional antennas were set up on the extreme south of the virtual workspace, which are representative of the position of the noonday sun in winter and summer. As a target point to generate the shadow model, a point near the city centre of Vienna city virtual workspace was chosen, near the entrance St. Stephen's Cathedral. The angle of the sun or declination, for its minimum and maximum during

winter and summer, to this point was found by using an online calculator (Hoffmann, 2015), see Figure 50.

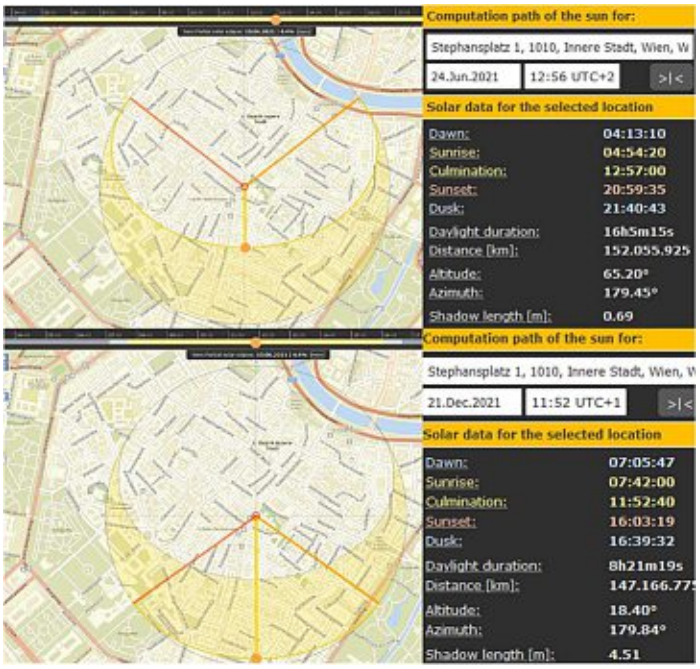

Figure 50: Calculation of suns maximum and minimum declination at midday to entrance of St. Stephens Cathedral in 2021
(Hoffmann, 2015)

As shown in Figure 50, the declination was found to be 65.2° in the summer (24th June 2021) and 18.4° in the winter (21st December 2021). The distance from the target point to the southern edge of the virtual workspace is 12.47 km, which together with the angles found in Figure 50 allows the height of the transmitters used to simulate the suns coverage to be calculated as shown in Figure 51.

A Line of Sight (LOS) model was then used, to simulate the transmitters coverage, representing sunlight with the intention of replicating the shadows caused by buildings and topography. The composite power-sum coverage from both these transmitters is the inverse of the suns shadowing for these 2 positions, see Figure 52. Although only two positions are considered due to time limitations, this process demonstrates that the suns shadowing can be approximately modelled using this method.

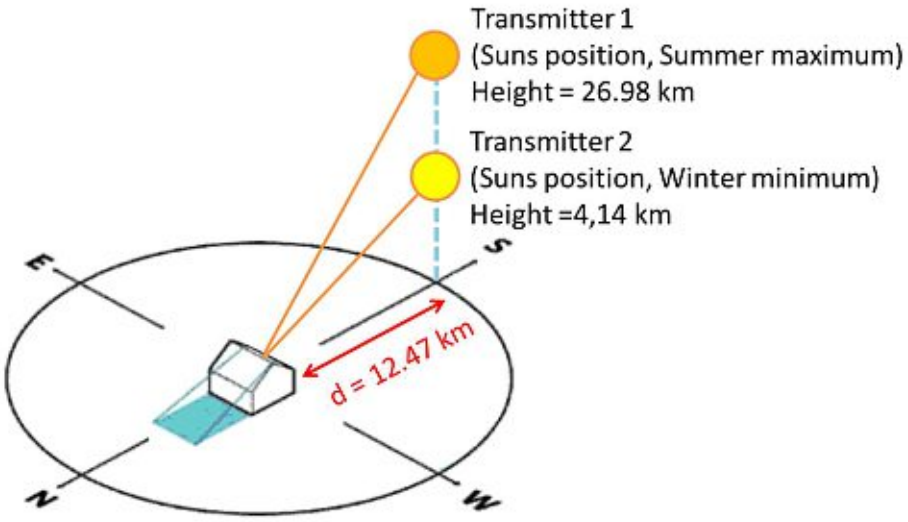

Figure 51: Heights of transmitters used to represent the suns position for summer maximum and winter minimum
Adapted from (Scheckel, 2013, p. 87)

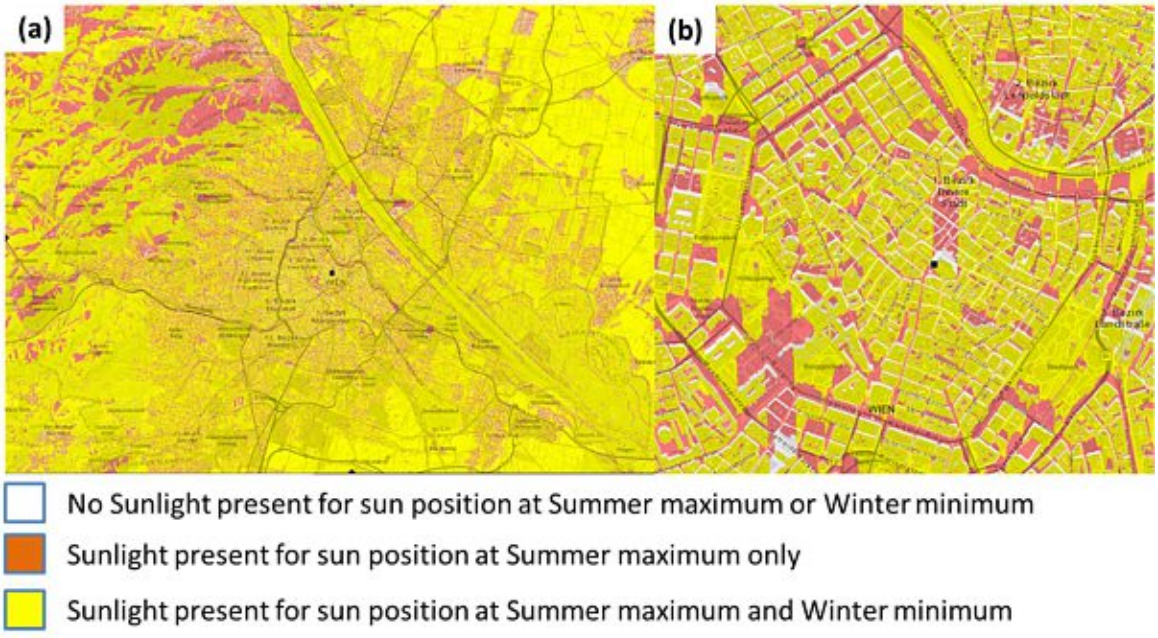

Figure 52: Simulated composite coverage of 2 transmitters located in the south of the virtual workspace as described for (a) complete Vienna Area, (b) inner city (Authors Illustration) Screenshots from ATDI HTZ communications v23, Vienna Area

5 Presentation of the results

In response to the first research question, solar irradiation data can be imported into a radio network planning software & filtered to building rooftops. The solar radiation data was successfully downloaded from PVGIS and imported onto a cartographic set in a macro (Western Europe), Regional (Austria) and city wide (Vienna) virtual workspace. The macro data set approached the memory limitations of the software/PC used to carry out the import and caused the software to crash often, therefore it was not possible to complete the next step, filtering to rooftop polygons, for the macro dataset. Importing the rooftop vector polygons from Open Street Map as a filter to the solar data was possible but using a 1:1 sampling ratio, i.e., 20m for the underlying DEM for the Austrian data set led to many sampling errors, see Figure 46. The import was repeated, iteratively increasing resolution until 0.3m was selected, where sampling errors were observed to be insignificant when compared to aerial photography of the area. Results for the solar irradiation data filtered to rooftop polygons can be seen in Table 22 and Table 23.

Table 22: Results of filtering PVGis irradiation data, Yearly average global irradiance on an optimally inclined surface, to OSM building outline polygons for Vienna

Threshold (KWh/m2 per year)	Vienna	
	Building Outline Polygons Covered (%)	Building Outline Polygons Covered (km2)
900	99.9985	93.22
1000	99.9985	93.22
1100	99.9985	93.22
1200	97.3049	90.709
1300	17.2607	16.091

Table 23: Results of filtering PVGis irradiation data, Yearly average global irradiance on an optimally inclined surface, to OSM building outline polygons for Austria

Threshold (KWh/m2 per year)	Austria	
	Building Outline Polygons Covered (%)	Building Outline Polygons Covered (km2)
900	98.4479	2348.4
1000	94.8155	2261.8
1100	83.4597	1990.9
1200	49.4576	1179.8
1300	24.7743	590.98
1500	0.9800	23.378
1700	0.0808	1.9286

In response to the second research question, it was found that suitable map data can be sourced with resolution sufficient to discern roof slope and orientation, see Appendix 1 and 2 for sources, however the radio planning software is incapable of processing this information and roof slope data is discarded during the pre-processing of the raw cartography data for use within the radio planning tool. This makes the radio planning tool unsuitable for assessment of regionwide rooftop solar potential evaluation.

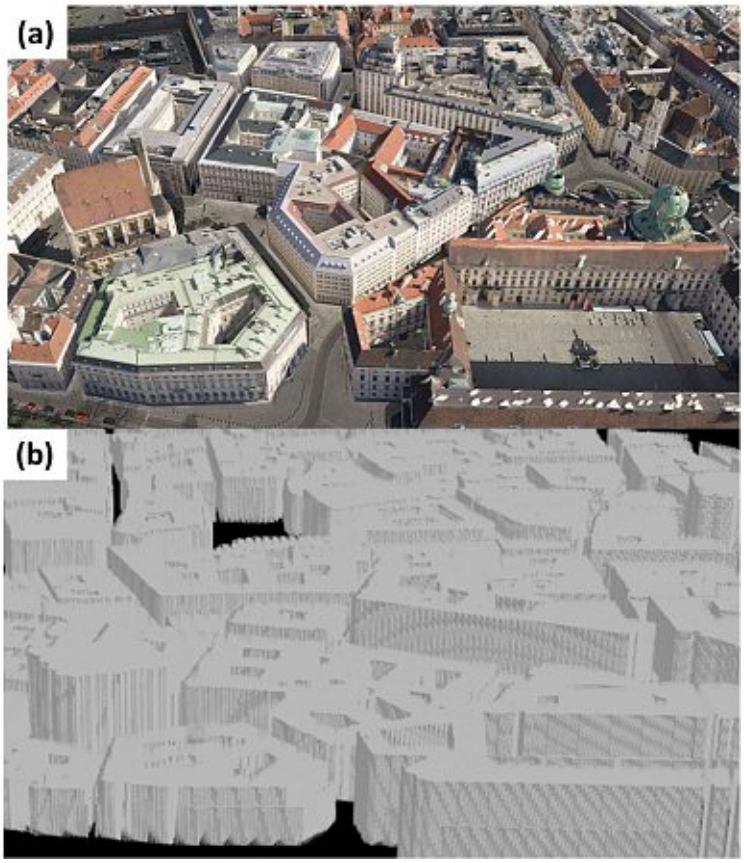

Figure 53: 3D view near the Presidential Chancellery, Vienna using (a) Google Earth, (b) Radio network planning tool
(Google LLC, 2021) (Advanced Topographic Development and Images, 2021) (Authors Illustration)

In response to the third research question, the parallax effect determines that simulating the suns position using an isotropic radiator within the radio planning tool is only possible over small areas, see Figure 54 and Figure 55.

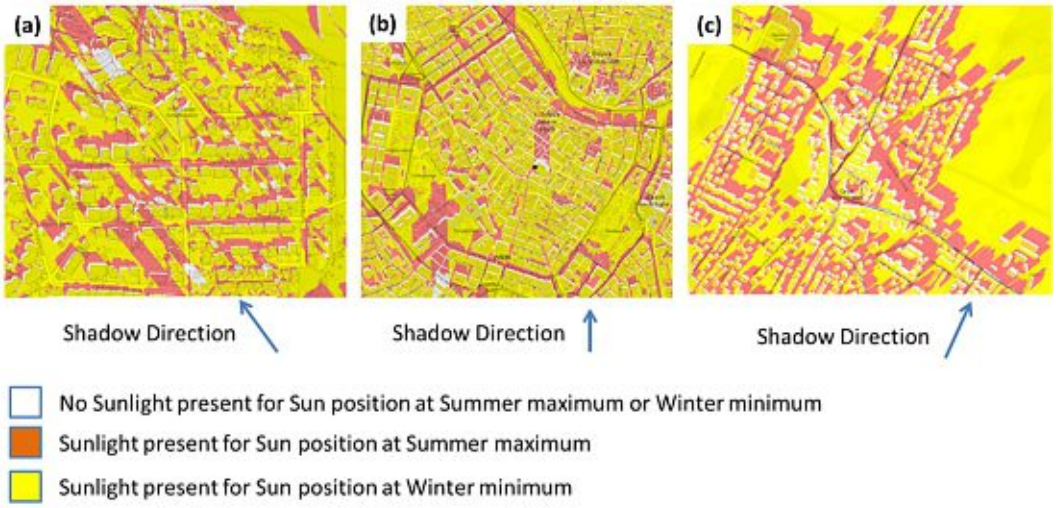

Figure 54: Coverage of 2 transmitters located in the south of the virtual workspace on (a) east of Vienna, (b) inner city and (c) west of Vienna in radio planning tool (Authors Illustration) Screenshots from ATDI HTZ communications v23, Vienna Area

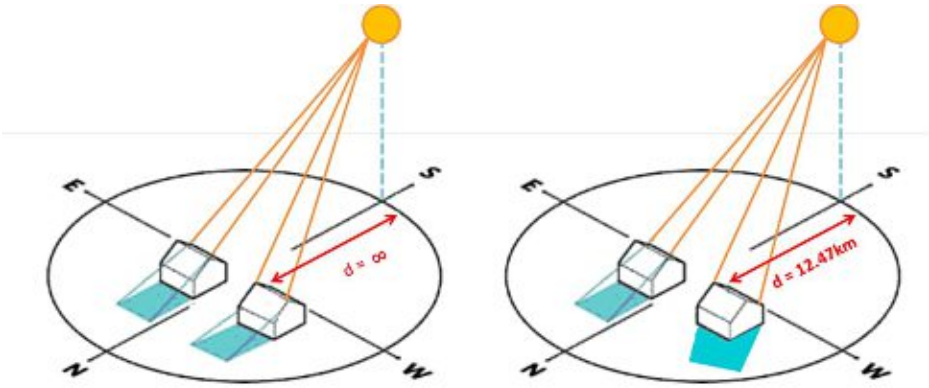

Figure 55: Parallax effect makes it impossible to generate an accurate shadow model of the suns position within the virtual workspace over a larger area
Adapted from (Scheckel, 2013, p. 87)

The parallax effect determines that positioning an omnidirectional isotropic radiator inside the virtual workspace makes it impossible to generate an accurate shadow model of the suns position over the entire area. Spot checks were made against the online sun/shadow calculator (Hoffmann, 2015) using this method for the Vienna data (33.5 x 27.5 km, 1m resolution) with sun position modeled at the extreme south of the virtual workspace, directly south (12.47km) from St. Stephens Cathedral. It was determined that the proposed solution loses accuracy within approximately 300m of the target point.

6 Conclusion

An IEA report concluded “that worldwide, cities with a population of ≥1.6 million account for only 25% of the potential rooftop solar PV generation in 2050 and that policies for realizing RTSPV potential need to focus on small cities. The IEA also report also notes that exactly these cities are often, “least prepared for implementing RTSPV, due to lack of data, limited resources, expertise, and constrained governance capacities. Regional or national governments can play a critical role in closing these gaps.” (OECD/IEA, 2016, p. 7)”

From the literature review in section two, studies on assessing RTSPV made in the period from 1992 to 2016, were found to have employed methods which have been predominantly statistical in nature, with only some methods taking GIS data as initial inputs. In more recent years, the majority of papers are based solely on GIS methods. Due to the nature of the GIS methodology, the major bottleneck to the widespread availability of rooftop solar potential mapping is the acquisition and processing of the orthorectified aerial photography, LiDAR or LRS cartographic data necessary for carrying out such studies on a national scale. The exception to this is Googles Project Sunroof which has dedicated massive mapping and processing resources to evaluating many areas in the US and to some extent Germany. Additionally, from the literature review, it can be seen that the software capabilities for processing data, once available, have evolved dramatically, with later methods employing machine learning to locate suitable positions for solar arrays on individual rooftops on a city-wide scale. The literature review also concluded that apart from custom written softwares or modelling scripts, the most popular GIS tools for this application are either ArcGis (Proprietary) or a QGIS/GrassGis (Open Source) combination.

To aid in the definition of a method of approach in section 3 and to better understand the processes involved, modelling exercises were carried out using tutorials and data for ArcGis and QGIS/GrassGis. Both processes were broken down to their component steps and flowcharted as illustrated in Figure 30 and Figure 36.

In section 4, a process was developed to allow the modelling and evaluation of regionwide rooftop solar potential within a radio network planning software. The concept begins with the premise that solar radiation data, once imported into the radio network planning tool, can be manipulated by filtering for building outlines and

adding successive masks for roof slope, azimuth and shading. The following research questions were developed to explore these areas, and a summary of the corresponding findings are given below.

1. Can solar irradiation data be imported into a radio network planning software & filtered to building rooftops?

Solar radiation data can be filtered to building outlines (for most practical purposes this is essentially the same as rooftop area) and quantified on a national scale and city-wide scale. Furthermore, it was found that import of solar data onto a macro virtual workspace for western Europe using a 100m resolution data set led to instabilities in the software which made further processing impossible, and further analysis on the macro level was discontinued. The cumulative results of filtering the solar radiation data against OSM building outlines for Vienna and Austria has been tabulated in Table 22 and Table 23. The IEA study has noted that it is not only important to be able to quantify rooftop solar potential, but also to be able to visualise the results. (OECD/IEA, 2016a) This can be achieved by exporting the results of the PVGis irradiation data filtered to OSM building outlines to google earth, see Figure 56. It should be noted that this visualisation data can be misleading as it presupposes that the building is unshaded from the surroundings and has a flat roof.

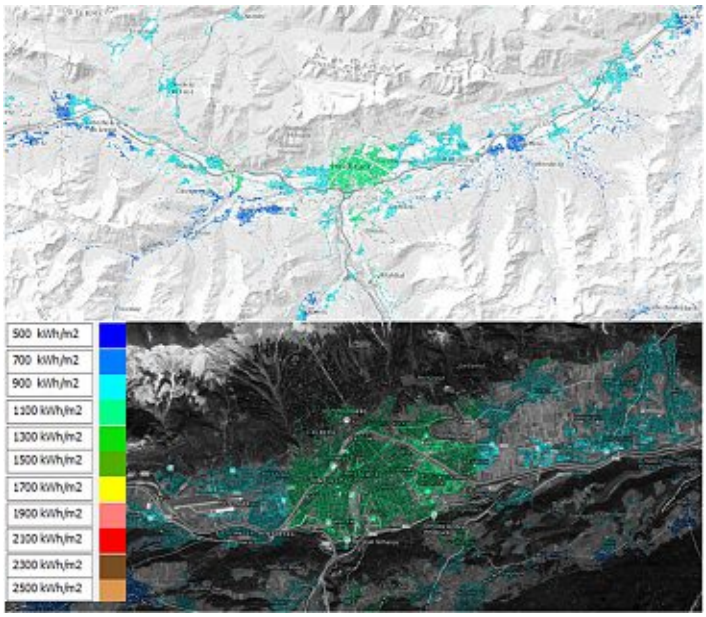

Figure 56: Results of filtering PVGis irradiation data, Yearly average global irradiance on an optimally inclined surface, to OSM building outline polygons and exported to Google earth, Innsbruck area
(Authors Illustration) Screenshot from ATDI HTZ communications v23 & Google Earth

2. Can cartography data be sourced with fine enough resolution to show roof slope/orientation, and can this data also be incorporated into the rooftop solar irradiation results?

Cartography data is available from many sources at the moment, see Appendix 1 & 2, and the availability and resolution of this data is growing. However, the pre-processing involved in generating cartography sets for radio network planning discards the roof slope data which would be necessary to evaluate rooftop solar potential, see Figure 57. This attribute of discarding the rooftop slope data invalidates the concept of this thesis that a radio network planning tool could be repurposed to evaluate regionwide rooftop solar potential.

Figure 57: 3D view of Linz & Salzburg City centers, (a) overview, (b) detail in radio planning tool
(Authors Illustration) Screenshots from ATDI HTZ communications v23, Linz & Salzburg Area

3. Can these results be further refined to include shading effects on building rooftops from the surrounding topography and buildings by simulating the sun as an isotropic radiator and line of sight calculation?

It was found that due to the parallax effect, developing a shadowing model from simulations of a single/multiple radio transmitters means that this method can only be applied over smaller areas dependent on the size of the virtual workspace. As an example, a virtual workspace which encapsulated the entire Vienna region, with a transmitter located 12.47km to the south in order to develop a shadowing model targeting the area around St. Stephens Cathedral started to lose accuracy within a 300m radius of the target coordinates. Increasing the size of the virtual workspace, in order to decrease the effects of parallax over the complete region would require

the resolution of the mapping data to be down-sampled to such an extent that no meaningful results can be produced.

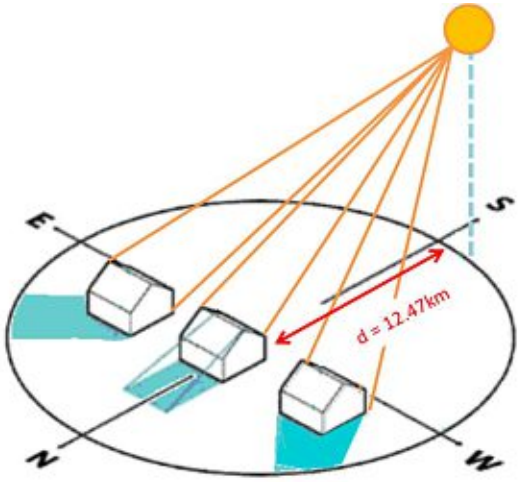

Figure 58: Example of the effects of parallax on shadow modelling
Adapted from (Scheckel, 2013, p. 87)

This study has attempted to overcome the cartographic data bottleneck by using lower resolution data, 100m resolution for macro areas (e.g. Western Europe), 20m range for national studies (e.g. Austria) and 1m for cities (e.g. Vienna). This data has been processed for use in radio network planning tools within the telecommunications industry and is available almost worldwide with varying resolution and freshness (less populated places will only have older or lower resolution data available). Although it was found that all rooftop slope data of such models has been discarded, one advantage of the data available from the telecommunications industry is that the topographical clutter (all obstacles to radio propagation on the earth's surface) is already classified in categories such as rural, suburban, urban, dense urban, industrial, woods and forests etc., see Figure 59.

It should be concluded that if value can be found from a method which employs off-the-shelf radio planning cartography, to assess RTSPV potential, it would be to generate inputs from the pre-categorised clutter data for use to improve the results of existing or modified statistical methods. For example, the IEA project that approximately 27% of the share of urban final electricity demand in India, the country where most growth in this area is expected, could be met by rooftop PV in cities, by 2050 (OECD/IEA, 2016a, p. 285). However, until 2021, acquisition of map data in India was heavily regulated making the use of GIS methods of rooftop solar potential evaluation impossible in many areas (Kumar, 2021). As mentioned in the literature review, several studies have been carried out using statistical methods which have classified the available rooftop area in a region by categories based on

building utilization. (Unger and Mohr, 1992) (Izquierdo et al, 2008, p. 933) (Schallenberg-Rodríguez, 2013) (Kurdgelashvili et al, 2016) (Hofierka & Kaňuk, 2009)

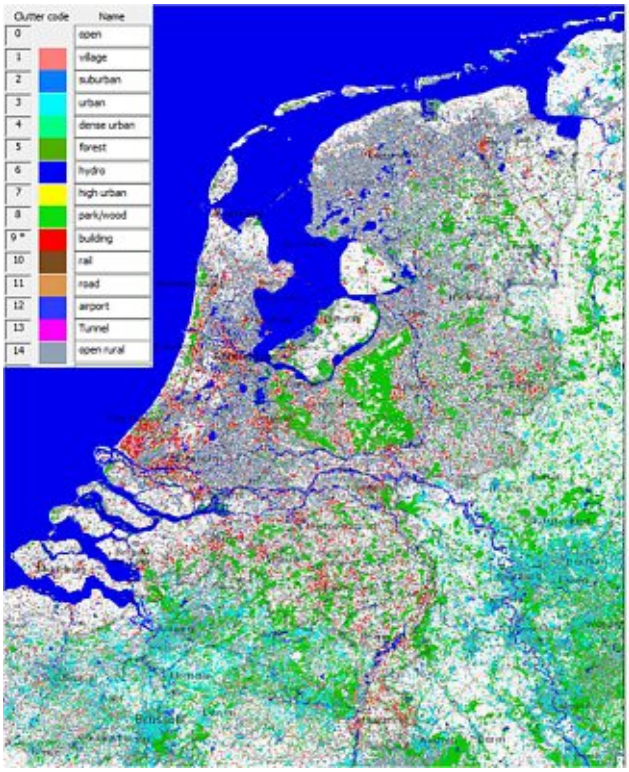

Figure 59: Example of categorized clutter data for the Netherlands
(Authors Illustration) Screenshots from ATDI HTZ communications v23

In the authors opinion, this would seem to be a promising interim solution until the results of more extensive studies made with detailed digital surface models are available. Furthermore, the author proposes that the roofs of buildings in industrial estates, which, from observation, tend to be large, flat and spaced apart enough that shadowing from vegetation does not impact their yearly irradiation, should be prioritised in any governmental subsidy scheme to promote rooftop solar. Prioritisation of these buildings would allow countries, the majority of which are behind schedule to meet their renewable targets, to rapidly increase the quantity of energy received from solar power without causing lengthy land use disputes. Adding rooftop solar in industrial areas would have the additional advantage that the electricity would most likely be consumed on site, or nearby, with minimal transmission losses. As the generation of suitable cartography data and evaluation of rooftop solar potential is a high effort exercise, OSM building outline vectors could be pre-filtered to identify these large, unshadowed flat roofed buildings in industrial areas using database and scripting tools as part of the preparation for targeted cartography data acquisition.

Bibliography

Advanced Topographic Development and Images, 2021. *LATEST AVAILABLE TERRAIN DATA.* [Online]
Available at: https://atdi.com/mapresources/
[Accessed 14 01 2021].

Aerometrex Inc., 2020. *Use of 3D city models for the Australian solar industry.* [Online]
Available at: https://aerometrex.com.au/photogrammetry-applications/use-of-3d-city-models-for-the-australian-solar-industry/
[Accessed 10 07 2020].

Asinari & Bergamasco, 2011. Scalable methodology for the photovoltaic solar energy potential assessment based on available roof surface area: application to Piedmont Region (Italy). *Sol. Energy,* 85(5), pp. 1041-55.

Asinari & Bergamasco, 2011. Scalable methodology for the photovoltaic solar energy potential assessment based on available roof surface area: Further improvements by ortho-image analysis and application to Turin (Italy). *Solar Energy,* 85(11), p. 2741—2756.

BloombergNEF/Solar Power Summit, 2019. *European Market Outlook,* Brussels: Solar Power Europe.

Blue Marble Geographics, 2021. *Global Mapper Overview.* [Online]
Available at: https://www.bluemarblegeo.com/products/global-mapper.php
[Accessed 19 01 2021].

Burke, J., 2017. *Mission Critical Radio Network Planning: Tools & Techniques,* Vienna: University of Applied Science, Technikum Wien.

Castellanos, Sergio & Sunter, 2017. Rooftop solar photovoltaic potential in cities: How scalable are assessment approaches?. *Environmental Research Letters,* 12(125005), pp. 1 - 7.

Castellanos, Sergio & Sunter, 2017. *Rooftop solar photovoltaic potential in cities: How scalable are assessment approaches?.* [Online]
Available at: https://www.researchgate.net/publication/321742090_Rooftop_solar_photovoltaic_potential_in_cities_How_scalable_are_assessment_approaches
[Accessed 10 07 2020].

Conkling, J., 2017. *Partnering with E.ON to bring Project Sunroof to Germany.* [Online]
Available at: https://blog.google/around-the-globe/google-europe/project-sunroof-germany/
[Accessed 14 01 2021].

EPA, 2020. *Green Power Equivalency Calculator - Calculations and References.* [Online]
Available at: https://www.epa.gov/greenpower/green-power-equivalency-calculator-calculations-and-references
[Accessed 20 01 2021].

ESRI, 2020. *Estimate solar power potential.* [Online]
Available at: https://downloads.esri.com/learnarcgis/estimate-solar-power-potential/solar_in_glover.zip
[Accessed 18 01 18].

ESRI, 2021. *Modeling solar radiation.* [Online]
Available at: https://pro.arcgis.com/en/pro-app/latest/tool-reference/spatial-analyst/modeling-solar-radiation.htm
[Accessed 03 01 2021].

European Commission, Joint Research Centre (JRC), 2019. *A high-resolution geospatial assessment of the rooftop solar photovoltaic potential in the European Union.* [Online]
Available at: https://www.sciencedirect.com/science/article/pii/S1364032119305179
[Accessed 10 07 2020].

European Commission's Joint Research Centre, 2020. *SARAH Solar Radiation Data.* [Online]
Available at:
http://re.jrc.ec.europa.eu/pvg_download/sarahdata/gh_0_year_sarah.zip
[Accessed 14 10 2020].

GisGeography, 2020. *5 Free Global DEM Data Sources – Digital Elevation Models.* [Online]
Available at: https://gisgeography.com/free-global-dem-data-sources/
[Accessed 10 07 2020].

Google LLC, 2017. *Project Sunroof data explorer: a description of methodology and inputs.* [Online]
Available at: https://www.google.com/get/sunroof/data-explorer/data-explorer-methodology.pdf
[Accessed 30 12 2020].

Google LLC, 2021. *Frequently Asked Question.* [Online]
Available at: https://www.google.com/get/sunroof/faq/
[Accessed 14 01 2021].

Google LLC, 2021. *Googel Sunroof- How it Works.* [Online]
Available at: https://www.google.com/get/sunroof/how-it-works/
[Accessed 14 01 2021].

Google LLC, 2021. *Google Earth.* [Online]
[Accessed 12 02 2021].

Google LLC, 2021. *Project Sunroof.* [Online]
Available at: https://www.google.com/get/sunroof#/p=0
[Accessed 14 01 2021].

Grodsky & Hernandez, 2020. Reduced ecosystem services of desert plants from ground-mounted solar energy development. *Nature Sustainability,* Volume 3, p. 1036–1043.

Hoffmann, T., 2015. *Suncalc.* [Online]
Available at: https://www.suncalc.org
[Accessed 15 01 2021].

Hofierka & Kaňuk, 2009. Assessment of photovoltaic potential in urban areas using open-source solar radiation tools. *Renewable Energy,* 34(10), p. 2206—2214.

Hofierka, Huld & Suri, 2007. *r.sun - Solar irradiance and irradiation model.* [Online]
Available at: https://grass.osgeo.org/grass76/manuals/r.sun.html
[Accessed 26 12 2020].

Hong, Lee, Koo Jeong & Kim, 2016. Development of a method for estimating the rooftop solar photovoltaic (PV) potential by analyzing the available rooftop area using Hillshade analysis. *Applied Energy,* Volume 194(C), pp. 320-332.

Instituto Tecnologico de Canarias, 2020. *mean global solar irradiation on the horizontal plane.* [Online]
Available at: http://meteodata.itccanarias.org/
[Accessed 24 12 2020].

Izquierdo, Rodrigues & Fueyo, 2008. A method for estimating the geographical distribution of the available roof surface area for large-scale photovoltaic energy-potential evaluations. *Solar Energy,* Volume 82, p. 929–939.

Jakubiec & Reinhart, 2013. A method for predicting city-wide electricity gains from photovoltaic panels based on LiDAR and GIS data combined with hourly Daysim simulations. *Solar Energy,* Volume 93, p. 127—143.

Karteris,Slini & Papadopoulos, 2013. Urban solar energy potential in Greece: A statistical calculation model of suitable built roof areas for photovoltaics. *Energy and Buildings,* Volume 62, p. 459—468.

Khanna, D., 2020. *Estimate solar power potential.* [Online]
Available at: https://learn.arcgis.com/en/projects/estimate-solar-power-potential/
[Accessed 18 01 2021].

Ko, Wang, Chen & Tsai, 2015. Evaluation of the development potential of rooftop solar photovoltaic in Taiwan. *Renewable Energy,* Volume 76, pp. 582-595.

Kodysh, Omitaomu, Bhaduri & Neish, 2013. Methodology for estimating solar potential on multiple building rooftops for photovoltaic systems. *Sustainable Cities and Society,* Volume 8, pp. 31-41.

Kumar, C., 2021. *Times of India.* [Online]
Available at: https://timesofindia.indiatimes.com/india/india-relaxes-mapping-policy-desi-private-firms-to-have-greater-access/articleshow/80922427.cms
[Accessed 18 02 2021].

Kurdgelashvili, Li, Shih & Attia, 2016. Estimating technical potential for rooftop photovoltaics in California, Arizona and New Jersey. *Renewable Energy,* Volume 95, pp. 286--302.

Lehmann & Peter, 2003. *Assessment of roof & facade potentials for solar use in Europe,* Aachen: Institute for sustainable Solutions and Innovations.

Lindberg, Sun, Grimmond & Tang, 2018. *Goteborg_SWEREF99_1200.* [Online]
Available at: https://umep-docs.readthedocs.io/projects/tutorial/en/latest/Tutorials/IntrodutionToProcessingSEBE.html
[Accessed 18 01 2021].

Lindberg, Sun, Grimmond & Tang,, 2018. *Solar Energy - Introduction to SEBE.* [Online]
Available at: https://umep-docs.readthedocs.io/projects/tutorial/en/latest/Tutorials/SEBE.html
[Accessed 18 01 2021].

Lorenzon, E., 1994. *Engineering of Photovoltaic Systems.* 1 ed. Madrid: PROGENSA.

MA 41 - Stadtvermessung, 2020. *Solarpotenzial3D.* [Online]
Available at: https://www.wien.gv.at/solarpotenzial3d/#/
[Accessed 14 01 2021].

Mainzer, Killinger, McKenna & Fichtner, 2017. Assessment of rooftop photovoltaic potentials at the urban level using publicly available geodata and image recognition techniques. *Solar Energy,* Volume 155, pp. 561-573.

Mansouri-Kouhestani, Byrne, Johnson, Spencer, Hazenonk & Brown, 2018. *Evaluating solar energy technical and economic potential on rooftops in an urban setting: the city of Lethbridge, Canada.* [Online]
Available at: https://link.springer.com/article/10.1007/s40095-018-0289-1#citeas
[Accessed 10 06 2020].

Mapdwell Inc, 2014. *Solar System Mappedwell.* [Online]
Available at: https://mapdwell.com/en/solar/cambridge
[Accessed 14 01 2021].

McClendon, B., 2012. *The never-ending quest for the perfect map.* [Online]
Available at: https://blog.google/products/maps/never-ending-quest-for-perfect-map/
[Accessed 14 01 2021].

Moore-O'Leary, Grodsky, Saul-Gershenz & Hoffacker, 2019. Techno-ecological synergies of solar energy for global sustainability. *Nature Sustainability,* Volume 2, p. pages560–568.

Mulvaney, D., 2017. Identifying the roots of Green Civil War over utility-scale solar energy projects on public lands acrossthe American Southwes. *Journal of Land Use Science,* 12(6), pp. 493-515.

National Renewable Energy Laboratory, 2020. *PVWatts Calculator.* [Online]
Available at: https://pvwatts.nrel.gov/
[Accessed 28 12 2020].

Nguyen & Pearce, 2013. Automated quantification of solar photovoltaic potential in cities. *International Review for Spatial Planning and Sustainable Development,* 1(1), pp. 49-60 .

OECD/IEA, 2016a. *Energy Technology Perspectives,* Paris: International Energy Agency.

OECD/IEA, 2016b. *Energy Technology Perspectives Annex H – Rooftop Solar PV Potential in Cities,* Paris: International Energy Agency, pp. 1-11.

OSM Buildings, 2020. *OSM Buildings.* [Online]
Available at: https://osmbuildings.org/data/
[Accessed 10 07 2020].

Paidipati, Frantzis, Sawyer, & Kurrasch, 2008. *Rooftop Photovoltaics Market Penetration Scenarios.* [Online]
Available at: https://www.osti.gov/biblio/924645
[Accessed 17 12 2020].

Palmer, Cole, Betts & Gottschlag, 2016. Assessment of potential for photovoltaic roof installations by extraction of roof tilt from light detection and ranging data and aggregation to census geography. *Institution of Engineering and Technology Renewable Power Generation,* 10(4), p. 467—473.

Pan Tech World, 2016. *Digita Photogrammetry.* [Online]
Available at: https://www.pantechworld.com/digital-photogrammetry/
[Accessed 14 01 2021].

Petrini-Monteferri, Posch, Bremer, Georges, Wichmann, Dürauer & Sam, 2014. *VERTISOL – das weltweit erste Verfahren zur großflächigen Erstellung von Solarkatastern für Gebäudefassaden dargestellt am Beispiel der Stadt Wien.* Salzburg, AGIT 2014 – Symposium und Fachmesse Angewandte Geoinformatik.

Pritt, M. D., 2014. *Fast Orthorectified Mosaics of Thousands of Aerial Photographs from Small UAVs.* Washington, DC, IEEE, p. 1—8.

PVGIS, 2019. *Photovoltaic Geographical Information System.* [Online]
Available at: https://re.jrc.ec.europa.eu/pvg_tools/en/tools.html

QGIS - GRASS-Wiki, 2016. *QGIS.* [Online]
Available at: https://grasswiki.osgeo.org/wiki/QGIS
[Accessed 31 12 2020].

Saunders, P. J., 2020. *Land Use Requirements of Solar and Wind Power Generation:Understanding a Decade of Academic Research.* 1 ed. Arlington: Energy Innovation Reform Project .

Schallenberg-Rodríguez, 2013. Photovoltaic techno-economical potential on roofs in regions and islands: The case of the Canary Islands. Methodological review and methodology proposal. *Renewable and Sustainable Energy Reviews,* Volume 20(C), pp. 219--239.

Scheckel, P., 2013. *The Homeowner's Energy Handbook: Your Guide to Getting Off the Grid.* 1 ed. North Adams, USA: Storey Publishing.

Singh & Banerjee, 2015. Estimation of rooftop solar photovoltaic potential of a city. *Solar Energy,* Volume 115, p. 589—602.

Software Informer, 2021. *ICS telecom 8.0.* [Online]
Available at: https://ics-telecom.software.informer.com/8.0/
[Accessed 12 02 2021].

Solar Energy Industries Association/Wood Mackenzie, 2019. *Solar Market Insight Report 2019 Q3,* Washington D.C.: SEIA/Wood Mackenzie Power & Renewables.

SolarGis, 2020. *Download solar resource maps and GIS data for 200+ countries.* [Online]
Available at:
https://solargis.com/file?url=download/Austria/Austria_GISdata_LTAym_YearlyMonthlyTotals_GlobalSolarAtlas-v2_GEOTIFF.zip&bucket=globalsolaratlas.info
[Accessed 15 11 2021].

SolarGIS, 2020. *SolarGIS.* [Online]
Available at: https://apps.solargis.com/prospect/detail/iF5lanTaFRr820TU/pv-electricity/hourly
[Accessed 26 03 2020].

Spanish Land Registry, 2013. *Spanish Cadastre.* [Online]
Available at: http://www.sedecatastro.gob.es/
[Accessed 25 12 2020].

Spatial Information Industry Promotion Institute, 2014. *Spatial Information Industry Promotion Institute (SPACEN).* [Online]
Available at: http://www.spacen.or.kr/main.do
[Accessed 14 01 2021].

Stadt Freiburg i. Br. - Geodatenmanagement, 2018. *3D-Stadtmodell Freiburg LoD2.* [Online]
Available at:

https://geodaten.freiburg.de/geonetwork/srv/ger/catalog.search#/metadata/1c576440-e5e1-4095-bff1-a14d76cec6f4
[Accessed 14 01 2021].

Stadt Freiburg i. Br. - Vermessungsamt, 2018. *3D-Stadtmodell Freiburg LoD1.* [Online]
Available at:
https://geodaten.freiburg.de/geonetwork/srv/ger/catalog.search#/metadata/164ceef4-6c67-4763-8100-c5799a2ea6d8
[Accessed 14 01 2021].

Stadt Wien-Stadtvermessung, 2020. *https://www.wien.gv.at/stadtentwicklung/stadtvermessung/geodaten/solar/solarmethodik.html.* [Online]
Available at:
https://www.wien.gv.at/stadtentwicklung/stadtvermessung/geodaten/solar/solarmethodik.html
[Accessed 21 09 2020].

Stadt Wien-Stadtvermessung, 2020. *Technologie - Airborne Laserscanning (ALS).* [Online]
Available at: https://www.wien.gv.at/stadtentwicklung/stadtvermessung/images/als-technologie.gif
[Accessed 20 09 2020].

State Energy Resources Conservation and Development Commission, 2019. *Assembly Bill No. 178 Energy: building standards: photovoltaic requirements.* [Online]
Available at:
https://leginfo.legislature.ca.gov/faces/billNavClient.xhtml?bill_id=201920200AB178
[Accessed 12 11 2020].

STATISTIK AUSTRIA, 2013. *Gebäude 1971 bis 2011 nach ausgewählten Merkmalen.* [Online]
Available at:
https://www.statistik.at/wcm/idc/idcplg?IdcService=GET_PDF_FILE&RevisionSelectionMethod=LatestReleased&dDocName=074079
[Accessed 18 02 2021].

Takebayashi, Ishii,Moriyama, Sakaki, Nakajima & Ueda, 2015. Study to examine the potential for solar energy utilization based on the relationship between urban morphology and solar radiation gain on building rooftops and wall surfaces. *Solar Energy,* Volume 119 , p. 362—369.

Unger and Mohr, 1992. *Theoretisches und technisches Potential von Solarthermie, Photovoltaik, Biomasse und Wind in Nordrhein-Westfalen,* Bochum: Ruhr-Universität Bochum.

ViennaGis, 2020. *Wien Umweltgut: Solarpotenzialkataster.* [Online]
Available at: https://www.wien.gv.at/umweltgut/public/grafik.aspx?ThemePage=9
[Accessed 10 07 2020].

Wiginton, Nguyen & Pearce, 2010. Quantifying rooftop solar photovoltaic potential for regional renewable energy policy. *Computers, Environment and Urban Systems,* 34(4), p. 345—357.

Wu, Leslie, Sawyer, Cameron, Brand, Cohen, Allen, Ochoa & Olson, 2020. Low-impact land use pathways to deep decarbonization of electricity. *Environmental Research Letters,* 15(7), pp. 1-13.

List of abbreviations

ATDI	Advanced Topographic Development and Images
BS	Base Station
CBECS	Commercial Buildings Energy Consumption Survey
DEM	Digital Elevation Model
DHI	Diffuse Horizontal Irradiance
DNI	Direct Normal Irradiance
DSM	Digital Surface Model
DTM	Digital Terrain Model
EIA	Energy Information Administration
ESRI	Environmental Systems Research Institute
GCR	Ground Cover Ratio
GIS	Geographic Information System
HVAC	Heating, ventilation, and air conditioning
IEA	International Energy Agency
LiDAR	Light Detection And Ranging
MIT	Massachusetts Institute of Technology
MS	Mobile Station
NREL	National Renewable Energy Laboratory
OECD	Organisation for Economic Co-operation and Development
OSM	Open Street Map
PR	Performance Ratio
PV	Photovoltaic
PVGIS	Photovoltaic Geographical Information System
RANSAC	Random Sample Consensus
RECS	Residential Energy Consumption Survey
RMS	Root Mean Square
RTSPV	Rooftop Solar Photovoltaics
SBR	Setback Ratio
USDOE	U.S. Department of Energy

List of figures

List of Tables

List of appendices

Appendix A1

International listing of data sources for DEM, DSM and geo-referenced vector polygons or raster data

Appendix A2

National listing of data sources for DEM, DSM and geo-referenced vector polygons or raster data

Appendix A3

Variables included in QGIS meteorological data file

Appendixes

A1

International listing of data sources for DEM, DSM and geo-referenced vector polygons or raster data

Description	Link
NASA Earth Data	https://search.earthdata.nasa.gov/search?m=2.951407120500747!-7.1015625!2!1!0!0%2C2
USGS web site Earth Explorer (Worldwide 1 arcsec SRTM and more)	http://earthexplorer.usgs.gov/
USGS web site Global data Explorer (Worldwide)	gdex.cr.usgs.gov/gdex/
USGS web site 3DEP (USDigital Elevation Data)	https://viewer.nationalmap.gov/basic/?basemap=b1&category=ned,nedsrc&title=3DEP%20View#/
Jaxa web site Digital Elevation Data	www.eorc.jaxa.jp/ALOS/en/aw3d30/data/index.htm
View Finder web site Digital Elevation Data	http://www.viewfinderpanoramas.org/dem3.html
SRTM 3 arsec DEM Data	https://srtm.csi.cgiar.orgsrtmdata/
Population data 1 arcsec (4SEC)	https://ciesin.columbia.edu/data/hrsl/
Palsar Forest/Non-Forest 25m	https://www.eorc.jaxa.jp/ALOS/en/palsar_fnf/data/2017/html
Sentinel satellite images 10 and 20m	https://scihub.copernicus.eu/dhus/#/home
World: Land and Water polygons	https://osmdata.openstreetmap.de/data/water-polygons.html
ICESAT-1; National Snow and Ice Data Center (H5 format)	https://nsidc.org/data/glah06
ICESAT-2 (ATL03); National Snow and Ice Data Center (H5 format)	https://nsidc.org/data/atl08
ICESAT-2 (ATL08); National Snow and Ice Data Center (H5 format)	https://nsidc.org/data/atl03/versions/3
ICESAT-1/2); Openaltimetry (CSV format)	https://openaltimetry.org/
Regional OpenStreetMap Vectors	https://extract.bbbike.org/
National OpenStreetMap Data Extracts	https://download.geofabrik.de/

A2

National listing of data sources for DEM, DSM and geo-referenced vector polygons or raster data

Description	Link
Artic: DEM data	https://www.pgc.umn.edu/data/arcticdem/
Argentina: Terrain data	https://www.ign.gob.ar/NuestrasActividades/Geodesia/ModeloDigitalElevaciones/Busqueda
Australia: Terrain data	http://services.ga.gov.au/
Austria: Terrain data	https://www.landinformationsystem.at/#/lisa/overview
Brazil: Terrain data	https://downloads.ibge.gov.br/downloads_geociencias.htm
Canada: Lidar	https://canadiangis.com/free-canada-lidar-data.php
Canada: Terrain data	https://www.rncan.gc.ca/information-topographique/10803
Cyprus: Terrain data	https://eservices.dls.moi.gov.cy/#/national/inspiregeoportalmapviewer
Denmark: Terrain data	https://download.kortforsyningen.dk/content/dhm-2007terr%C3%A6n-10-m-grid
England: Terrain data	https://environment.data.gov.uk/DefraDataDownload/?Mode=survey
Netherlands: Building Vector data	http://3dbag.bk.tudelft.nl/downloads
New Zealand: Terrain data	https://data.linz.govt.nz/
Norway: Terrain data	https://www.geonorge.no/
Phillipines: Terrain data	www.philgis.org
Poland: Lidar / DTM+DSM/ Vectors	https://mapy.geoportal.gov.pl/imap/Imgp_2.html
Scotland: Lidar data	https://data.gov.uk/dataset/abe9bb9d-b99e-4d43-bed2-06e7b4d5701d/lidar-composite-coverage-and-extents-for-scotland
Spain: Terrain data	http://www.ign.es/web/ign/portal
Uruguay: Terrain data	https://visualizador.ide.uy/ideuy/core/load_public_project/ideuy/
Wales: Lidar data	http://lle.gov.wales/Catalogue/Item/LidarCompositeDataset?lang=en

A3

Variables included in QGIS meteorological data file

No.	USE	Column name	Description
1	R	iy	Year [YYYY]
2	R	id	Day of year [DOY]
3	R	it	Hour [H]
4	R	imin	Minute [M]
5	N	qn	Net all-wave radiation [W m^{-2}]
6	N	qh	Sensible heat flux [W m^{-2}]
7	N	qe	Latent heat flux [W m^{-2}]
8	N	qs	Storage heat flux [W m^{-2}]
9	N	qf	Anthropogenic heat flux [W m^{-2}]
10	N	U	Wind speed [m s^{-1}]
11	O	RH	Relative Humidity [%]
12	O	Tair	Air temperature [°C]
13	N	pres	Barometric pressure [kPa]
14	N	rain	Rainfall [mm]
15	R	kdown	Incoming shortwave radiation [W m^{-2}] Must be >= 0 W m^{-2}.
16	N	snow	Snow [mm]
17	N	ldown	Incoming longwave radiation [W m^{-2}]
18	N	fcld	Cloud fraction [tenths]
19	N	Wuh	External water use[m^3]
20	N	xsmd	Observed soil moisture [m3 m^{-3} or kg kg^{-1}]
21	N	lai	Observed leaf area index [m2 m^{-2}]
22	O	kdiff	Diffuse radiation [W m^{-2}]
23	O	kdir	Direct radiation [W m^{-2}]
24	N	wdir	Wind direction [°]

(Lindberg et al, 2018)